# FIRST-DAY ROAD LOG:

# GEOMORPHIC AND TECTONIC DEVELOPMENT OF THE SANDIA MOUNTAINS

SEAN D. CONNELL[1], SPENCER G. LUCAS[2], KARL E. KARLSTROM[3], DANIEL J. KONING[1], KARL KRAINER[4], MATT HEIZLER[1], KURT RUDOLPH[5], LAURIE CROSSEY[3], ERWIN MELIS[6], GARY S. MORGAN[2], AND LESLIE MCFADDEN[3]

[1]New Mexico Bureau of Geology and Mineral Resources, 801 Leroy Place, Socorro, NM 87801; sean.connell@nmt.edu
[2]New Mexico Museum of Natural History and Science, 1801 Mountain Road NW, Albuquerque, NM 87104
[3]Earth and Planetary Sciences, University of New Mexico, MSC O3-2040, 1 University of New Mexico, Albuquerque, NM 87131-0001
[4]Institute of Geology, Innsbruck University, Innrain 52, Innsbruck, A-6020 Austria
[5]University of Houston and Rice University, 9 Rabbitbrush, Santa Fe, NM 87506
[6]John Shomaker and Associates, 2611 Broadbent Parkway NE, Albuquerque, NM 87107

**Assembly Point:** Parking lot for New Mexico Museum of Natural History and Science Annex (950 Eighteenth Street NW)
**Departure Time:** 7:30 AM
**Distance:** 78 miles
**Stops:** 4

**Views, landmarks, and outcrops are given using the clock system, where 12:00 is straight ahead, 3:00 is to the right, and 9:00 is to the left. Driving distances are given in miles.**

## SUMMARY

The Day 1 agenda for the field conference traces a counter-clockwise loop around the Sandia Mountains, where we will observe structural, stratigraphic, and geomorphic features associated with this basement-cored uplift, and discuss the geologic history of central New Mexico, with stops focusing on Proterozoic rocks, the Great Unconformity, Upper Pennsylvanian stratigraphy, and Cenozoic development of the rift-flanking Sandia Mountains (Fig. 1.01).

7:30 AM: Assemble caravan in parking lot for New Mexico Museum of Natural History and Science Annex.

8:00 to 11:00 AM: Stop 1 will examine Proterozoic features of the aureole of the Sandia pluton, an unusual downfaulted block of deformed Mesozoic sedimentary rocks, and Pleistocene piedmont alluvium. After an introduction to the geologic history of the Sandia Mountains, participants will split into two groups for separate hikes. A northern hike visits basement rocks at the southern end of Rincon Ridge that are part of the thermal and deformational aureole of the 1.45-Ga Sandia granite. On this northern hike, participants have an opportunity to observe deformational fabrics and discuss crustal evolution and the emplacement of the Sandia pluton. What can these features tell us about the tectonic history of the Sandia pluton and surrounding country rock?

A separate southern hike visits faulted Triassic and Jurassic sedimentary rocks, where the group will discuss how this allochthonous block of Mesozoic strata came to be located here. Does this outcrop represent an ancient landslide or is it an extensional tectonic klippe that was translated to its present location by early rift-related normal faulting? At this stop, we will also discuss alluvial stratigraphy and examine features of the Sandia pluton in scattered boulders of Sandia granite. Groups will swap leaders and routes midway through this stop at around 9:45 AM.

11:45 to 1:00 PM: Stop 2 examines the Great Unconformity near Doc Long Picnic Area, where participants can examine the nonconformable contact between Mesoproterozoic Sandia granite and Pennsylvanian sedimentary rocks of the Sandia Formation. The Great Unconformity represents a hiatus of approximately 1.1 billion years in the geologic record. At this stop, the group will learn about thermochronologic data that help constrain the timing and magnitude of basement unroofing of the Sandia granite, providing insights into the history of erosion before and during development of the Ancestral Rocky Mountains orogeny. Discussions will integrate upper Paleozoic stratigraphy, the role of the Transcontinental Arch, and regional tectonic controls on large-scale sedimentation and exhumation.

2:00 to 3:30 PM: Stop 3 examines the Great Unconformity at the base of the Crest of Montezuma, where rocks of the Pennsylvanian Sandia Formation nonconformably overly deformed Paleoproterozoic metasedimentary rocks. The group will discuss implications of a regional synthesis of upper Paleozoic stratigraphy, Pennsylvanian sedimentation, and Placitas area hydrogeology.

4:00 to 5:00 PM: Stop 4 examines a boundary between Neogene conglomerate and conglomeratic sandstone of the Santa Fe Group and underlying Cretaceous rocks of the Mancos Shale. Gravels in the Sierra Ladrones Formation (upper Santa Fe Group) recorded the unroofing of the northern Sandia Mountains. We discuss the nature of this boundary and how it has been used to interpret the uplift history of the Sandia Mountains and development of the adjacent Albuquerque Basin of the Rio Grande rift.

5:30 PM: New Mexico Geological Society BBQ at Rio Grande Nature Center State Park, 2901 Candelaria Road NW, Albuquerque, New Mexico 87107.

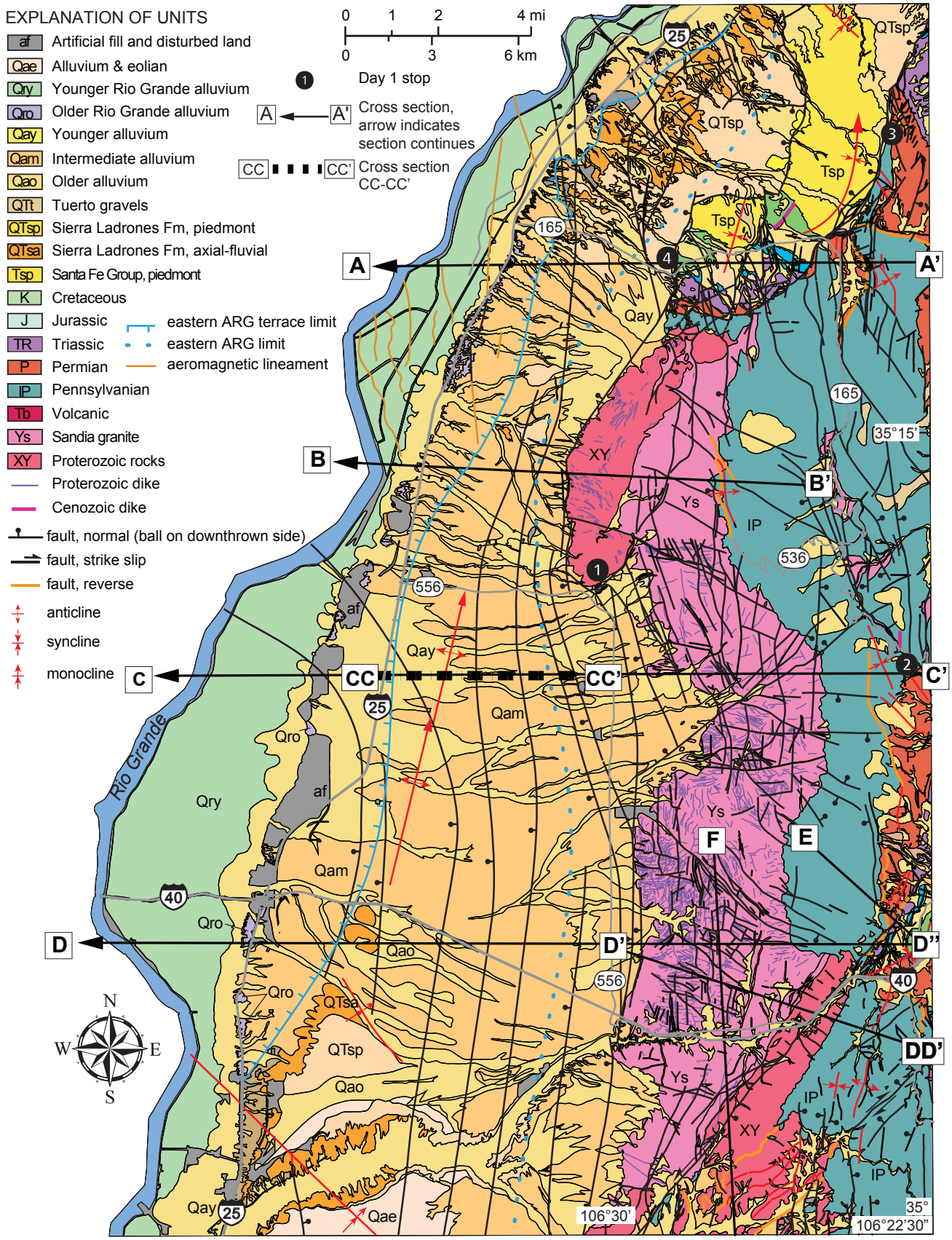



FIGURE 1.01. Geologic map of the Albuquerque area and Sandia Mountains (simplified from Connell, 2006). Cross sections shown in Figures 1.02, 1.06, and 1.11. Fault traces are shown to indicate continuity in the subsurface and do not denote offset relationships with overlying alluvium (units Qry, Qro, Qay, Qam, Qao, and Qae). Eastern limit of ancestral Rio Grande terraces is shown by blue hachured line; eastern limit of ancestral Rio Grande (ARG) deposits in Sierra Ladrones Formation is shown by dotted blue line.

**Mileage** Description *Distance to next entry*
**[Waypoint, decimal degrees, World Geodetic System 1984]**

**Waypoint 1.01 [N35.1016°, W106.6662°]**

**0.0** Assemble caravan at New Mexico Museum of Natural History and Science Annex parking lot at 950 Eighteenth Street NW. **Head west to parking lot exit, turning left (south) onto Eighteenth Street NW. ZERO ODOMETER AT THIS TURN.** *0.1*

**0.1** **Turn right (west) onto Mountain Road NW.** *0.3*

**0.4** **Turn right at stoplight onto Rio Grande Boulevard and head north toward on-ramp to Interstate 40.** *0.4*

**0.8** **At stoplight, merge onto east-bound I-40.** Quickly and safely move three lanes to the left to avoid local traffic congestion. *0.5*

**1.3** Cross Twelfth Street NW overpass and continue east on I-40. *0.6*

**1.9** **Move right onto lane that feeds into the north-bound on-ramp to I-25** (Exit 159C toward Santa Fe). Approach the "Big I," a local name for the intersection of I-40 and I-25**. Use off-ramp to merge onto northbound I-25.** *1.8*

**3.7** Continue north on I-25, passing under Candelaria Road (Exit 226). Our route along I-25 is near the deepest part of the Albuquerque Basin (Fig. 1.02). *0.5*

**5.2** Pass Montgomery/Montaño Boulevard overpass (Exit 228). *1.8*

**7.0** Cross over north-trending Albuquerque Metropolitan Arroyo Flood Control Authority (AMAFCA) diversion channel, which is part of a larger system of smooth-walled concrete channels designed to quickly divert floodwater collected across northeast Albuquerque to the Rio Grande at the north edge of the city, where water enters the river. AMAFCA was created in response to recurring and damaging flash-flood events that accompanied urbanization of the Albuquerque area during the middle of the 20th century. Severe floods in the 1940s prompted the U.S. Army Corps of Engineers to

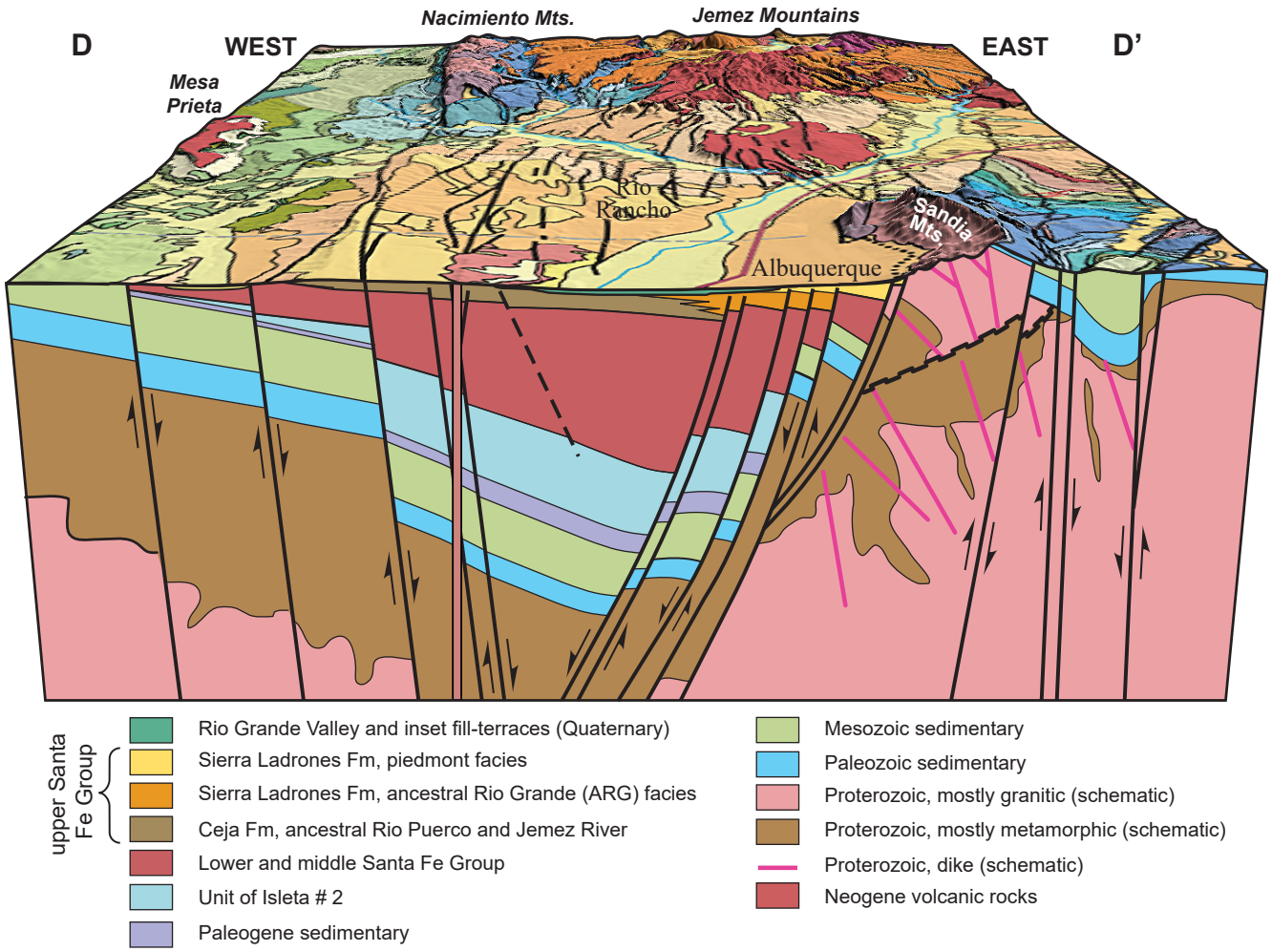



FIGURE 1.02. Block diagram of Sandia Mountains and Albuquerque Basin drawn along cross section line D–D' on Figure 1.01 (modified from Connell and Love, 2009).

recommend large-scale diversion channels and detention works. In 1963, the New Mexico Legislature established AMAFCA as a special-purpose political subdivision charged with planning, constructing, and maintaining metropolitan flood-control facilities (Peterson, 1992). Early construction of the North Diversion Channel (completed in 1966) and South Diversion Channel (completed in 1972) mitigated flood risks in Albuquerque by intercepting drainage from steep mountain-front arroyos and conveying storm runoff safely around the suburban core of Albuquerque. *0.3*

**7.3** Pass San Mateo/Osuna Boulevard overpass (Exit 230). We are near the depocenter of the Calabacillas subbasin. *0.1*

**7.4** Pass San Antonio Boulevard (Exit 231). Holocene and uppermost Pleistocene piedmont deposits derived from the Sandia Mountains form valley border fans that overlie middle Pleistocene fluvial deposits of the Edith Formation. Young alluvial deposits (unit Qay of Connell, 2008a) locally pose geotechnical challenges for construction and managed aquifer recharge due to compressibility, piping susceptibility, and hydrocollapse of weakly consolidated deposits (Clary et al., 1984). Hydrocollapsable soils associated with Holocene alluvium, which are locally less dense than the older piedmont deposits, will consolidate when saturated with water. These low-density sediments can compact and cause severe foundation damage when wetted from irrigation, intense rainfall, or broken pipes, leading to costly repairs for homes and infrastructure (Rinehart et al., 2017). Mapping locations of deposits that are prone to hydrocollapse is important for identifying suitable areas for managed aquifer recharge (Koning et al., 2019, 2026e). *0.9*

**8.3** Pass Paseo del Norte Boulevard (State Road 423 [NM 423], Exit 232). *1.6*

**9.9** Balloon Fiesta Park is about 0.75 miles (1.2 km) to the northwest. The park sits on middle Pleistocene alluvial deposits derived from the Sandia Mountains. These deposits overlie middle Pleistocene fluvial deposits of the Edith Formation, which was laid down by the ancestral Rio Grande (see Lambert, 1968; Connell et al., 2007). *0.6*

**10.5** Entering Sandia Pueblo land. **Take off-ramp (Exit 326) onto Tramway Boulevard (State Road 556 [NM 556]) and Roy Avenue.** Major features that define the skyline include: Nacimiento Mountains (Sierra Nacimiento) at 10:00, Jemez Mountains and basaltic lava flows and volcanic vents on Santa Ana Mesa at 11:00, and Sandia Mountains at 3:00. Upper Pleistocene and Holocene valley border deposits overlie the Edith Formation. To the west are abandoned and reclaimed gravel quarries in the Edith Formation. *0.4*

**10.9** **Turn right on onto Tramway Boulevard**, heading upslope and east toward the Sandia Mountains. *0.4*

**11.3** Ascend piedmont slope of Sandia Mountains (Fig. 1.03). Bison pastures to the south. *0.7*

**12.0** The rugged western face of the Sandia Mountains exposes 1.45-Ga Sandia granite, which intruded the 1.65–1.60-Ga metamorphic complex on Rincon Ridge. Pennsylvanian strata nonconformably overlie Proterozoic basement rocks.

The western flank of the Sandia Mountains (Figs. 1.02–1.04) defines the eastern structural margin of the Albuquerque Basin and preserves a tectonic and geomorphic record of rift-margin uplift, Neogene synrift basin filling, and alternating episodes of Pleistocene incision and aggradation. The Sandia Mountains are a basement-cored, east-dipping fault block that is capped by Paleozoic strata and characterized by a steep, west-facing escarpment with up to 1.4 km (0.9 mi) of topographic relief from crest to the upper (proximal) piedmont.

Geomorphic and soil-stratigraphic mapping of piedmont deposits integrates landform analysis, terrace and fan-surface correlation, and pedogenic characterization to reconstruct the late Cenozoic evolution of extensional basin margins (Fig. 1.05). Lambert (1968) produced the first detailed map of the Sandia Mountains piedmont. The alluvial stratigraphy was refined and expanded by Connell (1996) and incorporated into geologic quadrangle maps and a regional compilation by Connell (2008a). Discrete piedmont deposits and constructional surfaces are delineated using topographic expression, degree of dissection, surface clast armor, relative elevation above modern drainages, and crosscutting relationships (Fig. 1.05). Soil-profile development, as expressed by horizon thickness, pedogenic carbonate morphology stages, clay illuviation, rubefication, and desert pavement development, provides a relative




FIGURE 1.03. View of Rincon Ridge and Sandia Mountains.

chronologic framework that distinguishes older constructional fan remnants from inset younger depositional surfaces (see Connell and Wells, 1999 for descriptions of the northern flank of the Sandia Mountains).

We are traveling toward the structural boundary between the Albuquerque Basin and Sandia Mountains. Figure 1.06 is a cross section drawn along part of Paseo del Norte Boulevard, approximately 3 km (1.9 mi) to the south, that was constructed using water-supply and groundwater-monitoring wells drilled in the city of Albuquerque. Examination of lithologic cuttings from drilling activities and interpretation of borehole geophysical log data identified marker beds and aquifers that are depended on by the region (Connell, 1997). *1.4*

**13.4** At 11:00, Tabo Creek incised a deep canyon through Paleoproterozoic metamorphic rocks of Rincon Ridge (Fig. 1.07). The Rincon fault was named by Kelley and Northrop (1975) for a north–northeast-trending range-front bounding normal fault that marks the base of Rincon Ridge. The Rincon fault is treated as a northern segment of the larger Sandia Mountains frontal fault system. The Rincon fault is approximately 11 km (6.8 mi) long, dips between 65–76° SW, and bounds the western flank of Rincon Ridge and the northern Sandia Mountains (Connell, 2008a).

To the south, the Rincon fault displaces upper Pleistocene alluvial deposits in a down-to-the-west manner (Connell, 1996). The northern end of the Rincon fault splits into the Placitas and Ranchos faults near Stop 4. Such relatively recent displacements are important for assessing seismic hazards and the potential for earthquakes that could cause damage to homes and infrastructure (U.S. Geological Survey, 2024).

This stretch of Tramway Boulevard crosses a prominent inflection in the isostatic gravity field (Cordell, 1979). This inflection coincides with the eastern boundary of axial-fluvial deposits of the Sierra Ladrones Formation (ancestral Rio Grande deposits), which are, in turn, buried beneath a veneer of middle and upper Pleistocene piedmont alluvium. *0.6*

**14.0** Official Scenic Historic Marker (Fig. 1.08) honoring Doña Dolores "Lola" Chávez de Armijo, the State Librarian and an early women's rights pioneer who fought gender discrimination in 1912. The governor at the time sought to replace her because he considered women to be unqualified to hold office. The New Mexico Supreme Court ruled in her favor, paving the way for subsequent legislation allowing women to hold appointed office. Continue driving east, ascending a bajada formed by multiple drainages derived from the Sandia Mountains (Fig. 1.09). *0.9*

**14.9** **Turn left onto Forest Service Road 333 (FS 333)** toward La Cueva Trailhead and Juan Tabo Recreation Area. Cross a sliver of Sandia Pueblo land. The origin of Juan Tabó (or Juan Taboso) is not clear. He was either a local priest or a sheepherder who grazed his flocks in the canyon that now bears his name (Simmons, 1982). *0.2*

**15.1** Enter Cibola National Forest. *0.1*

**15.2** Hills on left are Paleoproterozoic metasedimentary rocks of the south-plunging nose of Rincon Ridge. *0.4*

**15.6** Park on right shoulder as directed.

**Waypoint 1.02 [N35.2025°, W106.5041°]**




FIGURE 1.04. Aerial view north, showing Rincon Ridge, Sandia Mountains, and associated piedmont slope. The black circle marks the location of Stop 1.

**STOP 1. Rincon Ridge and Structural Margin between Albuquerque Basin and Sandia Mountains.**

## INTRODUCTION

Stop 1 (Fig. 1.01) is at the northern end of a prominent eastward step in the mountain front that provides multiple perspectives into nearly 1.7 billion years of Earth history. At this stop, we will discuss exposed and buried geologic features and tectonic events that contributed to the development of the Sandia Mountains (Figs. 1.09–1.11). From this vantage, we can see Paleoproterozoic (1.68–1.65-Ga) metamorphic rocks on Rincon Ridge, the Mesoproterozoic (1.45-Ga) Sandia pluton and its contact aureole, upper Paleozoic strata nonconformably overlying on the Great Unconformity, a downfaulted block of Mesozoic rocks, and Pleistocene to modern piedmont deposits all within 2 km (1.2 mi) of the parking area. This locality presents an opportunity to integrate stratigraphy, structure, thermochronology, and geomorphology in the context of nearly one-third of Earth's history that ultimately led to uplifts and the development of the Rio Grande rift in central New Mexico.

East of Rincon Ridge, the Sandia pluton forms the rugged pinkish-colored western face of the Sandia Mountains (Figs. 1.03 and 1.07). Below the range crest, the Sandia pluton and surrounding country rock are nonconformably overlain by light-gray layered strata of upper Paleozoic strata that record deposition in a subtropical sea around 320 Ma. The boundary between these rocks is known as the Great Unconformity, a regionally extensive feature that in the Sandia Mountains represents nearly 1.1 billion years of Earth history missing from the rock record.

Participants will separate into two equal-size groups for two short hikes. The northern hike will examine Paleoproterozoic rocks on Rincon Ridge. The southern hike will look at a downfaulted block of deformed Mesozoic sedimentary strata and overlying Pleistocene alluvium. At about 9:45 AM, the groups will switch leaders and visit the other set of outcrops.

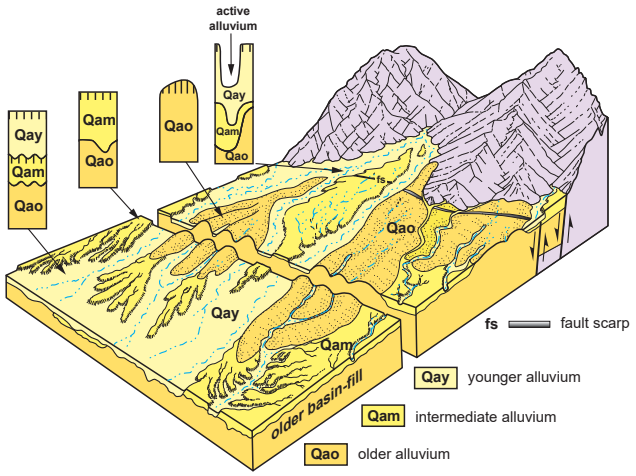



FIGURE 1.05. Morphostratigraphic sketch illustrating relative cross-cutting and soil-morphologic relationships used to differentiate alluvial deposits along piedmonts like the Sandia Mountains (modified from Peterson, 1981). Older piedmont deposits (unit Qao) tend to have rounded slopes with eroded soils and occupy interfluves between adjacent drainages. Intermediate-age units (Qam) tend to have well-preserved constructional tops with moderate soil-morphological development. Youngest units (Qay) occupy arroyos and low broad fans and exhibit weak soil-profile development.

## GEOLOGIC HISTORY

The Sandia Mountains form the uplifted eastern flank of the Albuquerque Basin of the Rio Grande rift (Fig. 1.02).

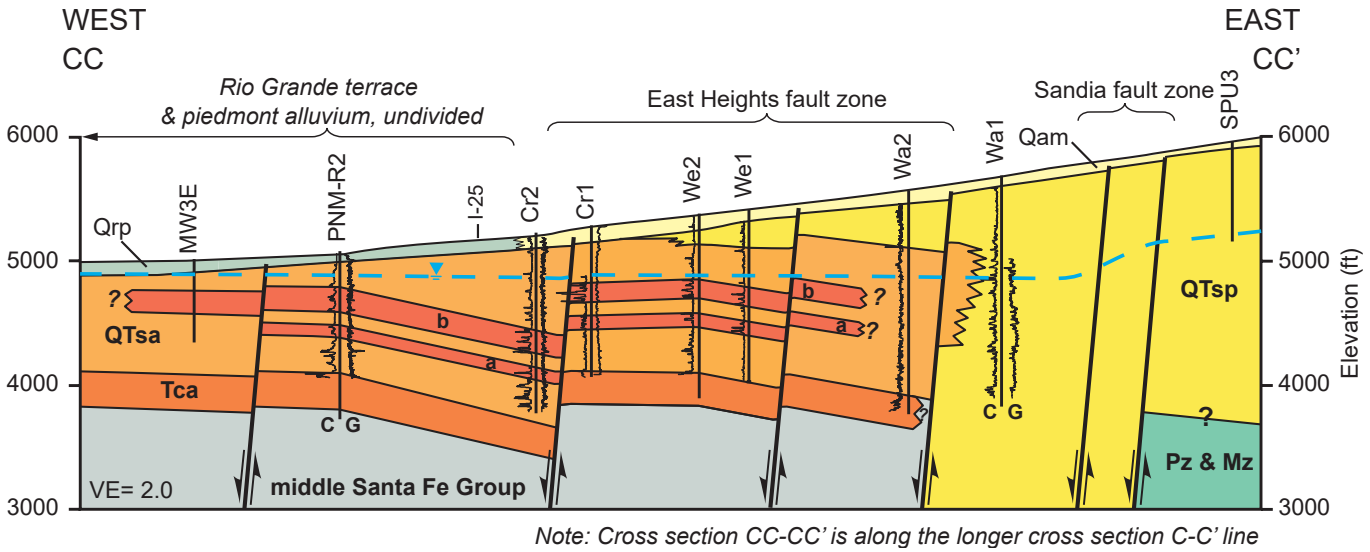



FIGURE 1.06. Geologic section (CC–CC') of the Sandia Mountains piedmont along Paseo del Norte Boulevard (see Fig. 1.01 for location). The geologic cross section is 3 km (2 mi) south of Tramway Boulevard and has been vertically exaggerated by a factor of two to highlight structural and hydrogeologic features across the Sandia Mountains piedmont (Connell, 1997). Municipal water-supply wells draw mostly from sand and gravel of the ancestral Rio Grande (QTsa) and piedmont (QTsp) lithofacies of the Sierra Ladrones Formation. Deposits of the ancestral Rio Grande (QTsa) once flowed within 1.6 km (1 mi) west of the mountain front, between the longitude of Eubank Boulevard and Browning Street NE. Well logs show electrical conductivity (C) and Gamma Ray (G) curves. Two laterally extensive silty sand marker units (a and b) are recognized in boreholes. Blue dashed line denotes water level based on measurements from the 1990s.




FIGURE 1.07. View to northeast of the mouth of Juan Tabo Canyon across Rincon Ridge. The face of Sandia granite forms the "shield" and "knife edge of the shield," which are well-known rock-climbing areas.




FIGURE 1.08. Historic marker honoring Doña Dolores "Lola" Chávez de Armijo.

The range is a basement-cored, east-dipping range capped by Pennsylvanian strata and characterized by a steep west-facing escarpment with as much as 1.4 km (0.9 mi) of relief from crest to proximal piedmont.

Major drainages (including Juan Tabo, Domingo Baca, Pino, Bear, Embudo, Embudito, and Tijeras Canyons) gather runoff from the Sandia Mountains and deliver sediment to the basin.

## Crustal Evolution

### Picuris orogeny

The oldest known rocks in the Sandia Mountains are 1.67-Ga metasedimentary and metavolcanic rocks of the Manzano Group (Karlstrom et al., 2004). On the east side of the Sandia Mountains, these rocks include the metarhyolite of the Monte Largo Hills (Timmons, 1995) that likely correlates with the 1.66-Ga Sevilleta metarhyolite in the Manzano Mountains. The schist we will see on the hike is correlated with the interbedded mudstone and sandstone protolith of the Blue Springs Schist (and quartzite). The quartzite on the crest of Rincon Ridge is likely correlative with quartzite of the upper Manzano Group in the Manzano Mountains (Holland et al., 2020). These rocks were deformed during Paleoproterozoic orogenesis and was subsequently intruded by the 1.45-Ga Sandia granite (Kirby et al., 1995).

The Sandia pluton preserves evidence of syntectonic emplacement during the Picuris orogeny. Within the aureole, composite gneissic foliation, partial melt pods, and shear-sense indicators record ductile deformation broadly synchronous with intrusion. The Seven Springs shear zone marks the structurally complex base of the pluton and exhibits top-to-the-northwest kinematics (Karlstrom et al., 1994; Kirby et al., 1995). These relations demonstrate that Mesoproterozoic magmatism, metamorphism, and deformation were intimately linked and reflect regional crustal tectonism associated with the Picuris orogeny (Daniel et al., 2013).

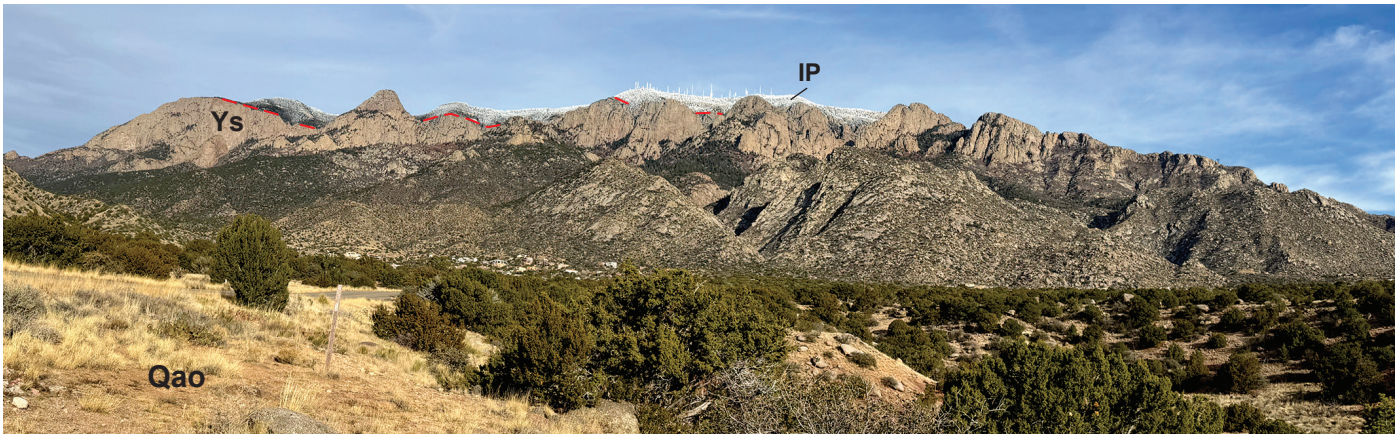



FIGURE 1.09. View of Sandia Mountains from Stop 1. The Sandia granite (Ys) was intruded at 10 km (6 mi) crustal depths at 1.45 Ga. Over the next 1.1 Ga, approximately 5 km (3.1 mi) of overlying rocks were eroded to the surface by 320 Ma to form the Great Unconformity, approximately marked by the red dashed line on this photograph.

### Ancestral Rocky Mountains orogeny

The Ancestral Rocky Mountains (ARM) orogeny represents a late Paleozoic episode of intracratonic, basement-involved deformation that reorganized the tectonic and depositional architecture of New Mexico. Initiation of ARM tectonism was broadly coeval with assembly of Pangea and progressive intercontinental deformation due to far-field stresses several distant plate margins (Kluth and Coney, 1981; Dickinson and Lawton, 2003; Leary et al., 2017). A detailed discussion of the ARM is presented at Stop 2.

### Laramide orogeny

During latest Cretaceous and Paleogene (Campanian–Eocene) time the western interior of North America became a structurally segmented foreland with basement-cored uplifts separated by intermontane basins due to compressional deformation associated with the Laramide orogeny. Laramide deformation in the Sandia Mountains is attributed to the presence of high-angle reverse faults in the Sandia Mountains and along the northwestern margin of the map area. These include the East and West Las Huertas and Cañoncito fault zones (Karlstrom et al., 1994, 2000).

Because the Sandia Mountains are one of tallest footwall uplifts of the Rio Grande rift and exhibit a significant extensional history, evidence for earlier faulting likely has been obscured by fault reactivation during Rio Grande rift extension. Karlstrom et al. (1999) described a "reverse-bend" on extensional faults on the back side of the Sandia Mountains that suggest structural inversion of Laramide faults; however, magnitudes of earlier contractional displacement are not well known. To the south in the Manzano Mountains, the Montosa fault is an east-verging, high-angle reverse fault with Paleogene displacement (~45 Ma) based on thermochronology (Ricketts et al., 2015). These styles of range-front geometries relative to the Great Plains to the east are broadly similar to the Front Range in northern New Mexico and Colorado, but with lower displacement or stronger structural inversion. Subsequent Neogene extension reactivated and overprinted many Laramide structures, complicating estimates of contractional displacement magnitude (Ricketts et al., 2015; Karlstrom et al., 2026).

By projecting the ridge crest of the rift-flanking uplifts on the eastern side of the Albuquerque Basin and using a geophysical model of the base of the synrift Santa Fe Group basin fill, we can see a relationship between the magnitude of rift-flank uplift and the basin depocenter (Fig. 1.10). Figure 1.12 shows the south-trending projection of range crests (solid black line) of the Sandia, Manzano, and Los Pinos Mountains. The black dashed line denotes the base of the Santa Fe Group (Grauch and Connell, 2013) showing that the highest elevation areas corresponds to the deeper parts of the basin. The overall "bow-shaped" geometry from Placitas to Tijeras, with maximum elevation corresponding to maximum throw, is a common feature of normal faults and highlights how fault segmentation influences seismicity in fault systems.

Questions remain as to the origin of a prominent midlevel bench on the Sandia Mountains (Figs. 1.12 and 1.13). In detail, the bench consists of smaller steps that in aggregate define a prominent feature in the mountain front that lies at the base of the cliffs beneath the crest line. Is it an uplifted erosional remnant marking a pause in uplift or is it defined by a complicated systems of faults, similar to the Knife Edge fault?

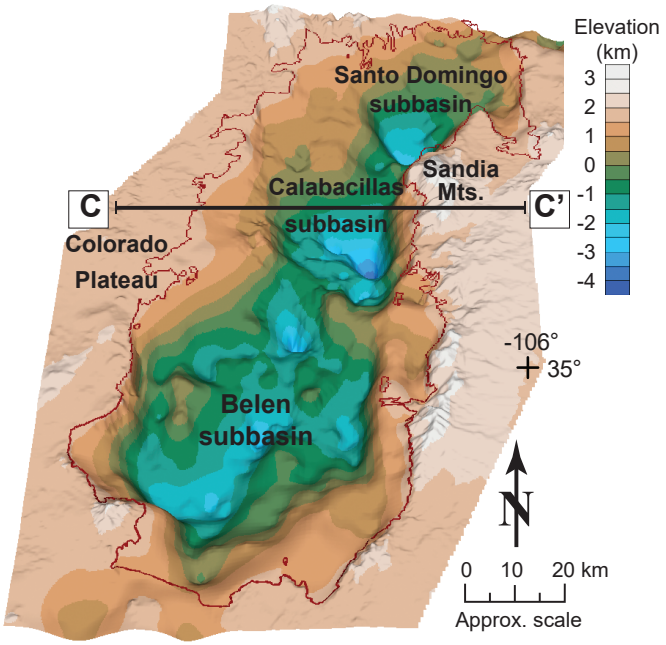



FIGURE 1.10. Geophysical model of the Albuquerque Basin, illustrating the base of Cenozoic Santa Fe Group synrift basin fill and major structural features (modified from Grauch and Connell, 2013). Based on gravity, magnetic, seismic, and deep borehole data, the basin is subdivided into three distinct subbasins. They are, from south to north, the Belen, Calabacillas, and Santo Domingo subbasins. The location of a cross section and block diagram across the Albuquerque Basin is shown by the C–C' line on Figure 1.11.

## STRUCTURAL FRAMEWORK

The Sandia Mountains exemplify the complex interplay of tectonic forces shaping the Albuquerque Basin, as shown by its basement-cored uplift and associated geomorphic features. The Sandia Mountains form a roughly 25-km (16-mi)-long basement-cored uplift that defines the eastern structural margin of the Albuquerque Basin. They are an east-dipping, basement-cored uplift capped by Pennsylvanian strata, with a steep west-facing escarpment and 1.4 km (0.9 mi) of topographic relief from crest to piedmont. Rincon Ridge is a secondary divide west of the crest with 1 km (0.6 mi) of relief. Major drainages, such as Tijeras Canyon, Juan Tabo, and Las Huertas Creeks enter the basin through structural segment boundaries.

The Sandia Mountains represent the uplifted eastern rift flank of the Albuquerque Basin and owe their present relief primarily to Neogene extensional faulting and footwall rebound (Kelley and Northrop, 1975; Kelley, 1977 and 1979; Woodward, 1977; Kelley et al., 1992; Roy et al., 1999; Grauch and Connell, 2013; Ricketts et al., 2015). Thermochronologic data indicate rapid cooling of the Sandia block at ~20–17 Ma, slowing by 16–14 Ma, and continuing to present (House et

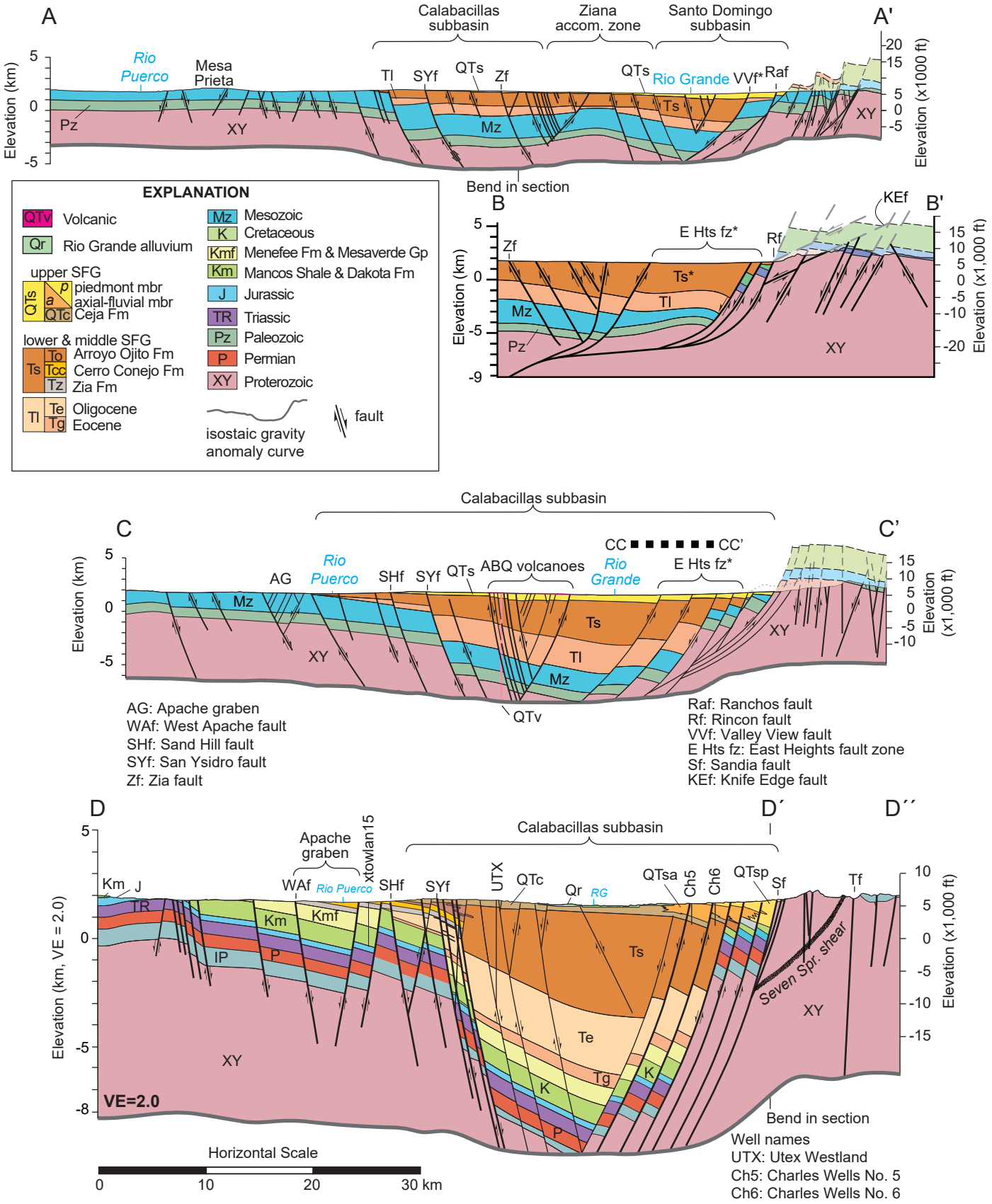



FIGURE 1.11. Geologic cross section across Rincon Ridge and the Sandia Mountains, from the northern flank of the Sandia Mountains (A–A'), across Rincon Ridge (B–B'), along Paseo del Norte Boulevard (C–C'), and between Menaul and Lomas Boulevards (D–D'). The asterisk on labeled faults denotes the approximate location of the Rio Grande fault of Russell and Snelson (1994). Cross sections A–A', C–C', and D–D' are modified from Connell (2008a, 2011). Cross section B–B' is from Ricketts et al. (2015).

al., 2003; Ricketts et al., 2016). Since Miocene time, approximately 3–5 km (9,800–16,000 ft) of Santa Fe Group strata accumulated in adjacent subbasins, particularly the Calabacillas subbasin, recording synrift subsidence and the progressive eastward tilting of basin fill (Grauch and Connell, 2013). Cross sections illustrate systematic thickening of Santa Fe Group strata toward the basin axis and the eastern structural margin (Figs. 1.02 and 1.11).

Structural interpretations of the Albuquerque Basin have evolved from early master-fault concepts (e.g., Bjorklund and Maxwell, 1961) to models emphasizing distributed, segmented normal faulting (e.g., Kelley and Northrop, 1975; Russell and Snelson, 1990, 1994; Grauch and Connell, 2013; Ricketts et al., 2015). Three principal geometries have been proposed (1) listric normal faults that flatten with depth and promote hanging-wall rotation; (2) dominantly high-angle, basement-involved normal faults defining steep half grabens; and (3) low-angle normal faults typical of highly extended terranes

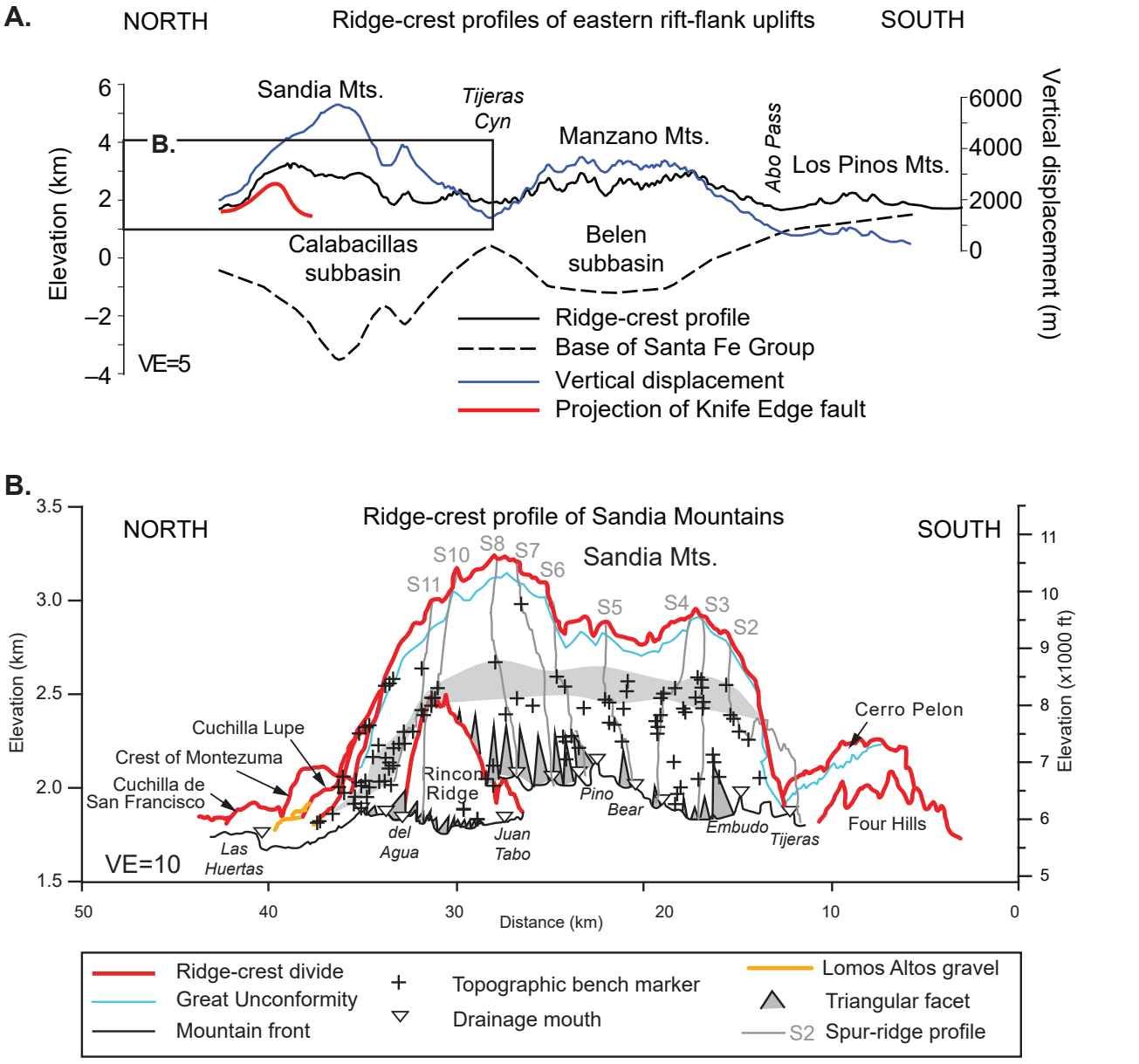



FIGURE 1.12. A (upper panel): South-trending projection of range crests (solid black line) of the Sandia, Manzano, and Los Pinos Mountains. Black dashed line marks the projected base of the synrift Santa Fe Group (Grauch and Connell, 2013) showing that highest elevation corresponds to deeper parts of the Albuquerque Basin. The Knife Edge fault is shown by the red line. Variations in overall vertical displacement (throw) along rift-bounding faults (blue line) is estimated by subtracting the base of Santa Fe Group from topographic profile (from Ricketts et al., 2015). Large canyons occupy the locations of major fault segment boundaries. The overall "bow-shaped" geometry from Placitas to Tijeras, with maximum elevation corresponding to maximum throw, is a common feature of normal faults and highlights how fault segmentation influences seismicity in fault systems. B (lower panel): Ridge-crest projection of Rincon Ridge and the Sandia crest line (modified from Connell, 1996), showing the structurally segmented character of the mountain front, including north-trending structural reentrants at the northern flank of the range. Gray lines (S10–S11) and crosses depict benches along west-trending spur ridges that are shown on Figure 1.13. The similarity in shape of Rincon Ridge and crest of the Sandia Mountains suggests that much of the present range-front relief was generated by faults along and west of the present mountain front.

(Wernicke and Axen, 1998; Axen, 2004). Modern rift models emphasize linkage of discrete fault segments and reactivation of inherited crustal weaknesses during progressive extension (Abbey and Niemi, 2020; Kolawole et al., 2021; Brune et al., 2023; Li et al., 2008, 2026).

Russell and Snelson (1990, 1994) interpreted seismic-reflection data to define a north-trending listric Rio Grande fault near the basin axis (Fig. 1.11). In their model, the Sandia Mountains form the footwall of a steep west-dipping master fault, and the basin is partitioned into oppositely tilted half grabens separated by a southwest-trending transfer zone. This interpretation became a widely cited archetype of segmented continental rifts (Grauch and Connell, 2013).

Subsequent integration of gravity, seismic, well, and geologic mapping data favors a distributed eastern margin fault zone rather than a single throughgoing axial structure (Figs. 1.11A, 1.11C, and 1.11D). Isostatic residual gravity data show pronounced minima along the eastern basin margin, consistent with thick accumulations of low-density synrift fill adjacent to the margin (Cordell, 1979; Grauch et al., 1999). Three-dimensional gravity inversion modeling delineates the Santo Domingo, Calabacillas, and Belen subbasins, each characterized by steep eastern structural gradients and predominant eastward tilting (Figs. 1.10 and 1.11; Grauch and Connell, 2013). A northwesterly trending antiform separates the Belen and Calabacillas subbasins, rather than a scissor-like transfer zone proposed by Russell and Snelson (1994)

Correlation of borehole geophysical logs and lithologic data from municipal wells demonstrates progressive northeastward thickening and tilting of Plio–Pleistocene basin fill that is not significantly offset across the projected trace of the Rio Grande fault, which projects along the western strands of the East Heights fault zone (Figs. 1.10, 1.11A, 1.11C, and 1.11D; Grauch and Connell, 2013). Seismic-reflection profiles similarly illustrate progressive eastward tilting without evidence for large displacement along a single basin-axis fault. Reexamination of industry seismic lines (Russell and Snelson, 1994) suggests that some reflections previously attributed to axial

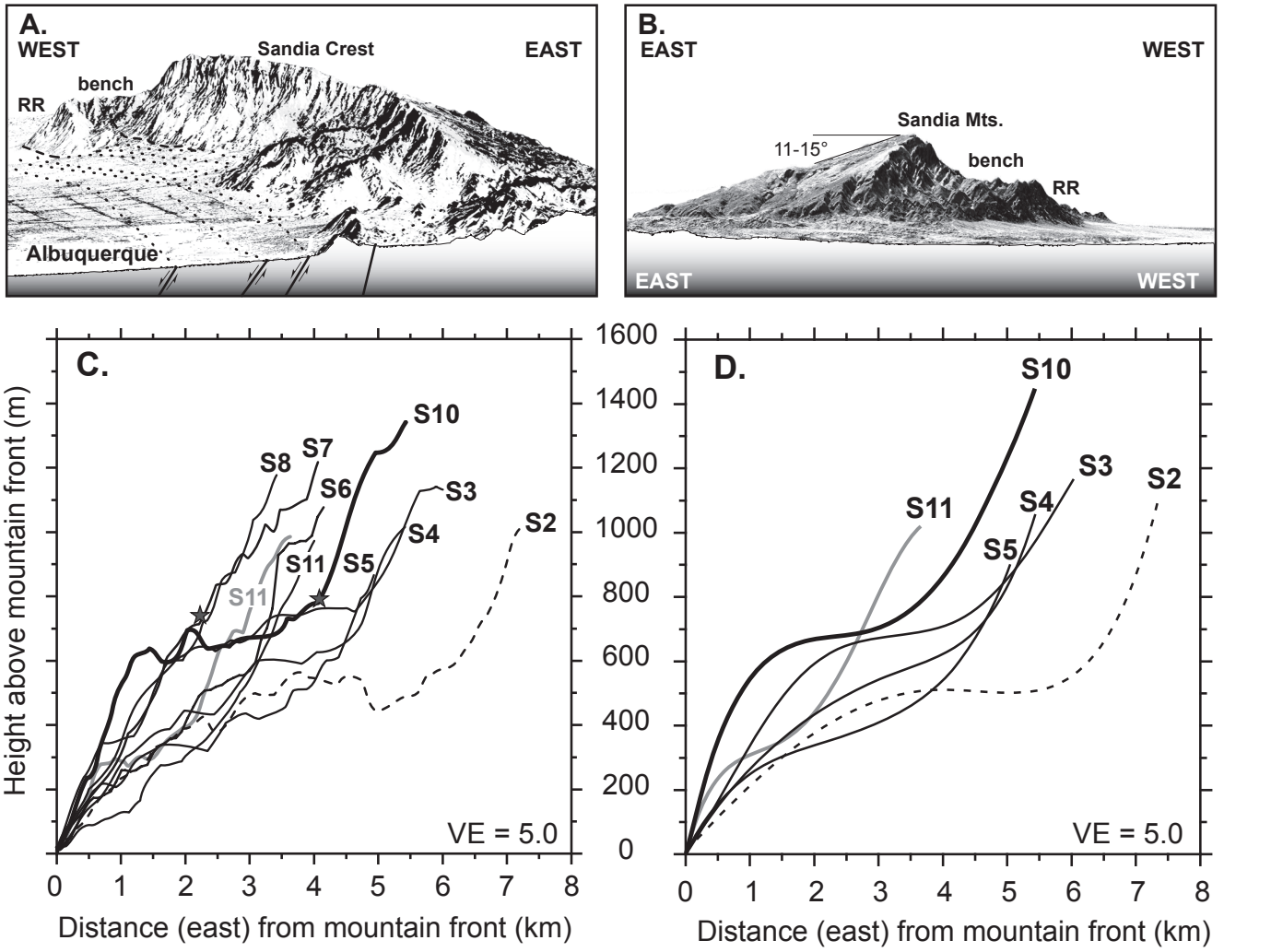



FIGURE 1.13. Geomorphology of the western face of the Sandia Mountains. A and B: Diagrams of the Sandia Mountains viewed from the southwest and north, respectively, showing a prominent topographic bench on the Sandia Mountains. C and D: Spur-ridge profiles illustrating this bench, from south (S1) to north (S11). See Figure 1.12 for locations of profiles. The gray star denotes the approximate location of the Knife Edge fault. Faceted spur ridges are common at the base of spur-ridge profiles. Smoothed spur-ridge profiles highlight the bench (smoothed using polynomial best-fit lines, $4<n<5$).

fault thickening may instead reflect pre-Santa Fe Group structure, early synrift stratigraphy, or velocity-model uncertainties (Russell and Snelson, 1994). Collectively, these observations diminish the requirement for a continuous Rio Grande master fault beneath the Rio Grande valley (Grauch and Connell, 2013).

Steep structural gradients along the eastern margin mark abrupt transitions from 3–5 km (9,800–16,000 ft) of Santa Fe Group fill to less than 1 km (0.6 mi) across narrow zones, consistent with 2–4 km (6,500–13,000 ft) of vertical separation accommodated by segmented basement-involved normal faults. Modeled basin-floor slopes correspond to observed bedding attitudes and syntectonic growth geometries within the Santa Fe Group (e.g., Connell, 2004). Apparent shallow dips on some seismic profiles can result from oblique line orientation, underscoring the importance of geometric corrections when evaluating fault dip.

Low-angle normal faults have been proposed locally along the Sandia and Ladron margins (Ricketts et al., 2015). In the Sandia Mountains, the west-dipping (~40°) Knife Edge fault is expressed by cataclastic vein networks in Proterozoic granite and may represent a rotated rift-margin structure (Fig. 1.14). The Knife Edge fault is recognized by a network of cataclastic (normal fault) veins, some cemented with calcium carbonate, in the Sandia granite (Fig. 1.12). The Knife Edge fault has a lower dip than those measured for other normal faults in the cross section (Fig. 1.11B), and lower than the approximately 60° surface dip predicted by fault mechanics (Anderson, 1905). This fault forms the east side of the ridge/bench that connects Rincon Ridge to Sandia Crest and suggests that fault dip has shallowed and the rocks in Rincon Ridge have been tilted east by about 20° in the footwall of the present-day mountain-front fault system (e.g., Sandia fault) due to isostatic unloading of the footwall (Ricketts et al., 2015; Karlstrom et al., 2026). Eastward tilting of Paleozoic strata (~15–20°) on the Sandia Mountains dip slope has been attributed to isostatic rebound and block rotation of the footwall during extension (Roy et al., 1999; Ricketts et al., 2015; Karlstrom et al., 2026). Although such structures may reflect rotated high-angle normal faults or localized detachments, they do not necessarily require a regionally extensive shallow-dipping master detachment in the upper crust. Listric geometries may nonetheless develop at midcrustal depths as faults sole into the brittle-ductile transition at depths of 8–10 km (5–6 mi) below the surface of the land (Axen, 2004).

Available geologic and geophysical data indicate that the northern Albuquerque Basin comprises interconnected, predominantly east-tilted subbasins bounded by a segmented eastern margin fault zone (Fig. 1.10). High-angle basement-involved normal faults dominate upper-crustal deformation, while depth-dependent (listric) curvature, block rotation, isostatic rebound, and structural inheritance contribute to the evolving rift architecture. This framework is consistent with progressive Miocene–Pliocene extension expressed through distributed fault systems rather than the displacement localized on a single axial master fault (see Russell and Snelson, 1994).

## GEOMORPHOLOGY

The Sandia Mountains sit within the Mexican Highlands section of the Basin and Range province and form a prominent rift-flank uplift along the eastern margin of the Albuquerque Basin. The basin occupies a transitional position between the narrow, well-expressed northern rift and the broader rift and Basin and Range to the south (e.g., Hawley, 1978; Chapin and Cather, 1990). As in many rift basins, the Albuquerque Basin is one of a series of half-graben basins and subbasins with alternating dip polarity across strain-accommodation zones (e.g.,

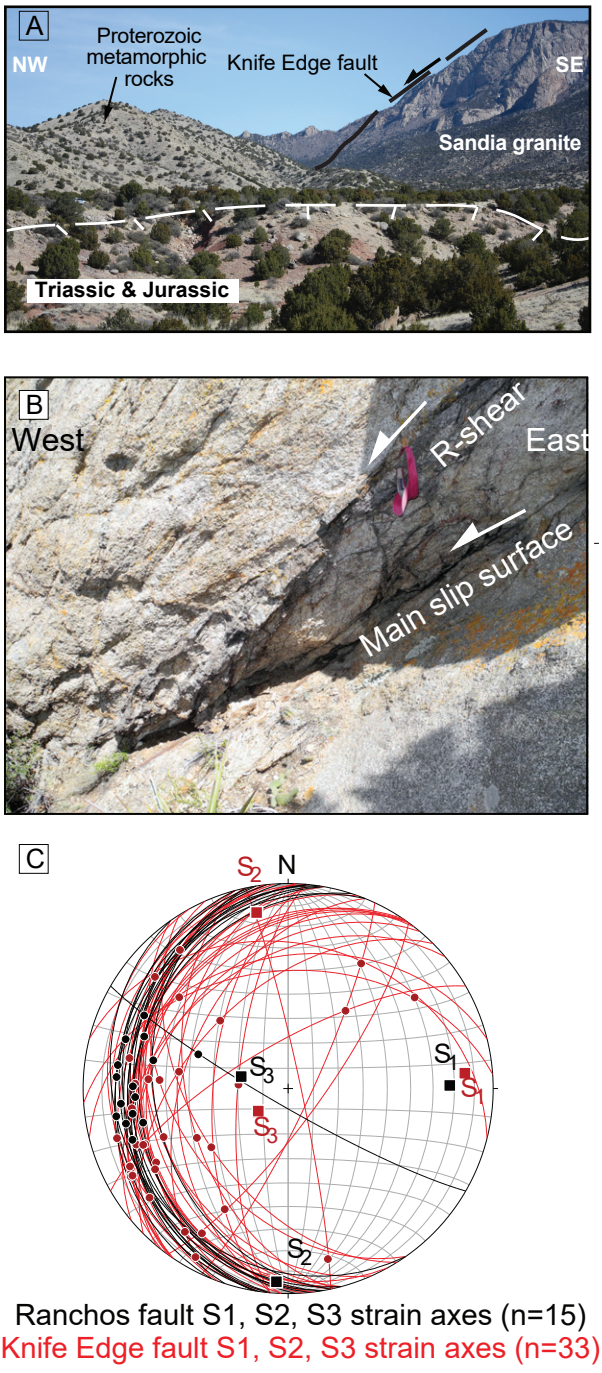



FIGURE 1.14. View to north from Stop 1. A: Precambrian metamorphic rocks. B: Knife Edge fault showing Riedel shears that indicate extensional movement. C: Low-angle fault dip of ~40°.

Chapin and Cather, 1994). Neogene extensional tectonism produced steep bedrock relief and pronounced topographic gradients along the Sandia range front (Figs. 1.13 and 1.15).

Progressive uplift of the Sandia Mountains block and subsidence of the adjacent basin generated a west-sloping piedmont that prograded basinward during the final stages of Santa Fe Group deposition at ~0.8 Ma (Connell et al., 2013). The resulting bajada extends nearly 13 km (8 mi) from the range front toward the Rio Grande and is composed predominantly of arkosic sandy gravel, mostly derived from Sandia granite. Proximal fan facies include boulder-rich debris-flow and sheetflood deposits; medial and distal facies consist of sandy pebble gravel that interfingers basinward with Rio Grande terrace deposits (Connell et al. 2007).

Within an embayment between Bear Canyon and Juan Tabo Creek, granitic bedrock is exposed in arroyo bottoms as much as 1.6 km (1 mi) west of the modern range front. These exposures reflect a shallowly buried pediment surface that is thinly veneered by piedmont deposits. Along the northern and central piedmont, segmentation produces alternating zones of aggradation, fan-head trenching, and partial abandonment of older geomorphic surfaces, and locally juxtaposes older basin-fill packages against younger deposits. Connell (1996) interpreted these patterns to primarily reflect tectonic segmentation and differential uplift rather than lithologic control alone.

## ALLUVIAL STRATIGRAPHY

The Sandia Mountains piedmont comprises coalescent alluvial fans, distributary-channel aprons, and inset arroyo networks that transport sediment from steep bedrock catchments into the Rio Grande valley. Preservation patterns, surface development, and incision are strongly influenced by mountain-front segmentation and early Pleistocene incision along the eastern basin margin. The alluvial stratigraphy of the Sandia Mountains piedmont records repeated episodes of fan construction, stabilization, and incision during Pleistocene time. Piedmont deposits consist of paleosol-bounded alluvial-fan and streamflow successions that interfinger basinward with inset terrace-fill of the Rio Grande valley (Connell and Wells, 1999; Connell et al., 2007). Proximal facies near canyon mouths are characterized by boulder-to-cobble debris-flow and sheetflood deposits, which grade distally into medial gravelly braided-stream facies and distal sandy to silty sheetflood and local over bank deposits. Granite boulders locally exceed 2.5 m (8 ft) in diameter and near-fan apices reach up to 11 m (36 ft) in diameter (Lambert, 1968).

Older (early to middle Pleistocene) deposits form high-standing fan remnants capped by well-developed Stage III–IV calcic soils and are locally faulted. Middle (middle to late Pleistocene) deposits are inset against these older surfaces, exhibit Stage II–III soil development, and grade basinward toward Rio Grande terraces. Younger (late Pleistocene–Holocene) deposits occupy active channels and low-lying fan aprons, show weak soil development, and are locally cut by faults (U.S. Geological Survey, 2024).

## FAULT ACTIVITY

Paleoseismic investigations indicate long-term slip rates ranging from 0.01–0.1 mm/yr (10–100 m/My) and recurrence intervals on the order of $10^4$–$10^5$ years (U.S. Geological Survey, 2024). As a thought experiment (Fig. 1.16), if 1 m (1.6 ft) of vertical displacement occurs per surface-rupturing event with recurrence of $10^3$–$10^4$ years, generation of 11–12 km (7–8 mi) of cumulative structural relief between the Great Unconformity beneath the basin floor and the range crest would require more than 10,000 rupture events. Even assuming larger per-event displacements of 2 m (6 ft) and longer recurrence times (~20 ky), several thousand events would be required to generate observed relief along the range front and hundreds of events along Rincon Ridge.

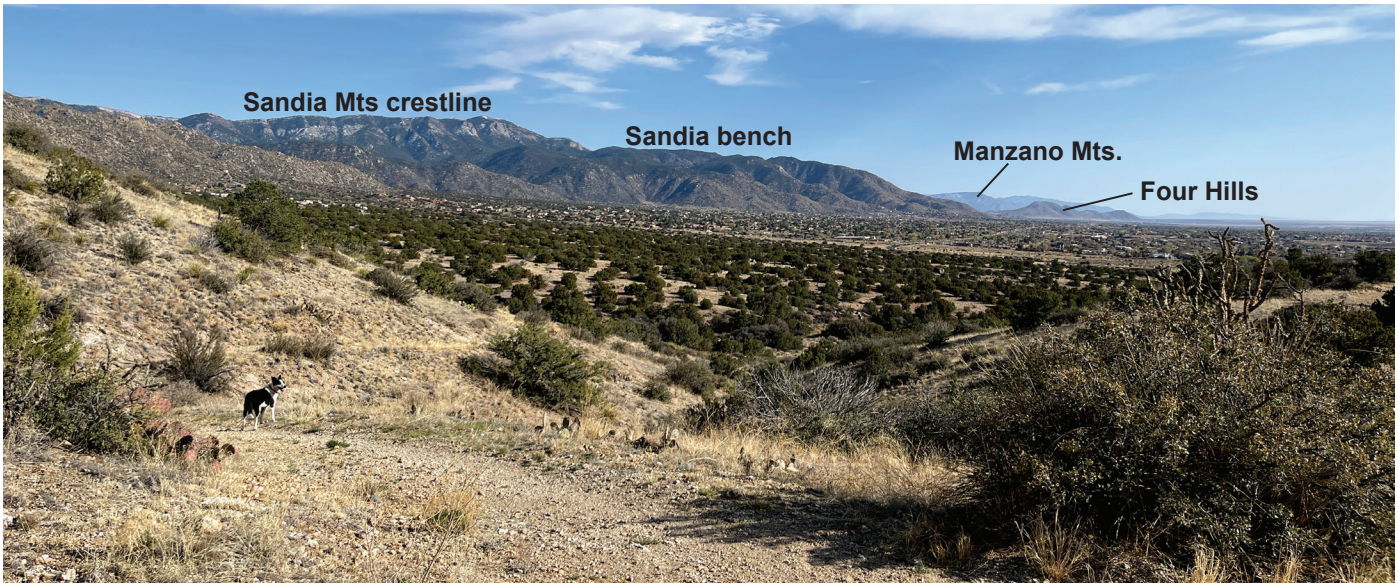



FIGURE 1.15. Panorama of embayment at the foot of the Sandia Mountains. The range front is punctuated by prominent midlevel topographic benches. The southern bench formed on the interfluves between Embudito and Embudo Canyons.

Although such estimates involve substantial simplifications—including the influence of isostatic response and differentiating uplift from exhumation (e.g., England and Molnar, 1990; Molnar and England, 1990)—they underscore the cumulative, incremental nature of rift-margin uplift and provide perspective on the tempo of landscape evolution and seismic-hazard potential along the faulted front of the Sandia Mountains.

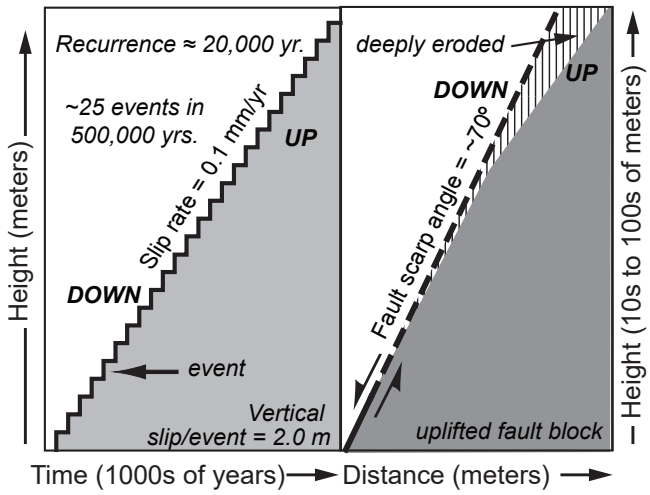



FIGURE 1.16. Thought experiment on how many earthquakes would it take to generate the present relief on Sandia Mountains assuming an average of 2-m (6-ft)-net vertical displacement per event. The left diagram illustrates mountain-front development as the summation of individual fault events of an arbitrary vertical offset. The right diagram envisions the long-term development of the mountain front as the serially faulted face retreats through erosion (eroded area shown by vertical lines).

## Group hikes

Two hikes examine rocks and features that span nearly 1.7 billion years of crustal evolution and landscape development in the Sandia Mountains (Fig. 1.17). The first hike ascends Rincon Ridge to examine Paleoproterozoic (1.68–1.60-Ga) metamorphic rocks of the Mazatzal province that were deformed during the 1.50–1.45-Ga Picuris orogeny and intruded by the 1.45-Ga Sandia granite. At outcrop scale, participants evaluate polyphase ductile fabrics (S0–S2), F2 folding, shear-sense indicators, contact aureole mineral assemblages (andalusite–sillimanite transitions), partial melts, and pegmatites that record syntectonic pluton emplacement and regional transpressive middle-crustal deformation.

The second hike descends into a small valley exposing faulted Triassic Chinle Group and Jurassic strata (Entrada–Morrison succession), where bedding-parallel slip, cross faults, and basin-margin structures illustrate Mesozoic inheritance and Cenozoic Rio Grande rift deformation along and across the Sandia Mountains. If you look east toward Sandia crest, equivalent strata would have been about 2 km (1.25 mi) above the Great Unconformity before they were eroded or faulted down the mountain front since ~20 Ma. The hike culminates on a degraded middle Pleistocene piedmont surface where the group will discuss alluvial stratigraphy, depositional processes, mountain-front geomorphology, and the tectonic and paleoclimatic controls that shaped the modern landscape.

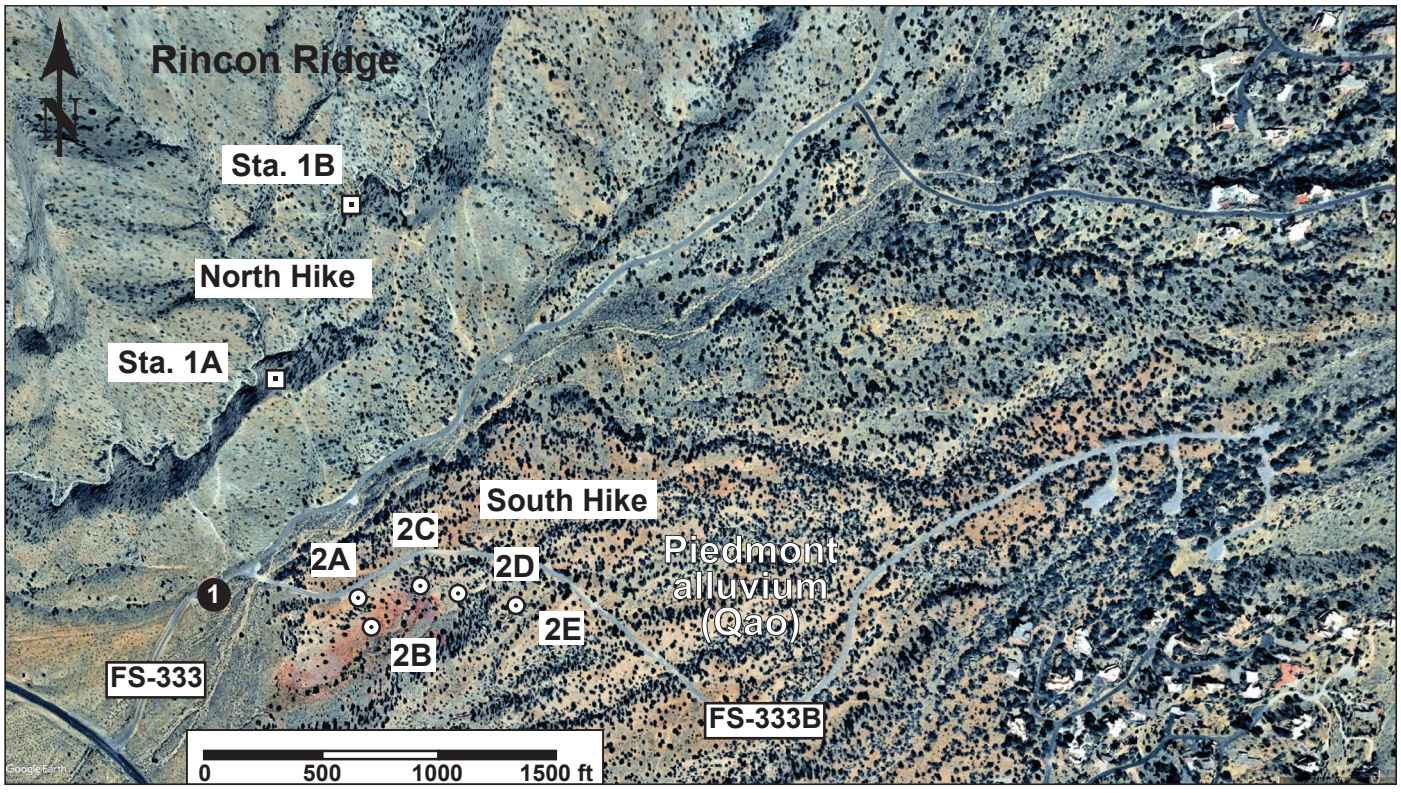



FIGURE 1.17. Aerial image showing station numbers for north (square) and south (circle) hikes (image from Google LLC, 2024). Access southern hike via La Cueva Road (FS 333B).

## NORTHERN HIKE: PROTEROZOIC FEATURES OF RINCON RIDGE

### Introduction

The continental crust and mantle lithosphere of New Mexico's portion of the North American plate formed during the Proterozoic via plate-tectonic addition of magmatic arcs and microcontinental fragments that became accreted to the Archean Wyoming province (Whitmeyer and Karlstrom, 2007). The oldest Paleoproterozoic rocks in northern New Mexico are part of the 1.75-Ga Yavapai province (Karlstrom et al., 2004; Hillenbrand et al., 2023, 2025). Most of New Mexico south of the Sangre de Cristo Mountains is underlain by 1.68–1.60-Ma rocks of the Mazatzal province (Karlstrom et al., 2004; Amato et al., 2008). Karlstrom and Keller (2005) proposed a northeast-trending deep crustal suture between the Yavapai and Mazatzal provinces located beneath the modern Jemez lineament (Magnani et al., 2004, 2005). Rocks of both provinces were deformed again between 1.50–1.45 Ga during the Picuris orogeny (Daniel et al., 2013). Thus, the basement rocks now exposed in numerous Cenozoic uplifts were deformed at middle crustal depths during multiple Proterozoic orogenic events (Hillenbrand et al., 2025). These rocks were exhumed during several Phanerozoic uplift and erosion intervals (Heizler et al., 2026; Karlstrom et al., 2026).

We are in an area where the 1.68–1.60-Ga rocks of the Mazatzal province underwent deformation during the 1.50–1.45 Ga Picuris orogeny and then were intruded by 1.45-Ga Sandia granite (Kirby et al. 1995). This pluton is one of a regionally important suite of ~1.4-Ga granites that intruded previously accreted basement provinces across the Southwest, from Wyoming to Mexico and along orogenic strike from southeastern California (Mojave province) to Labrador. The granites have a distinctive A-type chemistry and were previously thought of as anorogenic because they are generally less deformed than their country rock. However, Nyman et al. (1994), Kirby et al. (1995), and Shaw et al. (2005) observed deformed margins, aureoles, and shear zones that put them into an orogenic context. Their A-type ferroan and anhydrous character was interpreted by Frost et al. (2001) to result from anatectic melting of lower continental crust caused by basaltic underplating, rather than in subduction-related magmatic arcs. These plutons commonly contain mafic enclaves and magma-mingling textures where gabbro and diorite melts encountered granitic ones as we can observe on the southern hike. The interactions of magmatic, metamorphic, and deformation processes (Arnoff et al., 2016; Hillenbrand et al., 2025) will be discussed on the outcrops.

We hike up the southern spur of Rincon Ridge (Figs. 1.17 and 1.18) to examine highly deformed quartz-biotite schist and quartzite that have been called the Juan Tabo metamorphic rocks (Berkley and Callendar, 1979; Vernon, 1987). Rincon Ridge was mapped by Chris Andronicus, a member of Sandia Pueblo, with University of New Mexico professors Jeff Grambling and Karl Karlstrom. The results of this mapping were incorporated into the compilations of Connell et al. (1995) and Connell (2008a).

The oldest rocks on Rincon Ridge are 1.68–1.60-Ga rocks of the Juan Tabo metamorphic complex based on correlation with the Manzano Group (Holland et al., 2020). The inferred protolith was interbedded sandstone and mudstone. The Sandia pluton that intruded country rock about 10 km (6 mi) deep based on the metamorphic mineral phases observed in the pluton's aureole (Fig. 1.18). Early andalusite away from the pluton is replaced by sillimanite (Vernon, 1987, Connell et al., 1995) and sillimanite–potassium-feldspar assemblages occur with partial melting close to the pluton. The geometry of isograds in the aureole is reminiscent of contact metamorphism, but the polyphase ductile fabrics seen in the aureole record regional deformation. This led Vernon (1987) to introduce a combined term, regional contact metamorphism, for thermal softening from pluton intrusion in a large middle crustal zone that allowed regional deformation to be recorded.

Four metamorphic fabrics are seen here and illustrated on Figure 1.19. S0 is the original bedding of the protolith and is identified compositional layering. S1 is the oldest observed tectonic fabric and is a bedding-parallel foliation defined by the alignment of metamorphic minerals (i.e., mica alignments). S2 is the axial plane of F2 folds that fold both S0 and S1 fabrics. S2 represents a composite fabric of fold and flow alignments in a composite gneiss with an average northeast orientation. Closer to the pluton, this composite fabric contains partial melt pods (Fig. 1.19B). Shear sense is locally preserved (Fig. 1.19C) and the partial melts, pegmatites, and plastic flow in the aureole during D2 deformation (noted below) are all interpreted to have been broadly synchronous with pluton intrusion.

Two deformational events are recognized (D1 and D2). Near the pluton, D2 has transposed earlier fabrics. In areas away from the inner aureole, the earlier D1 event is recognized, where S1 fabrics are correlative with deformation associated with the 1.65–1.60-Ga Mazatzal orogeny as recorded by monazite dating (Karlstrom et al., 2016) and observed in syntectonic 1.65-Ga plutons (Brown et al., 1999) in thrust-sense, top-north shear zones in the Manzanita and Manzano Mountains to the south.

The main (D2) ductile deformation near the aureole immediately preceded final crystallization of the 1.45-Ga Sandia granite. The cooling pluton supplied heat to form syntectonic partial melts, but there is sparse to no evidence for ductile deformational fabrics across much of the pluton. This may also be due to temperatures above their critical melting fraction, where flowing magma does not record solid-state fabrics. Thus, deformation in the proximal pluton aureole is attributed to the 1.5–1.45-Ga Picuris orogeny (Daniel et al., 2013) that involved top-to-the-north thrusting in the Manzano thrust belt. The Sandia pluton itself was emplaced during northwest-directed transpressive deformation (Kirby et al. 1995). Tabular, subvertical, relatively late-stage pegmatites are interpreted to have formed at 1.45 or 1.43 Ga (Heizler et al., 2026) and are compatible with a northwest–southeast transpressive strain regime that was generated from a distant convergent plate boundary in Texas (Karlstrom and Humphreys, 1998). This 1.5-Ga plate boundary, inferred using neodymium (Nd) and hafnium (Hf) isotopic data, identifies 1.5-Ga crust of the more southerly

Shawnee province (Bickford et al., 2015; Hillenbrand et al., 2023) and its convergence with the 1.68–1.60-Ga crust of the Mazatzal province. Stresses propagated far into previously accreted provinces of southwestern Laurentia illustrate the widespread but heterogeneous Picuris orogeny deformation and metamorphism (Shaw et al., 2005) and the development of a proposed Picuris orogenic plateau (Hillenbrand et al., 2025). This convergence, for example in conjunction with flat-slab subduction, is invoked to have driven widespread lithospheric delamination in areas all the way to the Wyoming province to

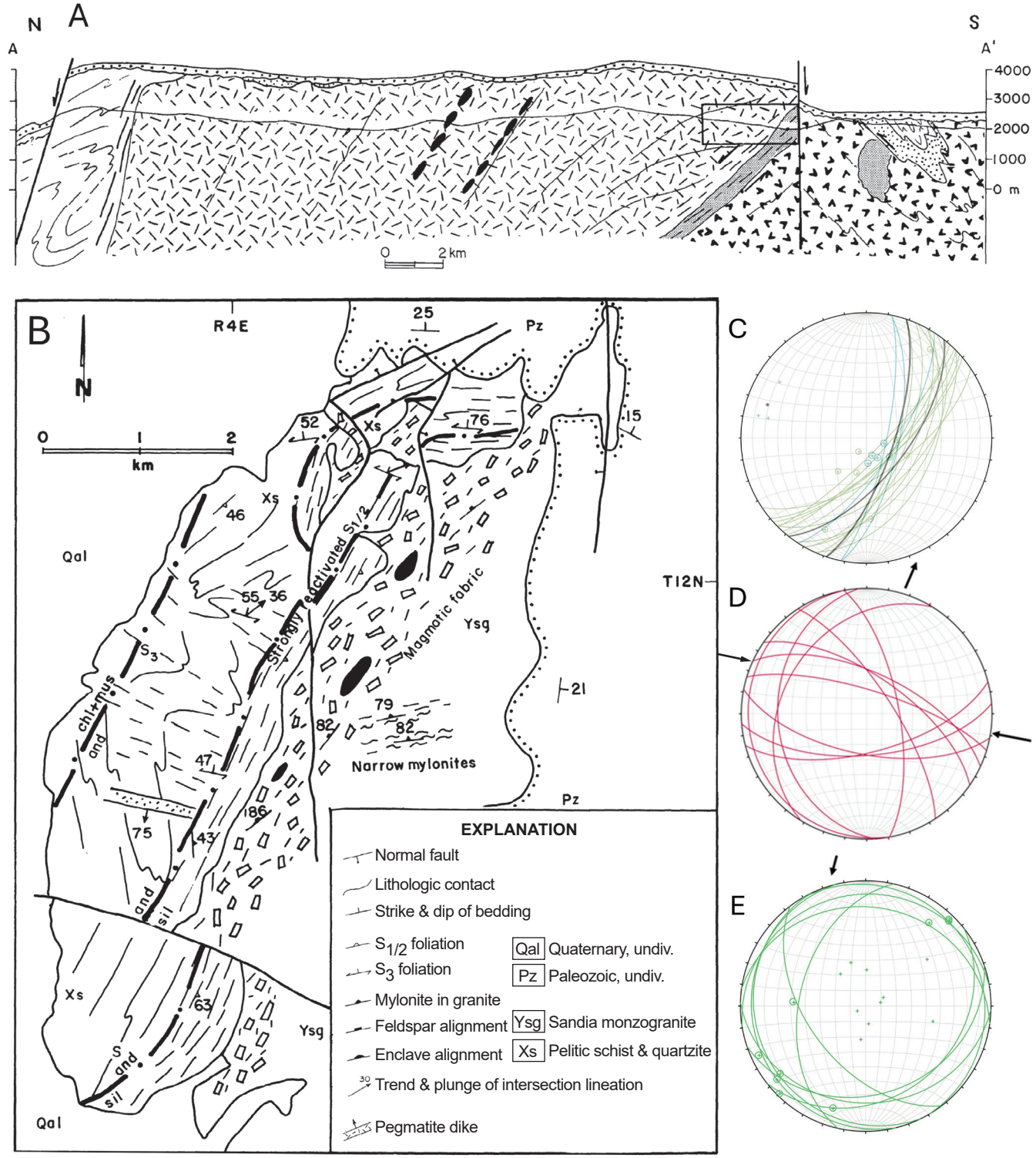



FIGURE 1.18. A: North–south cross section of Sandia pluton from Kirby et al. (1995). B: Detail of northern aureole of Sandia pluton (Kirby et al., 1995). C–E: Stereonets of metamorphic facies. C: S2 composite foliation and F2 hinge lines from Station 2A and 2B. D: 1.43-Ga pegmatite dikes from Juan Tabo Road showing conjugates and paleostress directions. E: Epidote-coated fault planes and slickenlines from station 1A and 1B show northeast–southwest subhorizontal slip on younger (likely Neogene) fault planes.

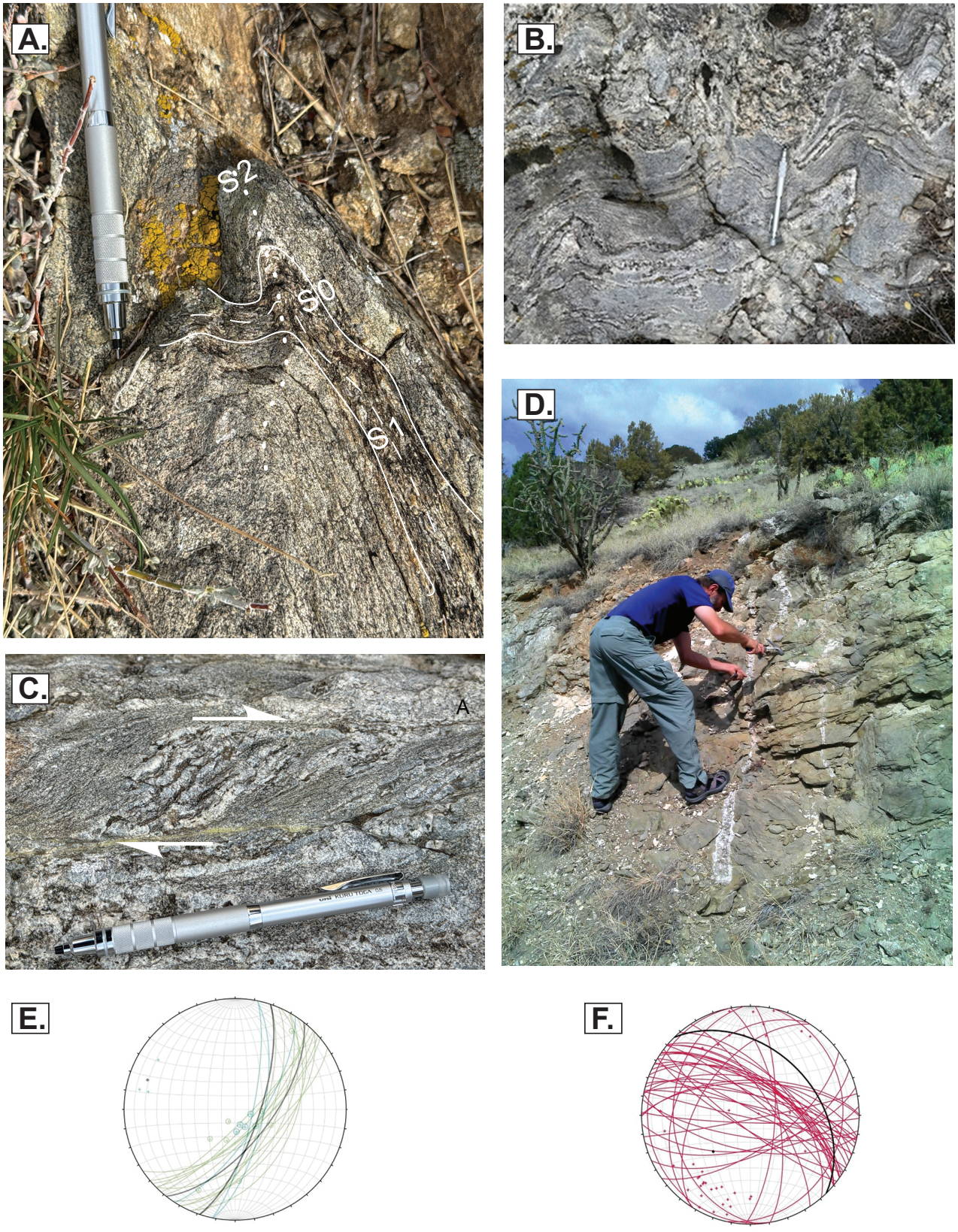



FIGURE 1.19. Basement features of Juan Tabo metavolcanic rocks. A: Three planar fabrics (surfaces): bedding (S0); first tectonic alignment of metamorphic minerals (S1); and axial plane of F2 fold of S0 and S1 (S3). B: Partial melt pods (leucosomes) indicate rocks were deforming (flowing) at partial melting temperatures in excess of 600°C. C: Right-lateral strike slip S-C fabrics with leucosome filling the sigmoidal S-planes and C-planes (shear planes) parallel to the dominant S2 foliation (040°/60° SE). D: Tabular pegmatite dikes strike NW and crosscut all fabrics in Juan Tabo schists indicating ductile deformation occurred prior to 1.73 Ga. Matt Heizler sampling a pegmatite for $^{40}Ar/^{39}Ar$ dating just up the road from La Cueva Trailhead (Heizler et al., 2026). E: Foliation and lineation from stations 1A and 1B of the northern hike. F: Crosscutting pegmatites from along the road to Juan Tabo Canyon include conjugates and a dominant set of northwest-striking tabular dikes.

explain the presence of 1.45-Ga A-type granites.

In this interpretation, Picuris-orogeny deformation overprinted earlier fabrics. In areas where this deformation occurred at high enough grade to cause widespread middle crustal flow, such as the near aureole of the Sandia Mountains and in the Picuris Mountains to the north, earlier fabric elements can be mostly or entirely transposed into 1.50–1.45-Ga deformational fabrics and are difficult to recognize. However, detailed petrochronology on zoned monazite and other syntectonic metamorphic minerals can be used to interpret intense later deformational events (Karlstrom et al., 2016; Hillenbrand et al., 2025).

## Northern Hike

### Waypoint 1.03 [N 35.2055°, W106.5021°]

#### Station 1A

Station 1A is at the high point of the ridge (Fig. 1.17). We will observe outcrop-scale features to identify the relative ages of several fabrics and folds. An important concept in structural geology is "Pumpelley's rule," which states that small-scale structures mimic the style and orientation of larger scale structures so that even small outcrops can serve as "Rosetta stones" for deciphering polyphase regional deformation. See if you can

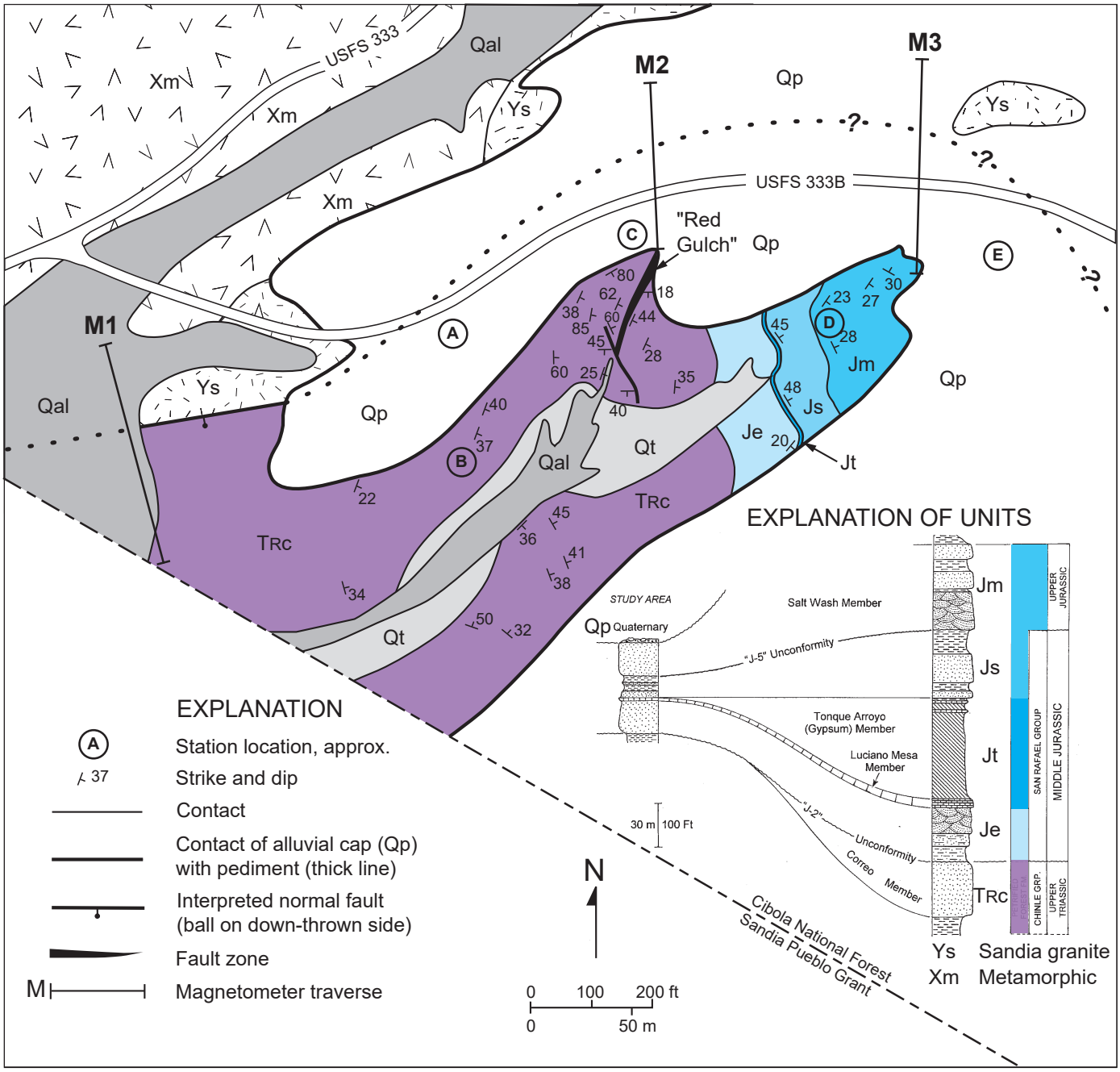



FIGURE 1.20. Geologic map of the Mesozoic inlier, Juan Tabo area (Van Hart, 1999). The boundary between Proterozoic and Mesozoic rocks was mapped using the results of ground-based magnetic-susceptibility surveys (M1–M3) described in Van Hart (1999).

identify relic bedding (S0), alignment of metamorphic minerals subparallel to bedding (S1), and folds of the composite S0/S1 foliation. In most outcrops the average orientation of the main fabric is 040°/60° SE, which is the orientation of composite S0/S1/S2 foliations interpreted to have formed due to heating in the pluton aureole just before final crystallization of the megacrystic unit of the Sandia pluton.

The tabular pegmatite dikes and fine-grained granites that crosscut schist and gneiss are not deformed, so ductile aureole deformation ended before their emplacement at 1.43 Ga (age from Heizler et al., 2026).

**Waypoint 1.04 [N35.2080°, W106.5011°]**

### Station 1B

Station 1B is in a sandy and rocky wash down the hill and to the north (Fig. 1.17). These outcrops illustrate rocks that were flowing at partial melt grade (>600°C) in the inner aureole of the Sandia pluton. Some things to observe and discuss include whether the main foliation is subperpendicular to main shortening direction (which it generally is), evidence for direction of flow parallel to foliation (called "general shear"), indications that partial melts preferentially developed or flowed through in certain compositional layers, evidence whether melt pods are in the places they accumulated or were "fluxed" through the outcrop area (i.e., the migmatite problem), and evidence for the direction(s) of extension based on boudinage of partial melt pods (leucosomes). In this case, both steep and subhorizontal extension can be seen within foliation plane as can happen by applying a flattening strain with a pancake-shaped strain ellipse.

## SOUTHERN HIKE: MESOZOIC FAULT BLOCK AND MOUNTAIN-FRONT GEOMORPHOLOGY

### Introduction

For the southern hike, we will descend into a small valley to visit an inlier of Triassic and Jurassic sedimentary rocks and discuss Cenozoic rift deformation of the Sandia Mountains and Albuquerque Basin (Fig. 1.17). This inlier was studied extensively by Van Hart (1999) and is summarized in a field guide to the Sandia Mountains by Van Hart (2023). We will then hike to the partially eroded surface of a middle Pleistocene alluvial deposit and discuss piedmont stratigraphy and the tectonic geomorphology of the Sandia Mountains. We will also observe meter-scale boulders and, in them, we can examine primary and secondary textures of the Sandia granite. Van Hart's (1999) detailed mapping and analysis of the Triassic and Jurassic strata here were based on comparison to the same stratigraphic units that are more completely preserved and better exposed near Placitas and in the adjacent Hagan embayment on the northeastern flank of the Sandia Mountains (Fig. 1.20 and Stop 4).

### Southern Hike

**Waypoint 1.05 [N35.2026°, W106.5013°]**

### Station 2A

From the parking area at Stop 1 (Fig. 1.17), walk along FS 333B to a small dirt parking area on right side of the paved road.

**Waypoint 1.06 [N35.2021°, W106.5012°]**

### Station 2B

Pale reddish-brown sandstone and pebbly sandstone assigned to the Upper Triassic Chinle Group (Fig. 1.21).

**Waypoint 1.07 [N35.2027°, W106.5003°]**

### Station 2C

This station will be difficult for us all to see at once, so we will temporarily separate into smaller groups to visit this exposure of faulted Chinle Group sandstone and mudstone (Fig. 1.20). Many of the faults are subparallel to the east–southeast-dipping bedding with slickenlines generally downdip, with a southerly rake, compatible with the bedding plane slip as strata adjusted to large-scale normal fault displacement. Northwest-striking cross faults have a similar trend to the faults that define the eastern margin of the Albuquerque Basin (Fig. 1.22) and may be related to the Sandia and La Cueva fault zones of Kelley and Northrop (1975).

A pediment is an extensive erosion surface overlain by a veneer of alluvium. As mentioned previously, much of the upper piedmont along the foot of the Sandia Mountains, west of Tramway Boulevard, forms a pediment, as illustrated by local outcrops of granite exposed in arroyo bottoms. This pediment surface has several meters of relief.

**Waypoint 1.08 [N35.2026°, W106.4994°]**

### Station 2D

Pale yellowish-brown fine-grained deformed sandstone assigned to the Jurassic Morrison Formation (Fig. 1.23). Look for exposures of the gypsiferous Todilto Formation on hillslopes. These are challenging to locate due to poor

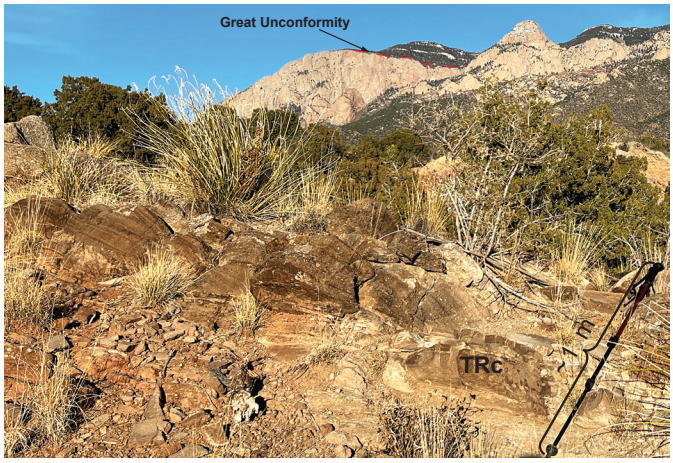



FIGURE 1.21. Triassic sandstone at Station 2B. The walking stick is approximately 1 m (3.2 ft) long.

exposures. Hike uphill to gravelly alluvium with scattered granitic boulders.

**Waypoint 1.09 [N35.2025°, W106.4985°]**

### Station 2E

We are standing on an erosional degraded constructional surface of middle Pleistocene piedmont alluvium derived from the Sandia Mountains. Look for subrounded and rounded pebbles, cobbles, and small boulders of blue-gray limestone that were derived from Pennsylvanian strata capping the crest of the Sandia Mountains, about 3.25 km (2 miles) east of this site.

Observe meter-scale boulders and infer depositional processes. Do these represent long-runout rock falls or were they transported by debris flows during large flooding events? Discuss tectonic, geomorphic, and paleoclimatic conditions that played a role in the development of the landscape. Compare

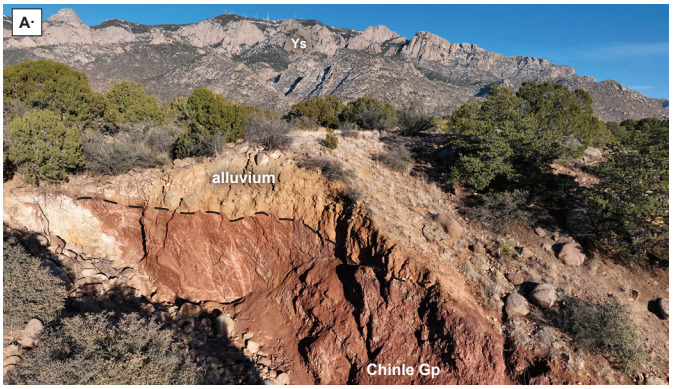



FIGURE 1.22. Faulted Mesozoic inlier at Station 2C. A: Triassic Chinle Group unconformably overlain by yellowish-brown Pleistocene piedmont deposits.



FIGURE 1.23. Photograph of Morrison Formation sandstone near Station 2D. These Mesozoic sedimentary rocks are overlain by a thin veneer of middle Pleistocene piedmont alluvium. The walking stick is approximately 1 m (3.2 ft) in length.

with hillslope processes responsible for development of pediment surfaces with those that created the prominent bench in the mountain front.

Given the ages of the Quaternary alluvial units that overlie the pediment, pedimentation processes likely involve comparable time spans of $10^4$ to $10^5$ years. Early workers recognized that a relatively stable base level and long time spans were required to form pediments (e.g., Oberlander, 1974). It is likely that widespread erosion along the mountain front enabled pedimentation implies relative base level stability. Otherwise, streams would incise canyons rather than sweep back and forth to produce widespread, relatively low-sloping erosional surfaces.

Another component of pediment formation is erosional retreat of the mountain front. Two processes related to hillslope retreat are weathering and corestone development. Corestones form through chemical weathering of jointed granitic bedrock, where near-surface groundwater preferentially alters mineral grains along joint planes and intersections. They are meter-scale boulders that are located relatively close to where they formed, such as along the foot of the Sandia Mountains. Once formed, rock fall, perhaps aided by earthquakes, or large rainfall events can transport these boulders a short distance down slope of the mountain front. Another product of weathering is grus derived from disintegration of granitic rock as feldspar grains decompose to clay, breaking the rock into loose, generally sand-sized particles.

Sediment transport is thought to occur during paleoclimatic changes that destabilize the landscape via changing vegetation density or storm-precipitation intensity (e.g., Bull, 1991). Did paleoclimate or tectonics also play a role in forming the topographic benches about midway up the mountain front? Was there a time of low-slip rates along the mountain-front faults where base-level stability facilitated pediment formation?

Many boulders on the alluvial surface have indentations located just above current ground level (Fig. 1.24). This notching may reflect preferential weathering during a time when the soil surface was higher than today. Clay in sediment can retain moisture, which facilitates the chemical transformation of mica in the granite to clay leading to disarticulation of feldspar and quartz grains in the granite, forming blankets of grus around the boulders. Subsequent erosion then lowered the ground surface by up to a meter, typically along the edges of incised drainage courses. Figure 1.25 contains photographs of magmatic features typically found in the Sandia granite.

### End of Stop 1. Return to vehicles.

**0.0** **REZERO ODOMETER before leaving parking area.** *0.1*

**0.1** **Return to Intersection of FS 333 and Tramway Boulevard, then turn left (southeast).** *1.4*

**1.5** Intersection of Tramway and Paseo del Norte Boulevards. **Continue south on Tramway Boulevard**. Cross a series of alluvial fans associated with drainages

that originate in the Sandia Mountains. Tramway Boulevard generally follows the trend of buried faults that separates thin (<30 m, [100 ft]) alluvium and Santa Fe Group basin fill on the left (west) from thicker deposits to the right (west). Piedmont deposits of the Sierra Ladrones Formation (upper Santa Fe Group) thicken considerably to the west (>100 m [>330 ft]) based on data from water-supply wells for the Sandia Heights community (according to well markers in Connell, 2006). *0.6*

**2.1** Cross Domingo Baca Arroyo drainage channel. *1.2*

**3.3** Cross Arroyo del Pino. A walking path along this arroyo is one of three developed trails that ascend to the crest of the Sandia Mountains. *0.1*

**3.4** Intersection of Tramway Boulevard and Simms Park Road, which is the main road access into Elena Gallegos Open Space. **Continue south on Tramway Boulevard.** *1.0*

**4.4** Cross Arroyo del Oso, a large canyon in the Sandia Mountains. Look for the bear statues on south side of Arroyo del Oso. These bronze sculptures of a mother bear and her two cubs are a tribute to the drainage's namesake (Oso is bear in Spanish). *0.2*

**4.6** Descend into a topographic low area associated with the radial flanks of fans emanating from Embudito and Embudo Canyons. *0.6*

**5.2** Intersection with Montgomery Boulevard. Gradually ascend toward the crest of an alluvial fan fed by Embudo Canyon. **Continue south.** *1.0*

**6.2** Intersection with Candelaria Boulevard. Continue south as Tramway Boulevard descends into a topographic low formed between mountain-front fans near the southern end of the Sandia Mountains. *0.4*

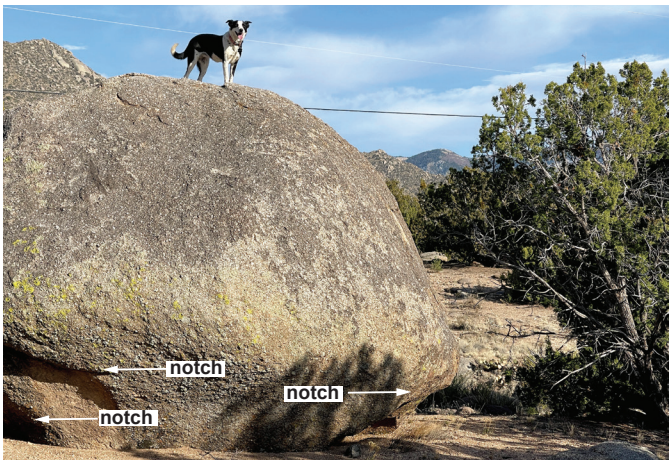



FIGURE 1.24. Boulder of Sandia granite on middle Pleistocene granitic alluvium near Station 2D. The indentation near the base of this boulder is likely due to enhanced near-surface weathering prior to erosion of the upper 0.5 m (1.6 ft) of alluvium.

**6.6** Intersection with Menaul Boulevard. Continue south. Just east of Tramway Boulevard is a shallow bedrock bench that has been cut by a north-trending strand of the Sandia Mountains fault system, a set of normal faults that define the structural margin of the Albuquerque Basin and Sandia Mountains. *1.0*

**7.6** Pedestrian bridge and intersection with Indian School Road that approximately coincides with a west-plunging axis of a fan associated with the mouth of Embudo Canyon to the east. *0.1*

**7.7** Intersection with Lomas Boulevard. The four low peaks ahead are part of a granitic salient known as Four Hills. *1.0*

**8.7** Pedestrian overpass and intersection with Copper Road. Ahead is the northern edge of proximal piedmont deposits of the ancestral Tijeras fan system. *0.6*

**9.3** Cross underneath I-40 overpass and **turn left (east) onto Central Avenue (Old Route 66).** *0.3*

**9.6** **Turn left at intersection with Four Hills Road, and proceed onto I-40 on-ramp, eastbound to Santa Rosa.** I-40 follows the course of Tijeras Canyon, a historic trail that connects the east side of the Sandia Mountains with the Albuquerque Basin. *1.0*

**10.6** Banded strata of Pennsylvanian limestone and shale forms skyline ridge ahead. Two stops today will closely examine Pennsylvanian strata. Pennsylvanian stratigraphy and late Paleozoic tectonics are summarized in Kues (2001), Kues and Giles (2004), and Lucas et al. (2026, in press). Pennsylvanian sedimentary rocks in the Sandia Mountains comprise




FIGURE 1.25. Features of Sandia granite (granodiorite) that can be observed on boulders and in the Sandia Mountains. The Sandia granite, like most 1.4-Ga A-type granites in the southwestern United States, contains numerous mafic enclaves. A: Mafic enclave that is interpreted to be comingled (and sometimes partially mixed) mafic magmas resulting from basaltic underplating that partially melted lower crustal rocks to form the granite. B: Evidence for such comingling of two partly immiscible melts is that tabular feldspars (inside rectangle) seem to have floated into the enclave and both are aligned in magmatic flow fabrics.

an approximately 586-m (1,923-ft)-thick stratigraphic section (Fig. 1.26). In ascending order the succession consists of (1) the Middle Pennsylvanian (Atokan–Desmoinesian) Sandia Formation, a primarily siliciclastic unit that includes coal deposited in a fluviodeltaic to shallow-marine environment; (2) the Middle Pennsylvanian (Desmoinesian) Gray Mesa Formation, composed of marine carbonate rocks; and (3) the Middle–Upper Pennsylvanian (Desmoinesian–Virgilian) Atrasado Formation and Upper Pennsylvanian (Virgilian) Bursum Formation, siliciclastic-carbonate strata representing shallow-marine and nonmarine depositional environments. *0.1*

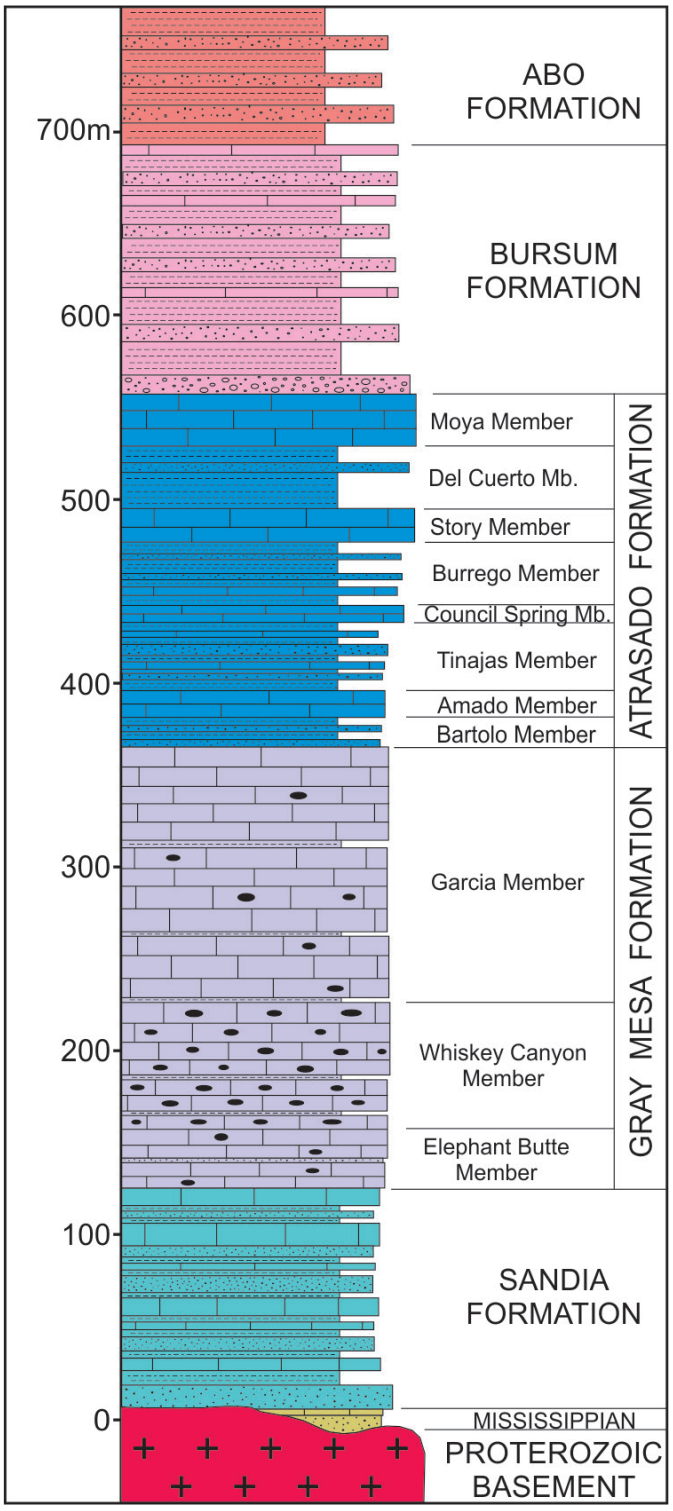



FIGURE 1.26. Generalized summary of Pennsylvanian lithostratigraphic units in the Sandia Mountains.

**10.7** Prominent joints in Sandia granite in roadcut on north side of I-25. *0.1*

**10.8** Village of Carnuel along north side of Tijeras Canyon. For the next 3.2 km (2 mi) we can see features of the southern Sandia Mountains (on left) and the northern Manzanita Mountains (on right).

The base of the Sandia pluton is a marked by the nearly 1-km (0.6-mi)-wide Seven Springs shear zone, which strikes northeast and dips 40° northwest (Fig. 1.27; Karlstrom et al., 1994; Kirby et al., 1995). In a northwest to southeast transect across this shear zone (not possible on this fieldtrip), one passes from the megacrystic main body of the Sandia granite to sheared megacrystic granite. Magmatic fabric in the pluton passes into solid-state shear zone fabrics exhibiting geopetal indicators of extensional shear sense of top to the northwest. The parallelism of magmatic and solid-state fabrics, and the presence of partial-melt leucosome tails around deformed megacrysts (now augen) indicate this shearing took place during emplacement of the Sandia granite (Kirby et al., 1995).

Tectonic lenses of quartzite and schist in the shear zone contain high-grade assemblages of sillimanite, potassium feldspar, and cordierite also indicating high-grade shearing. One then passes through a wide zone called the Cibola gneiss that contains tectonic slivers of quartzite and schist. Some areas are recognizable and dated to the ~1.65-Ga Cibola granite (orthogneiss). Some areas are megacrystic and some fine grained which, before it was dated (Karlstrom et al. 2004), led Kirby et al. (1995) to interpret this unit to be the sheared and partially melted base of the Sandia granite. Current interpretations are similar: space for emplacement of the 1.45-Ga syntectonic Sandia granite involved a top-northwest shear zone that developed in one of the many 1.65-Ga plutons that intrude the 1.68–1.60-Ga Manzano Group of the Sandia and Manzano Mountains.

The Tijeras greenstone of Connolly (1982) is correlated with the Isleta greenstone and other basalt–rhyolite metavolcanic units of the lower Manzano Group that are overlain by schist and quartzite. Thus, both the north and south aureoles of the Sandia granite are syntectonic with regional transpressive deformation and have regional contact metamorphic aureoles with highest grade rocks near the pluton versus andalusite and kyanite assemblages farther away as described by Kirby et al. (1995) and Karlstrom et al. (1994). *2.9*

**13.7** Blind curve ahead with Paleoproterozoic quartzite and aplite on left (north). On the right (south) is a succession of Pennsylvanian strata that overlies upper Mississippian red beds and paleosols of the Arroyo Peñasco and Log Springs Formations, which nonconformably overly Paleoproterozoic metasedimentary rocks. Stratigraphic sections of the Mississippian–Pennsylvanian strata on the ridge were restudied

by Lucas et al. (2021). Szabo's (1953) section 6 is characteristic (Figs. 1.28 and 1.29). The Mississippian strata there rest on Proterozoic basement (schistose mafic metavolcanic rocks) and are 16–20 m (52–66 ft) thick. They consist of an approximately 7-m (23-ft)-covered interval of sandstone and dolomite of the Arroyo Peñasco Formation, which is overlain by 10 m (33 ft) of sandstone and covered siliciclastic, reddish-brown mudstone of the Log Springs Formation. The overlying Sandia Formation contains approximately 55 m (180 ft) of quartzose sandstone, siltstone, and limestone. The section is capped by about 67 m (220 ft) of mostly cherty limestone of the Gray Mesa Formation. An interesting observation is the presence of Mississippian strata along the ridge here, which was first noted by Armstrong and Mamet (1974), and described by Armstrong and Mamet (1974, 1979) and Armstrong et al. (1979). There are no definitive exposures of Mississippian strata in the

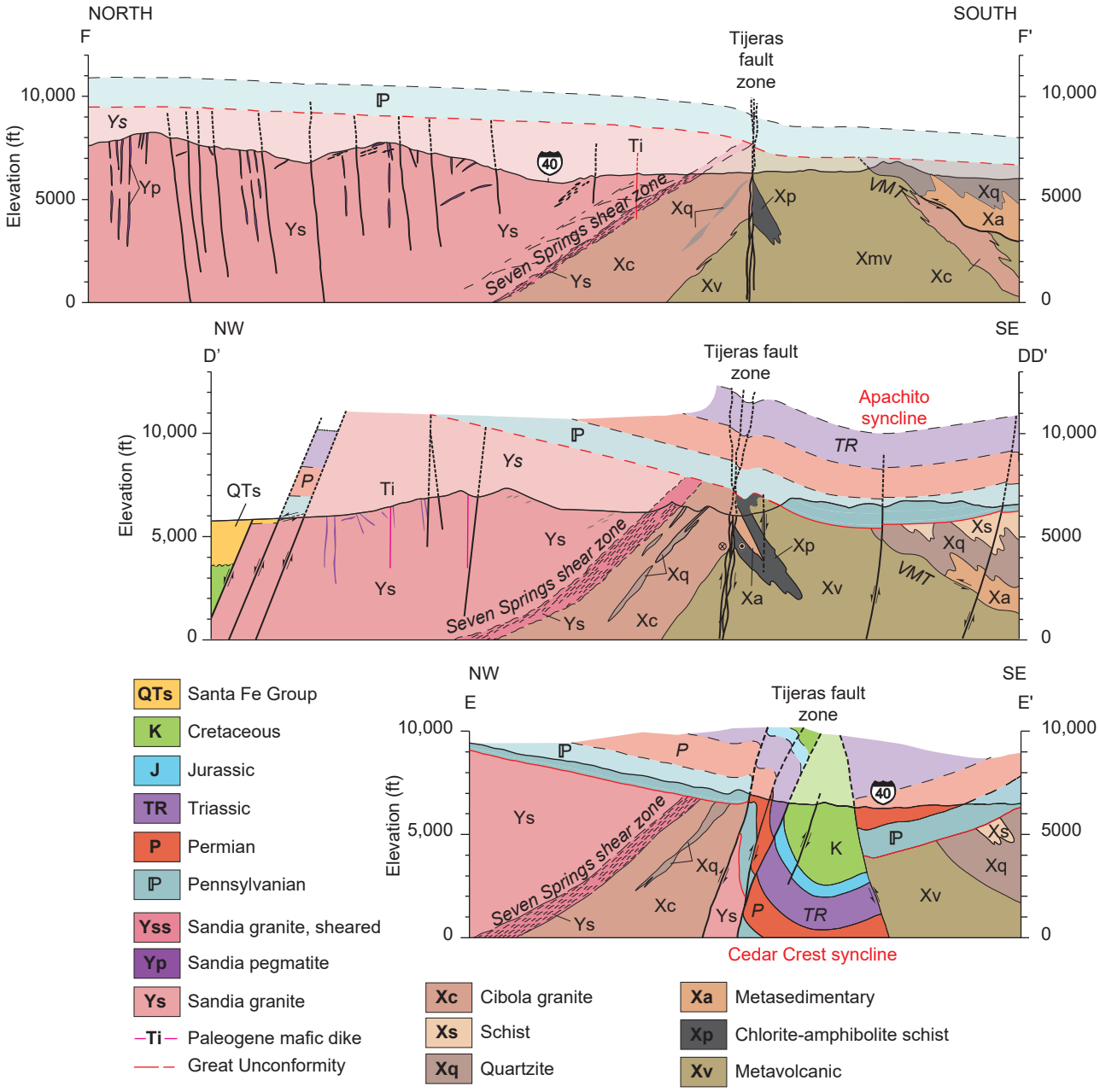



FIGURE 1.27. Geologic cross sections across Tijeras Canyon (Karlstrom et al., 1994, 1997) with locations discussed on Day 1. The northwestern edge of cross section D'–DD' shows an allochthonous block of Pennsylvanian limestone at the end of Lomas Boulevard that can be alternatively interpretated to be above a low-angle normal fault that was segmented by later high-angle normal faults, an ancient landslide block, or a down-faulted block of Paleozoic strata and the Great Unconformity. Cross section F–F' diagrammatically show alignments of comagmatic mafic enclaves and magmatic fabric in the Sandia pluton that mimics the NW-dipping base of the pluton formed by the Seven Springs shear zone (Kirby et al., 1994). This cross section also portrays zones of partial melting of 1.65-Ga Cibola gneiss in the Seven Springs shear zone that is gradational with part of the base of the Sandia pluton that was sheared with top-to-the-north shear sense at partial melt temperatures during pluton emplacement. Cross section E–E' shows the northeast-strike of the Tijeras fault zone, which is similar in strike with the Seven Springs shear zone, but is subvertical and records numerous Phanerozoic movements. See Figure 1.01 for cross-section locations.

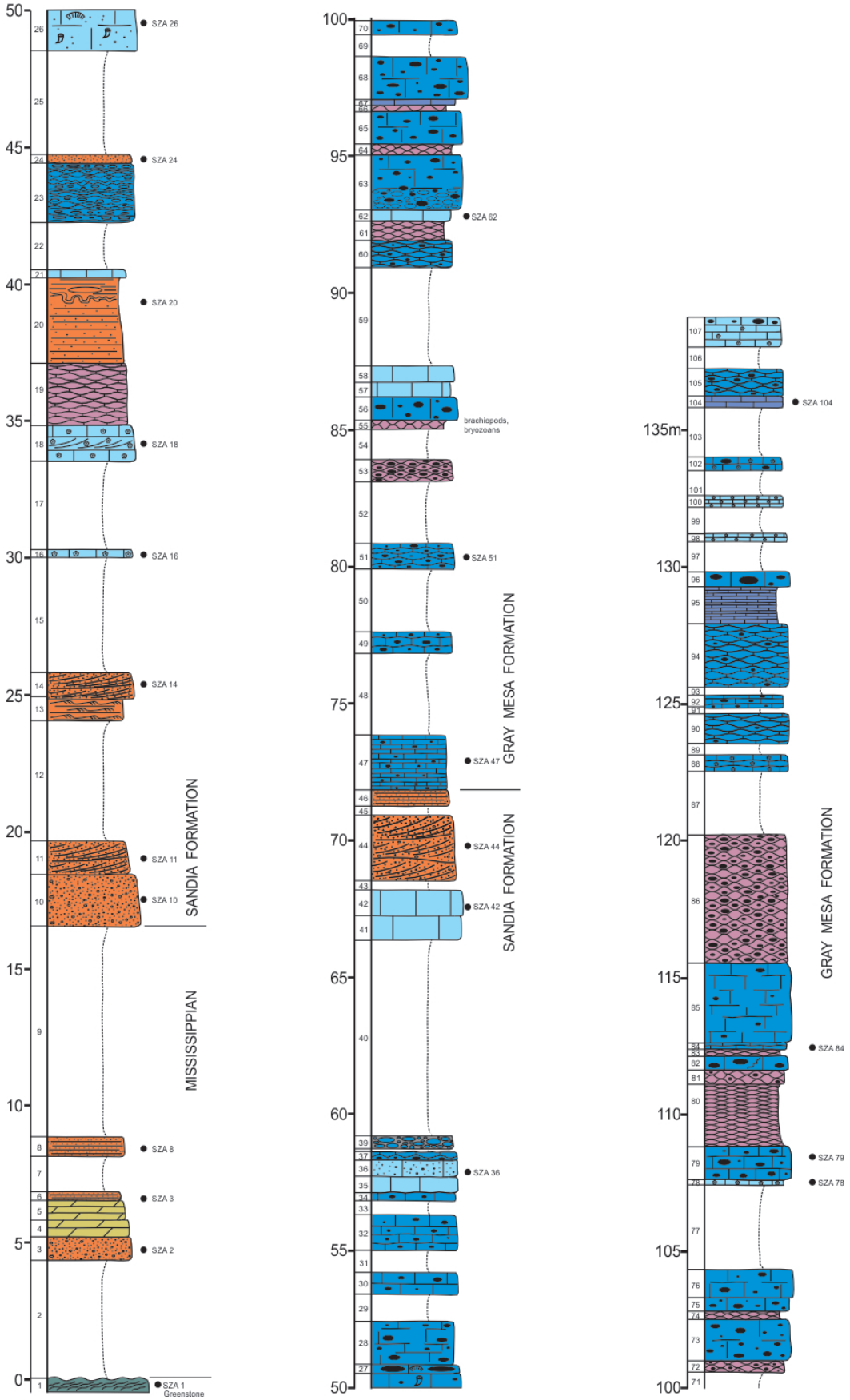



FIGURE 1.28. The Szabo 6 stratigraphic section of the Mississippian Arroyo Peñasco (unit 15) and Log Springs (units 6–9) Formations, and Pennsylvanian Sandia and Gray Mesa Formations. See Figure 1.29 for explanation of symbols.




FIGURE 1.29. Explanation of lithologic symbols in graphical drawings of measured Pennsylvanian stratigraphic sections (See Figs. 1.28, 1.33, 1.34, 1.39, and 1.45). On the sections, black dots with acronyms (e.g., THE-30) are the stratigraphic levels at which samples were collected for petrographic and/or microfossil analysis. Colored boxes with acronyms and numbers in subsequent stratigraphic column figures mark stratigraphic levels of fossil localities.

Sandia Mountains (i.e., the Sandia Formation rests on basement) until north of Sandia Crest. *1.0*

**14.7** Crossing buried trace of the Tijeras fault zone on the left. The fault is covered by locally derived colluvial deposits. The northeast-trending Tijeras fault is a has a long and complicated history of recurrent movement ranging from possibly the Proterozoic to the late Pleistocene (Connolly et al., 1982; Abbott and Goodwin, 1995; Kelson et al., 1999). The southwest projection of the Tijeras fault zone into the Albuquerque Basin nearly coincides with the location of Plio–Pleistocene volcanic fields. This trend also generally corresponds to a shift in regional patterns of stratal tilt. These features were used as evidence to suggest that the Tijeras fault zone continued across the Albuquerque Basin as an accommodation zone separating southern and northern subbasins (now called the Belen and Calabacillas subbasins, respectively; Russell and Snelson, 1994). Geologic mapping and aeromagnetic studies (Maldonado et al., 1999, 2007; Grauch and Connell, 2013) indicate that the Tijeras fault zone merges into, and probably connects with or is cut by, faults of the Hubbell Spring fault zone, instead of continuing across the basin as a discrete subbasin bounding structure as suggested by Russell and Snelson (1994). *0.4*

**15.1** Straight ahead is Cerro Pelon, a southwest-trending linear ridge, locally known as "Marcou's wall" that exposes carbonate beds of the Pennsylvanian Gray Mesa Formation (Fig. 1.30). Jules Marcou (1824–1898) was a Swiss-born geologist who accompanied the 1853 Whipple Expedition of the U.S. Army that traveled from Fort Smith, Arkansas to San Diego, California to establish a railroad route to the Pacific. On 8–10 October 1853, Marcou examined the geology of Tijeras Canyon and the Sandia Mountains to the north, and referred to the limestone-dominated strata (now called Middle Pennsylvanian Gray Mesa Formation) as "Mountain Limestone," an old British stratigraphic term that to modern understanding indicates a Mississippian age (Lucas, 2001). At the limestone outcrop just south of the hairpin turn in the creek, Marcou collected brachiopods and referred to this outcrop as a "grand perpendicular wall" (Marcou, 1858, p. 21). He also produced a sketch of the stratigraphy at the "wall," which

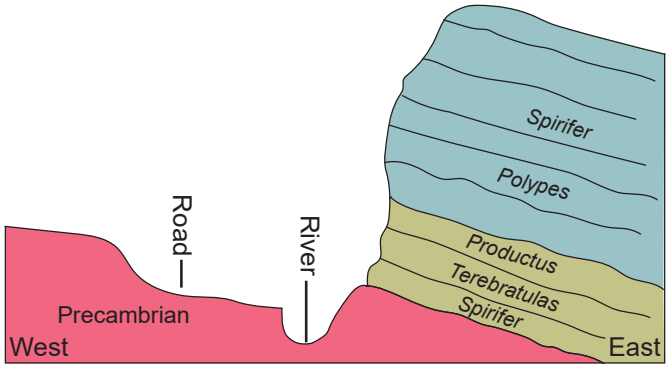



FIGURE 1.30. Jules Marcou's sketch of the "grand perpendicular wall" in Tijeras Canyon, a brachiopod-rich section of the Gray Mesa Formation. Redrawn from Blake (1856).

Blake (1856) published with Marcou's field notes (Fig. 1.30), labeling some of the layers with brachiopod genera names. The Pennsylvanian age of these strata was later realized by Herrick and Johnson (1900), among others, but Marcou's observations and sketch stand as the first relatively detailed description of a Pennsylvanian stratigraphic section in New Mexico. For more details on Marcou's work here, see Sutherland and Harlow (1973, p. 3–4) and Kelley and Northrop (1975, p. 15–19). *0.6*

**15.7** Upper Paleozoic carbonate and shale on roadcuts to left, now mostly covered by cement in an effort to mitigate rock fall. At 2:00 is Cedro Peak, a low hill spiked with communications towers. Lucas et al. (2014) described a complete local Pennsylvanian stratigraphic section there. The Tijeras cement plant is on the right (south). **Take off-ramp (Exit 175) on right that leads to State Road 14 (NM 14; the Turquoise Trail Scenic Highway).** *0.3*

**16.0** Stay left on NM 14 and drive north crossing under I-40. *0.8*

**16.8** Cross east Tijeras syncline. Reddish-brown sandstone and shale of the Permian Abo Formation are on the left. The Tijeras syncline exposes an Upper Cretaceous section consisting of the following units, in ascending stratigraphic order: Dakota Sandstone (Encinal Canyon, Oak Canyon and Cubero Members), Mancos Shale (Graneros, Greenhorn, Carlile, Juana Lopez, D-Cross, Tocito and El Vado Members), Crevasse Canyon Formation (Dalton, Gibson and Hosta Members), Satan Member of Mancos Shale, Point Lookout Sandstone, and an incomplete section of Menefee Formation. Lee (1912, 1917) described coal mines in the Gibson and Menefee intervals and referred to the area as the "Tijeras coal field," even though there was no economic coal production.

The Cretaceous section in the Tijeras syncline is important for establishing the continuity of the major Cretaceous facies (northwest–southeast: coal-bearing fluvial, shoreline, and offshore marine) across the Rio Grande rift and the northwest–southeast-trending shorelines of the Western Interior Seaway. According to Lucas (2026), this Cretaceous succession is similar to a correlative section in the southeastern San Juan Basin to the northwest, and to the Cretaceous successions at Placitas and in the Hagan embayment to the north. This section is southwest of the Hosta-Dalton merger and turnaround ("Cano Sandstone") of the Santonian regression-transgression of the Western Interior Seaway at Placitas and in the Hagan embayment to the north. The Tijeras syncline contains a coal-bearing facies tract of the Gibson Member that crops out again in the southeastern San Juan Basin near Guadalupe (Lucas et al., 2000). *0.2*

**17.0** Light-brown sandstones on ridge at 10:00 are marine shoreface deposits of the Upper Cretaceous Point Lookout Sandstone. *0.6*

**17.6** Strike valley in Upper Cretaceous Mancos Shale. *0.6*

**18.2** Gray-colored Mancos Shale on left. *0.6*

**18.8** Upper Cretaceous Point Lookout Sandstone at 3:00. *0.7*

**19.5** Reddish-brown mudstone of the Triassic Chinle Group on left. *0.4*

**19.9** Cross trace of the Tijeras fault zone. Fractured and faulted green and tan shale and sandstone of the Upper Jurassic Morrison Formation are exposed on right. *0.3*

**20.2** Moderately deformed gypsum beds of the Jurassic Todilto Formation exposed on the cut slope of church parking lot on the right (east). The church is built in an abandoned gypsum quarry. The Todilto Formation here is the Luciano Mesa Member, 2 m (6.6 ft) of dark gray kerogenic, finely laminated limestone, overlain by the Tongue Arroyo Member, massive white gypsum about 31 m (102 ft) thick. The bluff just east of the parking lot is Summerville Formation, which is 25 m (82 ft) in thickness and contains mostly ripple-laminated red-bed sandstone and variegated siltstone, shale, and nodular limestone. The Summerville is overlain by the Salt Wash Member of the Morrison Formation, 21 m (69 ft) of mostly trough-crossbedded, medium- to coarse-grained and locally pebbly sandstone. These are characteristic southern Colorado Plateau units and document the continuity of Middle and Upper Jurassic depositional systems well east of the plateau that extended east onto what are now the Southern High Plains (Lucas and Anderson, 1998; Anderson et al., 1999). *0.1*

**20.3** The Jurassic Entrada Sandstone on the right, approximately 22 m (72 ft) thick here, consists of a lower Dewey Bridge Member, which is 11 m (36 ft) of mostly ripple-laminated, very fine-grained, reddish-brown sandstone, and the overlying Slick Rock Member, which is trough-crossbedded, medium-grained, yellowish-gray sandstone about 11 m (36 ft) thick. The Entrada–Chinle contact here (now covered with concrete) consists of the Middle Jurassic Dewey Bridge sandstone disconformably on Upper Triassic Chinle Group mudstone, a hiatus of at least 40 My. *0.1*

**21.4** Road follows strike valley underlain by red beds of the Upper Triassic Chinle Group. The Triassic section in the Cedar Crest area is the Moenkopi Formation overlain by the Shinarump and Petrified Forest Formations of the Chinle Group. Triassic strata in the Cedar Crest area contains the following: (1) Middle Triassic (Anisian) Anton Chico Member of the Moenkopi Formation, which disconformably overlies Permian limestone of the San Andres Formation, as much as 65-m (213-ft)-thick of mostly grayish-red to pale-red litharenitic sandstone and siltstone; (2) disconformably overlying Shinarump (or Agua Zarca) Formation of the Chinle Group, as much as 100 m (320 ft) of mostly yellowish-gray sublitharenitic sandstone and extraformational conglomerate with clasts of quartzite and Paleozoic limestone; and (3) as much as 300 m (948 ft) of mostly reddish-brown bentonitic mudstone assigned to the Petrified Forest Formation, disconformably overlain by the Middle Jurassic Entrada Sandstone. Triassic strata here can be readily correlated with Triassic strata on the southern Colorado Plateau and on the southern High Plains, principally through lithostratigraphic correlation (e.g., Lucas and Heckert, 1995; Lucas et al., 1999, 2015). They are primarily fluvial deposits of the vast Late Triassic Chinle basin that once extended from Texas to Idaho and from Nebraska to eastern Nevada. *0.8*

**22.2** NM 14 veers to left offering the first views of the San Pedro Mountains and Gold Hills to the northeast. These uplands contain Oligocene subvolcanic and volcaniclastic rocks of the Ortiz Mountains volcanic field. *0.3*

**22.5** **Enter traffic circle and merge onto State Road 536 (NM 536) toward Sandia Crest.** *0.1*

**22.6** View of dip slope of Pennsylvanian Gray Mesa Formation at 10:00. Cuesta at 9:00 is underlain by reddish-brown Triassic sandstone and mudstone. *0.8*

**23.4** In the roadcut to the right, note reddish-brown sandstone and mudstone of the lower Permian Abo Formation overlain by thin dolomite beds and finer grained sandstones and siltstones at the base of the lower Permian Arroyo de Alamillo Formation of the Yeso Group (see Lucas and Krainer, 2026). *0.1*

**23.5** Abo Formation roadcut on right exposes the Cañon de Espinoso Member, which is characterized by laterally extensive sandstone sheets like those seen here. *0.7*

**24.2** Enter Cibola National Forest. Look for Auto Tour sign 6 and the depositional contact between Sandia Formation and overlying Gray Mesa Formation on right. *0.1*

**24.3** Cienega Canyon Picnic Area on left. *0.2*

**24.5** Great Unconformity exposed on right. **Turn left into parking lot for Doc Long Picnic Area.** *0.1*

**Waypoint 1.09 [N35.1743°, W106.3761°]**

**STOP 2. The Great Unconformity, Upper Paleozoic Stratigraphy, and Ancestral Rocky Mountains Orogeny.**

From parking lot, walk south along west shoulder of NM 536 for a view of the Great Unconformity. Watch for oncoming traffic and carefully cross highway as directed and only when it is safe to do so.

## THE GREAT UNCONFORMITY

The Great Unconformity represents one of the most significant erosional surfaces in the geologic record of the southwestern United States. The Great Unconformity marks where Paleozoic sedimentary strata overlie Proterozoic crystalline basement across a regional nonconformity (Dutton, 1882).

In New Mexico and adjacent regions, the stratigraphic expression of this unconformity varies widely. In Grand Canyon, southern New Mexico, and parts of Colorado, Cambrian strata rest directly on basement, whereas in many Ancestral Rocky Mountains (ARM) uplifts, Mississippian to Triassic strata overlie basement, reflecting substantial Proterozoic and Paleozoic erosion followed by diachronous burial of uplifted ARM blocks.

Basement rocks beneath the unconformity in New Mexico range from 1.75 to 1.1 Ga, with dominant age populations at 1.75–1.60 Ga and 1.45–1.33 Ga. In the Sandia Mountains, the Great Unconformity places Middle Pennsylvanian strata, and sparse and locally thin Mississippian units, on the 1.45-Ga Sandia Granite and its 1.65-Ga metamorphic aureole, which together represent the roof of the Sandia pluton.

Earlier workers attributed the Great Unconformity in northern New Mexico to the development of a broad northeast-trending Paleozoic highland extending from New Mexico to Minnesota called the Transcontinental Arch (Eardley, 1951). This arch explained the absence of lower Paleozoic strata across much of northern New Mexico; however, Carlson (1999) later emphasized that the arch likely consisted of multiple discontinuous northwest-trending basement highs that were reactivated episodically throughout the Phanerozoic, rather than a single continuous structural zone.

Detrital zircon studies have challenged both the continuity and even the existence of a coherent transcontinental arch, suggesting instead a more complex breached or segmented paleogeography (Myrow et al., 2003; Amato and Mack, 2012; Holland et al., 2023). In contrast, ARM uplifts are well documented as northwest-trending, fault-bounded basement highs associated with adjacent syntectonic basins, such as the Taos trough in New Mexico and the Paradox Basin in Utah (Leary et al., 2017). In northern New Mexico, these basement highs include the Zuni, Peñasco, Uncompahgre, Sierra Grande, Joyita, and Pedernal uplifts. The Sandia Mountains occupied a more proximal basinal position during Pennsylvanian time, receiving arkosic and carbonate sediments derived in part from the Pedernal uplift, approximately 50 km (31 mi) southeast of Stop 2.

These relationships suggest that the northeast-trending transcontinental arch and northwest-trending ARM uplifts are not causally related and may reflect distinct tectonic processes that operated at different times. In the Sandia Mountains and southward to at least the latitude of Socorro, New Mexico, strata older than Middle Pennsylvanian are largely absent, with local thin Mississippian deposits nonconformably preserved on Proterozoic basement. South of the approximate latitude of Truth or Consequences, New Mexico, upper Cambrian through Mississippian marine strata are present between Proterozoic basement and Middle Pennsylvanian rocks. Whether these lower and middle Paleozoic rocks were deposited farther north and subsequently removed, or whether northern New Mexico remained a persistent highland throughout much of the Paleozoic, is poorly resolved. Indeed, Bachman (1968) noted that lower and middle Paleozoic strata in southern New Mexico do not show northward landward facies transitions, and instead display irregular thickness patterns, with a general northward thinning and truncation just north of the latitude of the Caballo Mountains, approximately 200 km (124 mi) southwest of Stop 2.

Three regionally significant unconformities punctuate the lower and middle Paleozoic section in New Mexico (Bachman, 1968):

- The base of the Cable Canyon Sandstone (Montoya Group), where Upper–Middle Ordovician strata overlie Lower Ordovician rocks, representing a hiatus of ~25 My;
- The base of the Percha Formation, where Upper Devonian strata rest on Ordovician lithostratigraphic units, representing a hiatus of about 60 My; and
- The base of the Red House and Sandia Formations, where Middle Pennsylvanian strata overlie Upper Devonian rocks, representing a hiatus of ~55 My.

Thickness trends and truncation patterns are best explained by erosional removal beneath one or more of these unconformities (Kelley and Silver, 1952; Kottlowski, 1960, 1963; Bachman, 1968; Seager and Mack, 2003; Lucas et al., 2023). Kelley and Silver (1952, fig. 16) attributed the pre-Montoya and pre-Percha unconformities to epeirogenic uplift along a hinge line north of the Caballo Mountains, in southern New Mexico.

The most profound stratigraphic break is the pre-Pennsylvanian unconformity, which marks the onset of the ARM orogeny. This surface ultimately truncated all lower–middle Paleozoic strata preserved as far north as the Caballo Mountains and dominates the Great Unconformity record in the Sandia Mountains. Consequently, the northward thinning and disappearance of Cambrian through Mississippian strata can be attributed to the combined effects of two earlier epeirogenic unconformities and a final tectonically driven ARM erosional event. The original northern extent of lower and middle Paleozoic deposition, however, remains uncertain.

## Thermochronologic Constraints on Basement Exhumation

Thermochronologic analyses of the Sandia granite and its aureole provide critical constraints on the timing and magnitude of erosion associated with development of the Great Unconformity. Using $^{40}Ar/^{39}Ar$ dating of muscovite, biotite, and potassium feldspar, Heizler et al. (2026) reconstructed a temperature-time (T-t) path from Sandia pluton crystallization at 1.45 Ga to exposure near the surface by Pennsylvanian time.

Muscovite ages concordant with the 1.45-Ga U-Pb zircon age indicate rapid post-emplacement cooling through 400°C, consistent with intrusion at midcrustal depths of approximately 10–12 km (6.2–7.5 mi) under geothermal gradients of 30–35°C/km. Biotite ages of 1.43–1.40 Ga record cooling through 300°C during waning stages of the Picuris orogeny. Potassium feldspar multiple-diffusion-domain modeling indicates prolonged residence in the middle crust, with slow cooling from approximately 300°C to 250°C between 1.4 and 1.0 Ga, corresponding to only 2 km (1.25 mi) of exhumation over a span of 400 My.

Cooling accelerated between 1.0 and 0.8 Ga, with temperatures dropping to 150°C (~5 km [~3 mi] depth), likely reflecting uplift related to Grenville foreland deformation or early stages of Rodinian rifting (Mulder et al., 2017). Nearly half of the approximately 10 km (6 mi) of basement erosion required to expose the Sandia granite occurred prior to burial beneath Paleozoic strata and is recorded in the Proterozoic thermal history.

Thermal histories between 800 and 320 Ma are less well constrained and permit multiple interpretations, including continued erosion during Rodinia breakup (Ricketts et al., 2021), Cryogenian glacial erosion (Keller et al., 2019), or late Neoproterozoic erosion pulses (Thurston et al., 2024), potentially followed by shallow Phanerozoic burial.

Better constrained is that basement rocks were near the surface by Late Mississippian time and were subsequently reheated to 150°C by being buried by nearly 5 km (3 mi) of Phanerozoic strata, which are preserved in the adjacent Hagan embayment. Potassium feldspar spectra recording apparent ages as young as ~100 Ma reflect partial argon loss during this phase of burial and reheating.

The final phases of exhumation of the Sandia granite likely began during the Laramide orogeny, with the Great Unconformity surface remaining buried beneath 2–3 km (1–2 mi) of strata prior to Miocene time. Rapid late Cenozoic cooling through the 50°C isotherm during the past 10–20 Ma records uplift and exhumation of the Sandia Mountains as a Rio Grande rift flank (Ricketts et al., 2015).

Taken together, stratigraphic relations and thermochronologic data indicate that the Great Unconformity in the Sandia Mountains is a composite erosional surface formed through multiple pulses of exhumation spanning Proterozoic, Neoproterozoic, and late Paleozoic time. Rather than reflecting a single tectonic event or persistent Paleozoic highland, the Great Unconformity records a long and episodic history of basement residence, uplift, erosion, burial, and reexhumation that culminated in exposure during ARM deformation and eventual exhumation during Cenozoic extension.

## UPPER PALEOZOIC STRATIGRAPHY

Upper Paleozoic strata nonconformably overlie Proterozoic basement across the Great Unconformity (Fig. 1.31). The Mississippian Arroyo Peñasco and Log Springs Formations are locally preserved, overlain by synorogenic siliciclastic strata of the Sandia Formation (Fig. 1.32). The Sandia Formation consists of coarse-grained quartzose to subarkosic sandstone and conglomerate interpreted as syntectonic deposits of the ARM orogeny (Krainer and Lucas, 2013; Rudolf et al., 2026).

### Sandia Formation Reference Section

No type section of the Sandia Formation was designated when the unit was named (Herrick and Bedrant, 1900), nor was a type section designated by subsequent workers. Krainer et al. (2011) designated this succession near Doc Long Picnic Area as a reference section of the Sandia Formation (Fig. 1.33). Here, the base of the Middle Pennsylvanian Sandia Formation rests nonconformably on the Proterozoic Sandia granite. The Sandia Formation is 124 m (407 ft) in thickness here. Throughout the Sandia Mountains, the thickness of the Sandia Formation varies greatly, ranging from as little as a few meters in thickness to more than 100 m (328 ft) thick. This variation in thickness indicates paleorelief on the nonconformity at the base of the Sandia Formation was as much as 100 m (328 ft; Krainer and Lucas, 2013).

At the reference section (Fig. 1.33), the Sandia Formation is a succession of alternating shale, sandstone and pebbly sandstone, fossiliferous limestone, and a few covered intervals. The formation rests nonconformably on Proterozoic granite and is overlain by cherty limestone of the Middle Pennsylvanian Gray Mesa Formation. The Sandia Formation is divided into three parts:

- Part A: lower, heterolithic interval that is 69 m (226 ft) in thickness and composed of alternating shale/siltstone, sandstone, pebbly sandstone, (quartzose) sandy limestone, and limestone;
- Part B: middle limestone that is 21 m (69 ft) in thickness and composed of bedded limestone; and
- Part C: upper sandstone that is 34 m (112 ft) in thickness and composed of coarse-grained, cross-bedded sandstone, sparse limestone, and covered intervals.

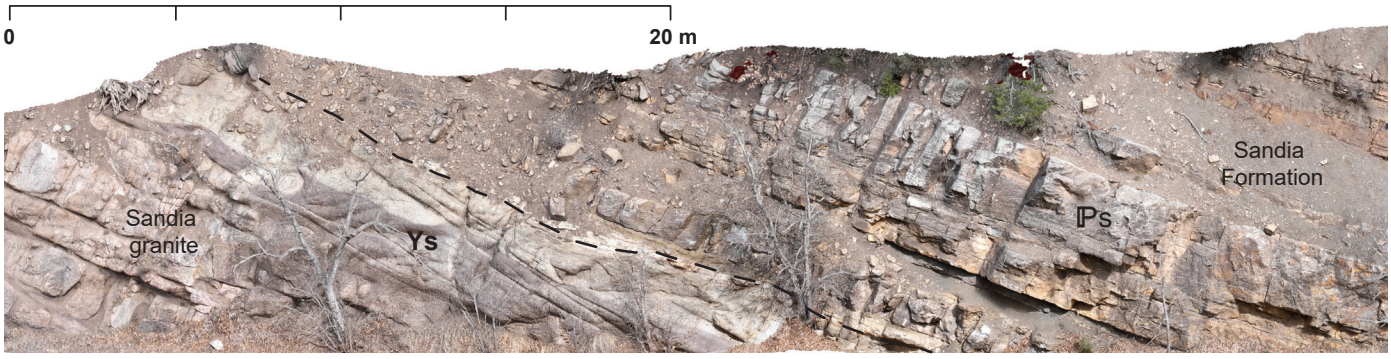



FIGURE 1.31. Photogrammetric model of the Great Unconformity separating Sandia granite (Ys) from overlying grus and sedimentary rocks of the Sandia Formation (IPs). Except for the base, the Sandia Formation is quartzose; however, overlying strata become arkosic toward the top of the Pennsylvanian section.



FIGURE 1.32. The Great Unconformity (at level of the person's left knee) between the Proterozoic Sandia granite and overlying Middle Pennsylvanian Sandia Formation near the Doc Long Picnic area. Photograph was taken from the base of the reference section of the Sandia Formation).

At the Doc Long reference section, the Sandia Formation is composed of alternating shale, sandstone, pebbly sandstone, fossiliferous limestone, and covered (probably shale) intervals that indicate deposition in mostly marine environments ranging from high-energy shoreface to low-energy deeper shelf (Krainer et al., 2011). Pebbly sandstone and sandstone are interpreted as fluviodeltaic (containing no fossils in sandstone and little or no calcite cement) to upper shoreface deposits (which are fossiliferous in calcite-cemented sandstone). Muddy limestone units (wackestone and floatstone) were deposited in a deeper, open-marine shelf environment below the wave base; grainstone and rudstone indicate deposition in a shallow, high-energy, open-marine environment. Three mudstone units contain fossil plants dominated by hydrophilic species and thus indicative of the very wet climates inferred for much of Atokan Euramerica (Lucas et al., 2026, in press).

Several transgressive cycles are recognized in the Sandia Formation, most commonly starting with pebbly sandstone and sandstone with an erosional base, upward fining and grading into siltstone/shale and limestone. Tectonics of the ARM orogeny as well as autocylic processes such as changes in climate likely played a major role in sedimentation patterns, on which glacioeustatic sea-level changes were imprinted. However, it is difficult to disentangle the relative influences of subsidence, climate, and eustacy in Sandia Formation strata due to the complexity of lateral facies changes and widely distributed exposures.

Sandstone in the Sandia Formation are quartz rich and mostly feldspar poor, whereas sandstone in the overlying upper Gray Mesa and Atrasado Formations are mostly feldspar rich. Baars and Stevenson (1984) attributed this quartz-rich interval to the shedding of sediments from the quartzite-cored San Luis uplift in northern New Mexico and southern Colorado. This was followed by an ARM pulse that uplifted granitic basement in the Uncompahgre uplift of northern New Mexico and southern Colorado.

This sediment-source explanation is challenging because other than the San Luis uplift, there is little or no evidence in New Mexico of quartzite-cored ARM uplifts that preceded exhumation of granite-cored uplifts. Furthermore, Sandia Formation strata are found as far south as Socorro County, many hundreds of kilometers away from the San Luis uplift with few intervening ARM-aged uplifts. The Pedernal uplift, located approximately 50 km (31 mi) southeast of Stop 2, is the most likely source of coarse-grained clastic detritus in the Sandia Formation. The petrography of Sandia sandstone is consistent with at least some exposed granite in the source area, as some of these sandstone intervals are subarkose.

Another explanation for the abundance of quartz detritus and relative paucity of feldspar in the Sandia Formation may be the result of deposition in a humid paleoclimate, which would have promoted rapid weathering of feldspar to clay. Thus, Sandia Formation sandstone likely included more feldspar than was preserved, but the humid Atokan climate altered most of the feldspar to clay. This is consistent with an inferred drying trend through the Pennsylvanian that can be identified across the Euramerican portion of the Pangean tropics, resulting in much greater weathering (and chemical reduction) of feldspars in the Sandia Formation than in the younger, post-Atokan units (Lucas et al., 2026, in press).

## ANCESTRAL ROCKY MOUNTAINS

The ARM orogeny represents a late Paleozoic episode of intracratonic, basement-involved deformation that reorganized the tectonic and depositional architecture of New Mexico. Initiation of ARM tectonism was broadly coeval with the assembly of Pangea and the progressive intercontinental suturing along the southern Laurentian margin (Kluth and Coney, 1981; Dickinson and Lawton, 2003; Leary et al., 2017).

In central New Mexico, ARM deformation consisted of basement-involved uplifts and adjacent flexural basins (Kluth and Coney, 1981; Dickinson and Lawton, 2003). Basin modeling and isopach analysis indicate that rapid tectonic subsidence began in Atokan to Missourian time (~320–306 Ma) in many basins, marking the principal phase of uplift and flexural loading associated with ARM deformation (Rudolf et al., 2026). In the Sandia Mountains, ARM tectonism commenced in early Atokan time, with synorogenic deposition of coarse-grained Sandia Formation strata resting directly on Mississippian rocks or Proterozoic basement, and development of localized depocenters such as the Taos–Rainsville trough in northern New Mexico.

In the Sandia Mountains, the expression of the ARM is preserved in the Pennsylvanian stratigraphic record. The basal Sandia Formation consists of coarse-grained, mostly quartzose sandstone and conglomerate that have been interpreted as synorogenic deposits shed from nearby uplifts during early ARM deformation (Krainer and Lucas, 2013; Lucas et al., 2025a). These strata locally rest unconformably on Mississippian carbonates or nonconformably on Proterozoic basement, documenting renewed uplift and erosion at the onset of rapid Atokan subsidence. Overlying Desmoinesian–Virgilian

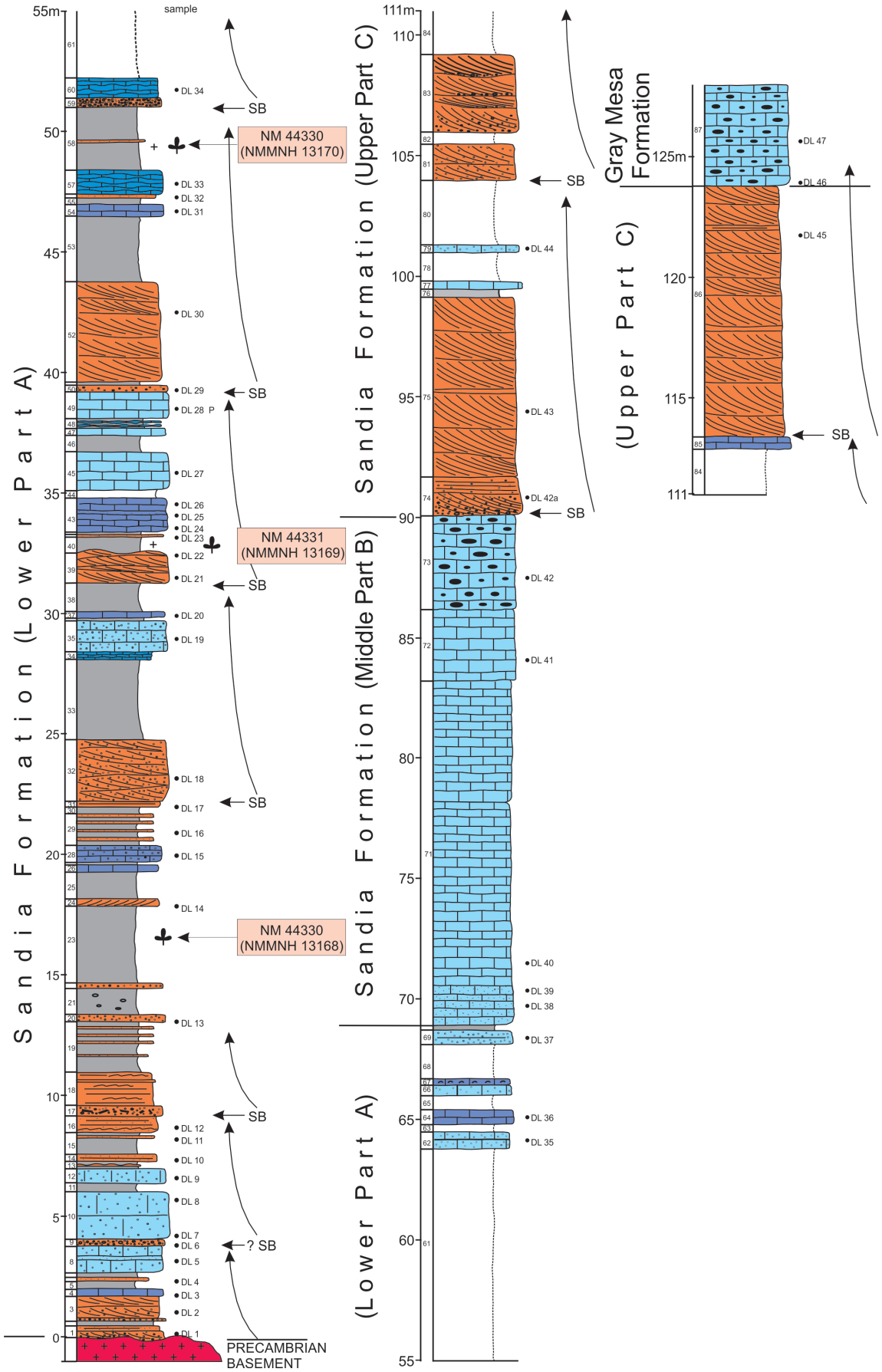



FIGURE 1.33. Reference section of Sandia Formation near Doc Long Picnic Area. See Figure 1.29 for explanation of symbols.

marine carbonate rocks of the Gray Mesa and Atrasado Formations record episodic marine transgressions into actively subsiding basins flanking emergent structural highs. Angular discordances, growth relationships, and coarse proximal facies within the Sandia and Manzano Mountains indicate syndepositional tectonism and differential accommodation consistent with ARM kinematics (Kottlowski, 1968; Krainer and Lucas, 2013). Collectively, these features demonstrate that the Sandia Mountains region occupied a tectonically active position of the ARM in central New Mexico, recording both uplift of basement blocks and flexural subsidence of adjacent Pennsylvanian basins during late Paleozoic orogenesis. The structural grain established during ARM contraction exerted long-term influence on subsequent Mesozoic sediment routing and Cenozoic fault reactivation.

The stratigraphic signature of the ARM orogeny includes syntectonic conglomerate, progressive onlap onto basement-cored uplifts, basinward-thickening sedimentary wedges, and regionally significant unconformities, notably the middle-Wolfcampian surface to the southeast. Subsidence histories document an initial moderate Late Mississippian–Early Pennsylvanian phase followed by accelerated Late Pennsylvanian–early Permian subsidence, and ultimately a transition to more regionally uniform Permian sag following waning tectonic relief. Provenance studies further indicate sediment routing from emergent ARM uplifts and increasing Gondwanan influence during Pangean continental collision to the southeast (Leary et al., 2020). Collectively, the ARM orogeny established the fundamental structural grain and sediment-dispersal patterns that controlled late Paleozoic basin evolution in New Mexico and exerted long-lived influence on subsequent Mesozoic and Cenozoic tectonism.

### End of Stop 2. Return to vehicles.

**0.0** **REZERO ODOMETER. Turn left and continue north on NM 536** as we cross the eastern dip slope of the Sandia Mountains. *0.1*

**0.1** Weathered Sandia granite on right. *0.2*

**0.3** Quartzose veins crosscut Sandia granite at bend in road across Barro Canyon. Durable quartz veins protrude from the outcrop due lack of biotite and associated weathering. Road bends southwestward and crosses a canyon. *0.1*

**0.4** Cross north-striking, west-down fault that repeats the Pennsylvanian stratigraphic section on the hanging wall (on west). *0.2*

**0.6** Tejano Road on right, just beyond bend in NM 536. As we head west and upslope, we are moving down the stratigraphic section. *0.2*

**0.8** Gray Mesa Formation on right. *0.1*

**0.9** Contact between Sandia and Gray Mesa Formations near mile marker 3. *0.1*

**1.0** Sandia Formation on right. *0.1*

**1.1** Weathered dike in Sandia Formation on right. *0.1*

**1.2** Road bends left and crosses Tejano Canyon. Look for Auto Tour sign 9 on right. The roadcuts near and across Tejano Canyon provide some of the most extensive and accessible exposures of Pennsylvanian strata in the Sandia Mountains (Fig. 1.34). Smith (1999) measured and described stratigraphic sections through units he identified as the Sandia and Madera Formations along the Tejano Canyon roadcuts. Smith (1999) interpreted meter-scale stratigraphic alternations within the

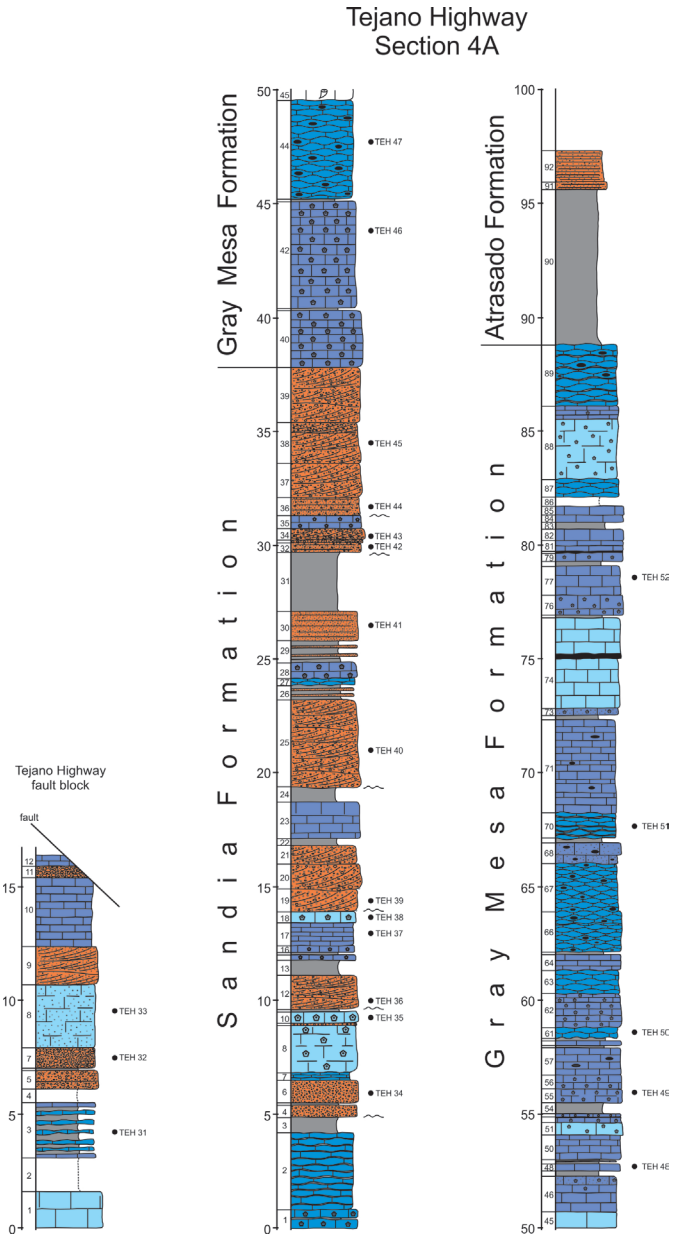



FIGURE 1.34. An example of part of the Pennsylvanian stratigraphic section at the Tejano Canyon highway cut (N35.1850°, W106.3888°, NAD83). See Figure 1.29 for explanation of symbols.

exposed succession as depositional cycles with estimated durations of approximately 200,000 to 473,000 years, attributed to long-eccentricity orbital forcing. Lucas et al. (2026, in press) reexamined the Tejano Canyon exposures and interpreted them as fault-bounded blocks of Sandia Formation and Gray Mesa Formation and concluded that the Atrasado Formation is not fully represented at this locality. Lucas et al. (2026, in press) offered an alternative interpretation of the depositional patterns in the Tejano Canyon roadcut section, revisiting and reassessing the conclusions of Smith (1999) regarding finer-scale depositional cyclicity. Fusulinid and conodont assemblages from the roadcut indicate predominantly early Desmoinesian ages for the exposed strata, implying a more limited temporal span than inferred by earlier studies (Lucas et al., 2026, in press).

Rather than revisiting the differing interpretations in detail, the reader is encouraged to examine these papers. In any case, this roadcut example illustrates some of the broader challenges of evaluating orbitally forced cyclicity in Pennsylvanian successions, particularly where structural complexity, incomplete exposure, and limited independent age control can complicate stratigraphic correlation and temporal resolution. *0.2*

**1.4** Road heads southwest. Sandia Formation on right. Note the change in bedding dips toward the east. *0.4*

**1.8** Gray Mesa Formation on left. *0.4*

**2.2** Switchback and intersection with Forest Service Road 536 (FS 536). Gray Mesa Formation is discontinuously exposed for the next half a mile. *0.1*

**2.3** Ridge top at 3:00 is capped by ledge-forming beds of the Gray Mesa Formation; underlying Sandia Formation is poorly exposed beneath dense shrubbery. *0.1*

**2.4** Sandstone of the Sandia Formation on left. Proceed slightly downsection as road bends to west. *0.1*

**2.5** Cross Great Unconformity. Sandia granite exposed on the left. *0.3*

**2.8** Road bends left near mile marker 5. A fault drops Gray Mesa Formation down to the west. *0.2*

**3.0** Elevation 8,000 ft (2,438 m) sign post. *0.2*

**3.2** Gray Mesa Formation on left. *0.2*

**3.4** Tree Spring on right. Atrasado Formation on left. *0.1*

**3.5** Gray Mesa Formation limestone on left. *0.1*

**3.6** Tree Spring Trailhead on left. Look for reddish-brown mudstone and limestone of the upper Atrasado Formation. In 1956, a jaw fragment with two molars of the American mastodon (*Mammut americanum*) was found here (Kelley and Northrop, 1975; Lucas, 1987). This fossil is unusual because it is one of the rare records (of which there are fewer than one dozen) of American mastodon in New Mexico, and its occurrence provides a high-elevation record at 2,582 m (8,471 ft). Mammoths were grazers that preferred lowland savannas and parklands, not mountainous terrain. What this mammoth was doing at such a high elevation is not clear. See Morgan and Lucas (2026a) for more details. *0.5*

**4.1** Reddish-brown strata of the Atrasado Formation on left. *0.2*

**4.3** Atrasado Formation exposed in roadcuts. View ahead of Ortiz Mountains in middle ground and the Sangre de Cristo Mountains framing the skyline. *0.3*

**4.6** Atrasado Formation. Note pullout for Lagunita Spring on right. *0.1*

**4.7** Entrance to Sandia Ski Area on left (Fig. 1.35). Sandia Peak Ski Area (formerly La Madera Ski Area), which was established in 1936 within the Sandia Ranger District and is the ski hill closest to Albuquerque. Development of modern lift-served skiing and the resort accelerated as access and facilities improved over the decades, culminating in the construction of the Sandia Peak Tramway by Robert Nordhaus and Ben Abruzzo. In 2023, the ski area entered a joint venture with Mountain Capital Partners. *0.3*

**5.0** View of San Pedro Mountains between 2:00 and 3:00. *0.1*

**5.1** Greenish claystone of the Atrasado Formation. *0.2*

**5.3** Auto Tour sign 13 and entrance to Balsam Glade Recreation Area. **Turn right (north) onto State Road 165 (NM 165) toward Placitas.**

**0.0** **REZERO ODOMETER.** *0.1*



FIGURE 1.35. Photograph of Sandia Ski Resort taken from Balsam Glade. Ski runs sit on the eastern dip slope of Gray Mesa Formation limestone.

**0.1** Cross gate and follow NM 165, an unimproved dirt road that connects to Placitas at the northeastern flank of the Sandia Mountains. Along the way, note discontinuous exposures of Sandia Formation. The U.S. Forest Service may close this gate (and its northern counterpart in Placitas) at any time during the winter months, so check with the Sandia Ranger District before traveling on this road. *0.7*

**0.8** Partial view of Hagan embayment and Ortiz Mountains on right (northeast). At the upcoming hairpin turn (Fig. 1.36), near-vertical beds of quartzite are within sheared Sandia granite. These beds are about 10–15 m (33–49 ft) thick and were interpreted by Kelley and Northrop (1975) to be metaquartzite. This interpretation is supported by observations at the hairpin that these subvertical beds of quartzite and schist are similar to the Manzano Group where is has been intruded by Sandia granite. Read et al. (1999) proposed that these quartzite beds may be correlative to the Del Padre Sandstone, a member of the Mississippian Arroyo Peñasco Formation. A challenge with a Mississippian age assignment is that outcrops of Del Padre Sandstone to the south in the northern Manzano Mountains and north of Sandia Crest are at most 2 m (6.6 ft) thick (Armstrong et al., 1979; Lucas et al., 2021, 2026). The cumulative thickness of the quartzite beds does not neatly fit the regional stratigraphic setting. Possible Mississippian quartzite beds are recognized on the Balsam Glade divide (see above). However, these strata are thin and subhorizontal, and may not be related to the subvertical beds at the hairpin turn. Thus, these near-vertical quartzite layers may more likely be correlative to the Proterozoic Manzano Group. *0.1*

**0.9** Continue north on road and descend into Capulin Canyon, a tributary to Las Huertas Creek. *0.6*

**1.5** Sandia Formation on left. *0.1*

**1.6** View ahead across Capulin Canyon and Palomas Peak (Fig. 1.37). Note dip slope of northeastern Sandia Mountains with ledge-forming limestone of Gray Mesa and Sandia Formations on left.

The Gray Mesa Formation section at Palomas Peak (and in this part of the Sandia Mountains) is unusual in having a thick bioherm at its top (Figs. 1.38 and 1.39). Perkins (1959) described this section in detail with a focus on carbonate sedimentology. Perkins identified cycles (clastic-bioclastic rhythms) in the section but did not propose a driver, only noting tectonics, climate, or eustasy as potential drivers.

Lucas et al. (2026, in press) provided a detailed description of the Palomas Peak section (Figs. 1.38 and 1.39). In this section, the Gray Mesa Formation is 122 m (400 ft) in thickness and contains cliff-forming limestone intervals that are as much as 23 m (75 ft) in thickness. Most of the bedded facies of the Gray Mesa Formation are composed of lithotypes that are well known from other Gray Mesa sections:

- Planar-bedded limestone, 0.3–2.3 m (1.0–7.5 ft) thick, mostly cherty with bed thicknesses between 10 and 20 cm (<8 inches).
- Wavy-bedded limestone, cherty to very cherty, containing black chert nodules (as much as 30 cm [12 inch] in diameter) and irregular chert lenses. Wavy bedded limestone units are up to 4.8 m (16 ft) thick, forming steep cliffs. Some of the even-bedded, sparsely wavy-bedded limestone units contain abundant crinoid fragments (crinoidal wackestone).
- Nodular limestone, partly bedded, cherty to very cherty, with beds ranging in thickness from 0.2–3.5 m (0.7–11.5 ft). Bedded limestone is typically muddy (bioclastic mudstone to wackestone); fossils visible on outcrop are sparse and include crinoid debris, sparse fusulinids (unit 20), brachiopods (units 22 and 57), and bryozoa (unit 57).
- Two massive to indistinctly bedded limestones are present in the lower part; one is 0.8 m (1.7 ft) thick (unit 26) and the other is 1.7 m (5.6 ft) thick (unit 28).
- A prominent cliff-forming algal mound facies (units 61 and 62) of indistinctly thick bedded to massive limestone up to approximately 20 m (66 ft) thick is developed near the top of the Gray Mesa Formation (Figs. 1.38 and 1.39). This prominent mound facies can be traced laterally over several hundred meters and varies in thickness. The massive mound facies is developed on top of indistinctly wavy-bedded cherty limestone with black chert nodules and lenses, followed by indistinctly medium-bedded limestone that grades into the massive mound facies. The massive mound facies is overlain by 1.2 m (4 ft) of wavy-bedded cherty limestone, a 0.5-m (1.6-ft)-thick covered interval, and 0.7 m (2.3 ft) of bedded crinoidal limestone containing chert. The crinoidal limestone unit marks the top of the Gray Mesa Formation. *0.2*



FIGURE 1.36. Hairpin turn exposing sheared near-vertical quartzite and Sandia granite.



FIGURE 1.37. View to north of Palomas Peak.

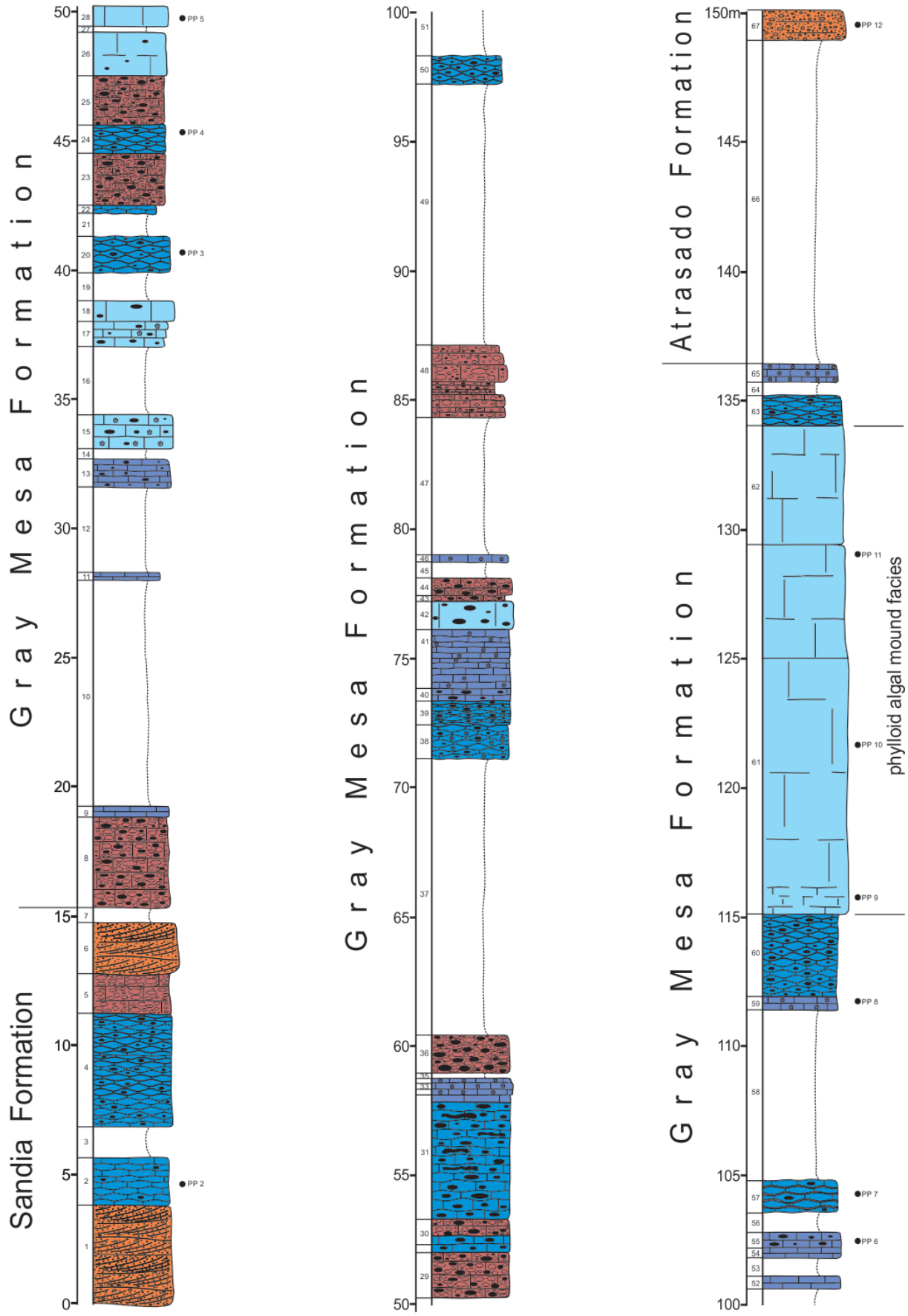



FIGURE 1.38. Palomas Peak Pennsylvanian section. See Figure 1.29 for explanation of symbols.

**1.8** Sandia granite on left. *0.3*

**2.1** Palomas Peak Trailhead (Forest Service Trail 66). *0.3*

**2.4** Sharp right turn, passing a side canyon to Capulin Canyon. The area on left has been subdivided into private residential lots. Las Huertas Spring is located in this drainage and it serves the community there. This spring is




FIGURE 1.39. Two views of the bioherm in the Gray Mesa Formation at Palomas Peak. A: Overview of upper part of Gray Mesa section, with bioherm labeled. B: Closeup of the bioherm.

anomalous in that it is oversaturated with $CO_2$ resulting in deposition of large volumes of travertine that line the creek from here to Las Huertas Picnic Area and to the north. Figure 1.40 shows water ponded behind rimstone dams, where slight turbulence from overflow enhances $CO_2$ degassing and travertine precipitation, creating a positive feedback that progressively increases dam height. Many of these travertine-bearing springs across the western United States are associated with deeper fluids that, although low in volume, are geochemically potent additions into a groundwater system (e.g., Newell et al., 2005). *0.3*

**2.7** Weathered Sandia granite on right. Enter Las Huertas Canyon, the second largest drainage on the Sandia Mountains. *0.2*

**2.9** Faults cutting Sandia granite. *0.6*

**3.5** Las Huertas Creek Picnic Area on left. *0.1*

**3.6** Weathered Sandia granite with dark-gray xenoliths or comagmatic enclaves. *0.4*

**4.0** Cross Las Huertas Creek. *0.2*

**4.2** Deeply weathered Sandia granite and sandy (granitic) at the base of Sandia Formation. *0.1*

**4.3** Faulted Gray Mesa Formation limestone. *0.1*



FIGURE 1.40. Springs feeding Las Huertas Creek are commonly underlain by travertine.

**4.4** Cross Las Huertas Creek. *0.1*

**4.5** Sandia Cave Trailhead on right (east). *0.5*

**5.0** Helical metal staircase ahead leads to Sandia Cave in limestone cliffs of the Gray Mesa Formation (Fig. 1.41). *0.2*

**5.2** Cross Las Huertas Creek. *0.4*

**5.6** Limestone of Gray Mesa Formation on left. *0.2*

**5.8** Note outcrops of Garcia Member of Gray Mesa Formation. There are three members of the Gray Mesa Formation that can be recognized north of Palomas Peak. These units are, in ascending stratigraphic order, Elephant Butte, Whiskey Canyon, and Garcia Members. Both the Elephant Butte and Garcia Members contain sparse chert nodules in contrast to the Whiskey Canyon Member, which is distinguished by abundant chert. It is worth noting that the few sandstone beds in the Elephant Butte and Whiskey Canyon Members are rich in quartz, as is observed in sandstone in the Sandia Formation. The arkosic composition appears to have begun in the Garcia Member. *0.1*

**5.9** Las Huertas Creek on right. For the next mile, keep your eyes open for locations where travertine in the creek becomes sparse. The reduction of carbonate cement on the floor of the creek may be due to faulting and shallow burial of the Great Unconformity, which likely influences groundwater flow patterns. *0.1*

**6.0** Garcia Member of the Gray Mesa Formation on left. *0.3*

**6.3** Subrounded cobbles and boulders of stream deposit associated with Las Huertas Creek. *0.2*

**6.5** Atrasado Formation shale on left. *0.2*

**6.7** Cross Las Huertas Creek. *0.1*

**6.8** Stream alluvium of Las Huertas Creek on right. *0.1*

**6.9** Atrasado Formation shale and limestone. *0.3*




FIGURE 1.41. Photographic panel of Gray Mesa limestone, showing at least 3 upward-coarsening parasequences. Entrance to Sandia Cave is in middle of an upward-coarsening sequence.

**7.2** Quaternary silt and very fine-to fine-grained sand on left. *0.1*

**7.3** Cross gate. Pavement begins. *0.2*

**7.5** View of Crest of Montezuma at 1:00. The Atrasado Formation is underlain by thick ledges of Gray Mesa limestone. Sandia Formation and underlying Sandia granite are poorly exposed in the lower slopes. *0.6*

**8.1** Entering San Antonio de las Huertas, an 18th century Spanish colonial land grant near the present-day Placitas, New Mexico. This grant was established in 1765 as a buffer settlement founded by Governor Tomás Vélez Cachupín for settlers and Genízaros ("detribalized" Native Americans) facing Apache raids. *0.2*

**8.3** Orangish-yellow Yeso Group strata in the valley on right. *0.3*

**8.6** Reddish-brown sandstone and shale of Abo Formation. *0.4*

**9.0** Hill at 12:00 is underlain by coarse-grained piedmont facies of the Santa Fe Group, which were derived from the northern flank of the Sandia Mountains during Neogene time. *0.1*

**9.1** Enter village of Placitas. **Turn right onto Camino del Tecolote.** *0.3*

**9.4** Reddish-yellow Holocene alluvium on valley floor. *0.3*

**9.7** Roadcuts on left are fault slivers of the Brushy Basin Member of the Jurassic Morrison Formation. **Turn right onto dirt road.** *0.2*

**9.9** **Park on access road to private residence near western edge of the Crest of Montezuma.** Figure 1.42 shows members of the Gray Mesa Formation that can be seen on the Crest of Montezuma. Although the sites we will be examining are on land managed by the Bureau of Land Management, you must first get permission from private landowners. Walk east on footpath to lower slope where we can see Sandia Formation overlying steeply tilted Paleoproterozoic metasedimentary rocks (Fig. 1.43). Then walk up to view the Gray Mesa Formation.

**Waypoint 1.10 [N35.3144°, W106.4064°]**

**STOP 3. Great Unconformity and Upper Paleozoic Stratigraphy at Crest of Montezuma.**

## PLACITAS AREA HYDROGEOLOGY

The Placitas area occupies a complicated structural ramp along the southeastern margin of the Santo Domingo subbasin, forming three principal hydrologic systems: (1) a mountain system in fractured Proterozoic granite and Pennsylvanian carbonate; (2) a structural ramp system dominated by Mesozoic shale and sandstone; and (3) a basin-fill aquifer system composed of Santa Fe Group sediments. The Sierra Ladrones Formation forms the primary basin-fill aquifer in western Placitas, whereas Pennsylvanian carbonate aquifers are only locally productive, and Permian and Mesozoic shale-dominated units generally exhibit low transmissivity except where enhanced

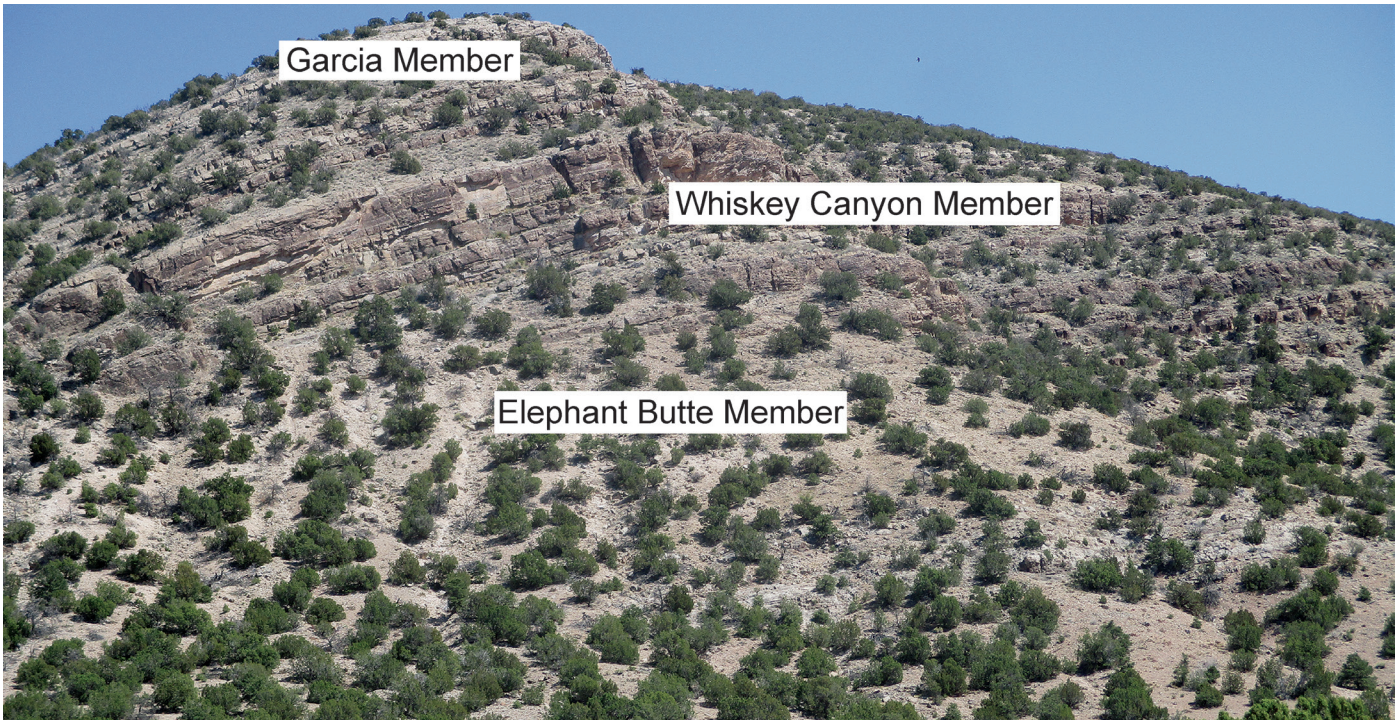



FIGURE 1.42. The Gray Mesa Formation at the Crest of Montezuma.

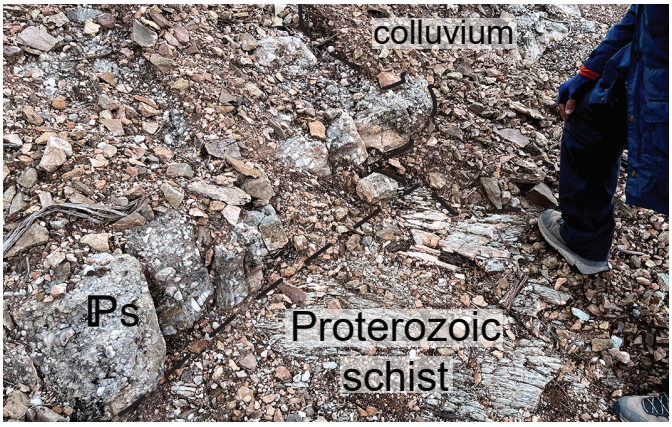



FIGURE 1.43. Angular nonconformable contact between pebbly sandstone of the Pennsylvanian Sandia Formation overlying Paleoproterozoic schist.

by fracturing. Faults including the Rincon–Ranchos, Lomos, Valley View, and Caballo–Escala systems compartmentalize groundwater flow, locally impeding recharge, promoting spring discharge, and producing spatially variable well performance. Water levels are variable and, although recharge from mountain-front infiltration and springs may approach or exceed current withdrawals, multiple datasets indicate long-term declines on the order of 0.22–0.76 m/yr (0.75–2.5 ft/yr) in many water-supply wells, reflecting structural compartmentalization, variable recharge, and increasing groundwater use during six decades of development (Johnson et al., 2002; Melis, 2026).

The main springs in each of the springsheds along our route (Cienega, Capulin, and Las Huertas) have slightly different geochemical signatures. In part, this may reflect that the springsheds are bounded by faults. Las Huertas drainage contains somewhat unusual carbonic springs that have lined its bed with travertine. A longitudinal sampling of Las Huertas Creek shows variation in the external $CO_2$ ($C_{ext}$), which is the portion of the total dissolved inorganic carbon that cannot be explained by dissolution of limestone in the Pennsylvanian aquifer system. The highest $C_{ext}$ inputs are recorded at the source springs high in the drainage and from another source near the Las Huertas Picnic Area. Both of these inputs correspond to north-trending normal faults (e.g., Lagunita and Ellis faults of Kelley and Northrop, 1975) that offset basement and may have Laramide ancestry. Las Huertas Creek waters below the picnic area are a mix of Las Huertas and Capulin springsheds and show declining $C_{ext}$ effects downstream. Las Huertas springs are an example of travertine-depositing carbonic springs found throughout the Southwest that have "lower-world" characteristics of high $CO_2$, sometimes with mantle-derived $^3He$. (Las Huertas has not been analyzed for helium isotope composition.) They are interpreted to be manifestations of what could be called "xenowhiffs" (i.e., foreign gases entrained in the near-surface groundwater system) due to subtle but measurable mantle and magmatic degassing at depth and migration of small volumes of geochemically potent fluids up faults (Crossey et al., 2026).

Stable-isotope compositions of springs in the Sandia Mountains have best-fit slopes that are lower than the Global Meteoric Water Line, indicating meteoric recharge is modified by limited evaporative effects with a strong contribution from winter precipitation. Springs to the south, in the nearby Manzano Mountains, exhibit a similar but more evaporatively influenced deuterium–oxygen trend that generally reflects recharge derived from lower-elevation precipitation and a smaller snowmelt component. This contrast is consistent with the slightly higher mean elevation of recharge in the Sandia Mountains (2,438 m [8,000 ft]) relative to the slightly lower mean elevation in the Manzano Mountains (2,134 m [7,000 ft]), where colder temperatures and greater snow accumulation enhance the winter precipitation signal in the Sandia Mountains springs. Because groundwater in the Placitas area is largely from the Sandia Mountains, the isotopic composition of local groundwater likely reflects this higher-elevation recharge source. Crossey et al. (2026) noted that temporal differences between earlier and more recent isotopic datasets may partly reflect climatic variability, including differences in winter temperature and snowpack between 20th century conditions and more recent sampling periods.

## PENNSYLVANIAN STRATIGRAPHY

The Crest of Montezuma is a north-trending structural reentrant that exposes a nearly complete Pennsylvanian section (Sandia, Gray Mesa, and lower and middle Atrasado Formations). Combined with the strata across the Montezuma fault to the north (middle–upper Atrasado and a complete section of Bursum Formation), the entire local Pennsylvanian section can be assembled here (Lucas et al., 2026, in press). We will examine a location (Figs. 1.42 and 1.44) where most of the Gray Mesa Formation is well exposed at the Tecolote B section of Lucas et al. (2026, in press). Locally along the ridge, a thin Mississippian section (mostly carbonate) is present between the basement and the base of the Sandia Formation.

At the Tecolote B section, the exposed thickness of the Gray Mesa Formation is 170 m (558 ft). The Gray Mesa Formation is mostly composed of limestone with some covered intervals, sparse conglomerate, and thin sandstone beds. A lithologic subdivision into Elephant Butte, Whiskey Canyon, and Garcia Members is possible (Figs. 1.42 and 1.44).

The Elephant Butte Member includes units 1–18 of the Tecolote B section and is 22.5 m (74 ft) in thickness. It is composed of thin conglomerate beds, sandstone, different types of limestone (most with little or no chert), and covered intervals. Covered intervals are 0.9–4.3 m (3–14 ft) thick and probably represent shale or siltstone.

The Whiskey Canyon Member is 78.5 m (258 ft) thick. It is composed mostly of cherty limestone with a few covered intervals that are 0.8–3.1 m (2.6–10.2 ft) thick and probably represent shale or siltstone. Limestone is represented by different lithotypes that are also known from other Gray Mesa sections. Many of the limestone intervals contain abundant chert. Individual limestone beds are 0.7–6.2 m (2.3–20.3 ft) thick. The Garcia Member is 69 m (226 ft) thick. Covered intervals in the Garcia Member are 0.3–5.1 m (1–18 ft) in thickness.

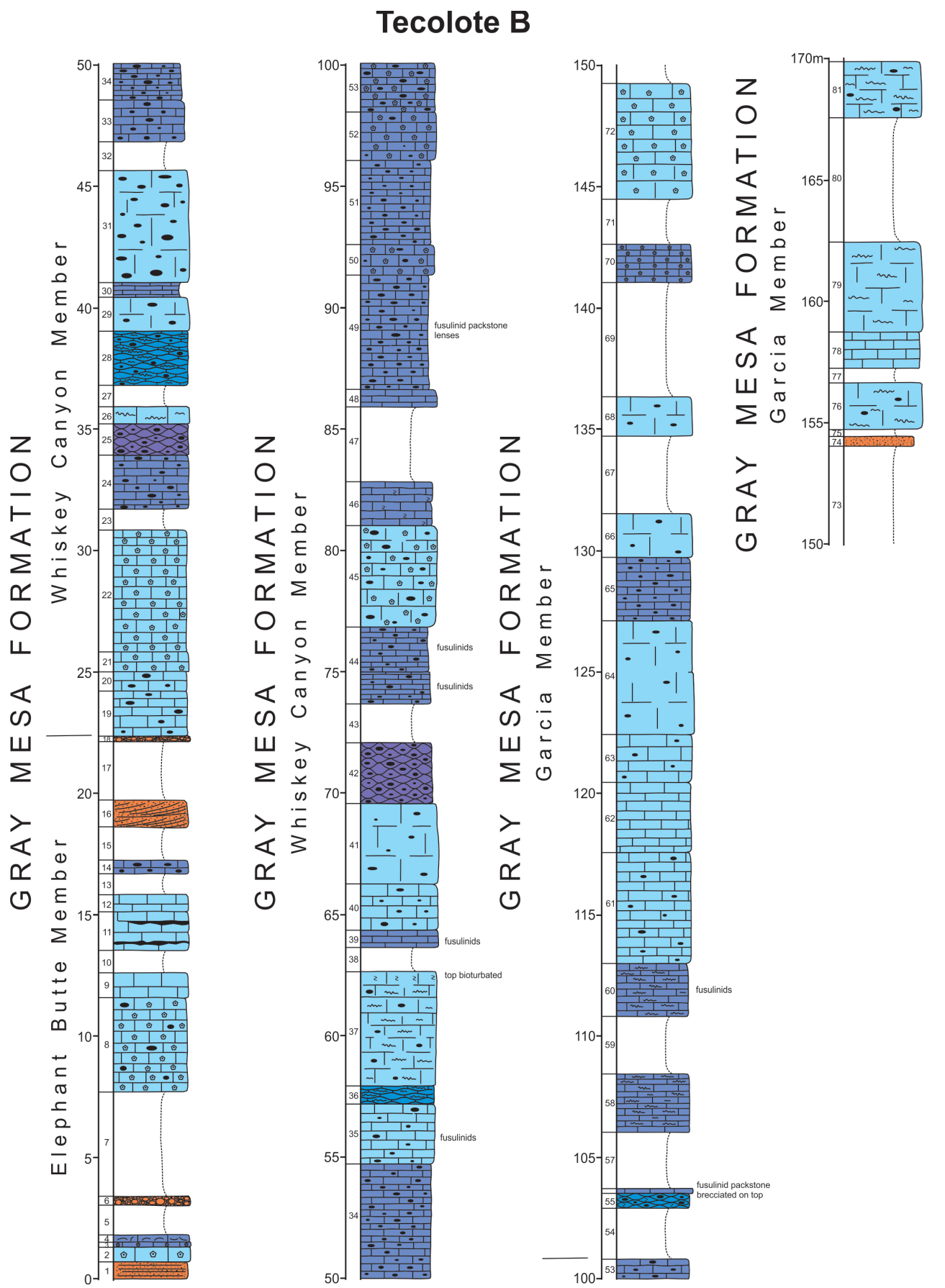



FIGURE 1.44. Tecolote B section of most of the Gray Mesa Formation at the Crest of Montezuma. See Figure 1.29 for explanation of symbols.

Limestone intervals are 0.2–4.8 m (< 3 ft to 16 ft) in thickness.

A striking characteristic of the Whiskey Canyon Member is the abundance of chert, which serves as a key distinguishing feature across known outcrops—from the type section in the Mud Springs Mountains near Truth or Consequences, New Mexico, to its northernmost exposure here at the Crest of Montezuma. This pervasive chert provides an important basis for interpreting silica sources and depositional conditions during late Paleozoic time.

Traditionally, chert in marine limestone has been interpreted as biogenic in origin, derived primarily from siliceous sponges and/or diatoms. However, an alternative model proposed by Cecil (2004, 2015) and Cecil et al. (2014) suggests that silica was sourced from quartz-rich, eolian dust. This interpretation is supported by the observation that upper Paleozoic chert is commonly associated with strata deposited under semiarid paleoclimatic conditions (e.g., Soreghan et al., 2023) and typically contains abundant detrital quartz silt and fine-grained sand dispersed within a chert matrix.

Detrital quartz grains (≤20 μm) commonly exhibit corroded margins indicative of dissolution. Cecil (2004) proposed that eolian abrasion damaged the crystalline lattice of quartz grains during transport, enhancing their susceptibility to dissolution in marine settings and facilitating subsequent reprecipitation as microcrystalline quartz (i.e., chert). Based on this mechanism, Cecil et al. (in press) proposed that chert in the Gray Mesa Formation of central New Mexico was largely derived from the dissolution of eolian dust.

Samples from the Whiskey Canyon Member at the Tecolote B section (Fig. 1.44, units 25 and 28) support this interpretation. These limestones contain abundant chert, both in massive beds and in nodular forms, characterized by angular detrital quartz grains (<20 μm) and fine-grained sand with corroded grain surfaces. The morphology of these grains is consistent with eolian transport and subsequent deposition in a marine environment, indicating an eolian-marine sediment source. Dissolution of these grains provided silica for the reprecipitation of microcrystalline quartz in the chert. Detrital zircon U-Pb age spectra further support this model. Limestone samples from the Tecolote B section show two well-defined age peaks, suggesting a relatively local siliciclastic source. In contrast, chert samples display a broader distribution of zircon ages, consistent with sediment derived from a more expansive source region and transported by wind.

The presence of abundant eolian-marine dust in the Gray Mesa limestones has broader paleoenvironmental implications. It indicates widespread semiarid conditions across tropical Pangea during the Atokan–Desmoinesian transition, consistent with regional changes in wetland floras and sedimentologic indicators of climate variability. This interpretation highlights the importance of atmospheric dust flux as a significant control on silica cycling and chert formation in late Paleozoic marine systems.

**End of Stop 3. Return to vehicles.**
**Retrace route (0.8 miles) to NM 165.**

**0.0** **REZERO ODOMETER.** *0.7*

**0.7** Placitas Post Office on left. *0.7*

**1.4** Mile marker 6. Just north of NM 165, Hibben and Bryan (1941) reported the remains of *Mastodon* and *Equus* (taxa characteristic of the Rancholabrean Land Mammal Age) within the valley floor alluvium near the village of Placitas (see Kelley and Northrop, 1975, p. 72–73). See paper by Morgan and Lucas (2026b) for details. In the same area, Bruce Huckle (1999, written communication) of the University of New Mexico Maxwell Museum reported Archaic (6–2 ka) projectile points in this deposit (see Connell et al., 1995). *0.5*

**1.9** Upper Jurassic Morrison Formation on left. At Placitas, Jurassic strata are exposed on fault blocks at the northern end of the Sandia uplift, and most of the published information on the Jurassic section at Placitas is on geologic maps (Kelley and Northrop, 1975; Connell et al., 1995; Menne, 1999). A complete Jurassic section was measured as four overlapping sections on different fault blocks (Fig. 1.45). Anderson and Lucas (2000) briefly reported on this section, which consists of, in ascending stratigraphic order, the Entrada, Todilto, Summerville, and Morrison Formations. Lucas (2018) provided a more extensive description of Morrison Formation strata.

At Placitas, the basal member of the Morrison Formation, the Salt Wash Member, is as much as 71 m (233 ft) in thickness and consists of fine- to coarse-grained, feldspathic sandstone, with pebbly (conglomeratic) zones as much as several meters thick. In addition to the pebbly beds, other distinguishing features are trough cross-bedding, presence of clay rip-up clasts, and nonmarine bioturbation. The overlying Brushy Basin Member is as much as 49 m (161 ft) thick and consists of greenish, mostly smectitic claystone with thin interbeds of dark-weathering fine-grained sandstone and nodular limestone. This is a relatively thin section of the Brushy Basin Member, and this claystone-dominated unit has likely been tectonically thinned by faulting. The uppermost member of the Morrison Formation, the Jackpile Member, is as much as 21 m (69 ft) thick locally and consists of trough- and planar-crossbedded kaolinitic sandstone. The Cretaceous Encinal Canyon or Oak Canyon Members of the Dakota Sandstone disconformably overly the Jackpile Member. A Jurassic section near Placitas is exposed south of Stop 4. *1.3*

**3.2** Fire station on right. Low ridges of Santa Fe Group piedmont deposits at 3:00. At 9:00 are views of the north-plunging flank of the Sandia Mountains. Sandia granite is overlain by Pennsylvanian strata. The narrow Rincon Ridge trends north-south to the west and is composed of metamorphic rocks. A west-east ridge connects Rincon Ridge to the north end of the shield. *0.6*

**3.8** Mile marker 4. On left (south), Pleistocene gravels—likely correlative to the Tuerto gravels of Stearns (1953) in the adjacent Hagan embayment—overly

conglomeratic piedmont deposits of the Sierra Ladrones Formation (upper Santa Fe Group). The Santa Fe Group overlies Mancos Shale. *0.1*

**3.9** Mancos Shale on left, near intersection with El Vado Road. *0.3*

**4.2** **As directed, pull onto right shoulder near Placitas**

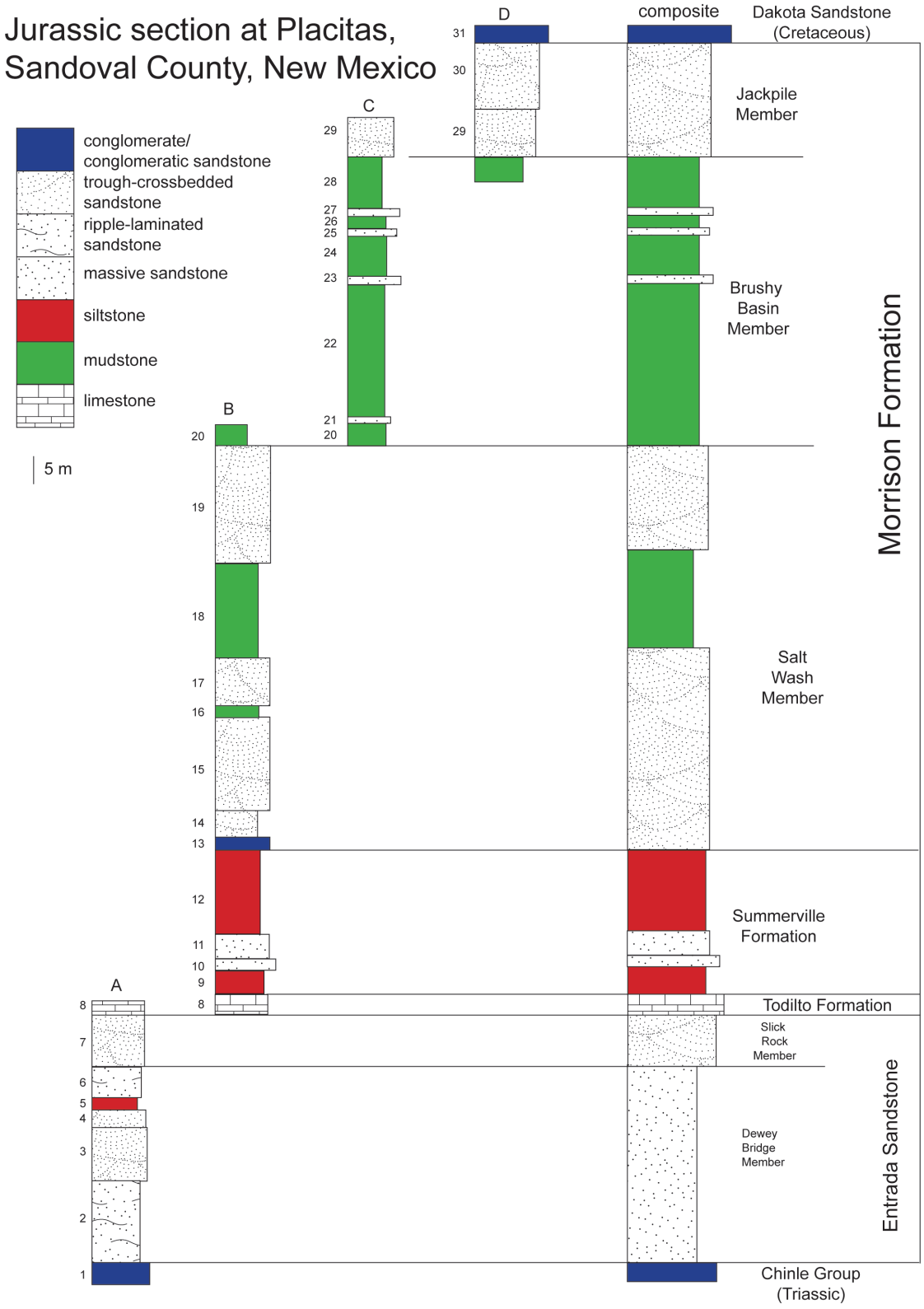



FIGURE 1.45. Stratigraphic sections of Jurassic strata measured at Placitas, Sandoval County, New Mexico. A, B, C, and D represent four overlapping sections measured on different fault blocks, and the column on the right is the composite Jurassic section (from Lucas, 2018).

**Historical Marker.** Use extreme caution when parking and leaving your vehicle. This site is along a blind curve and the traffic can be swift, especially near the end of a workday. Should the volume of vehicular traffic be high, consider using the parking areas west of this stop. **A Forest Service parking lot is 0.8 miles on the left; another parking area is down the road, 1.3 miles on the right.**

**Waypoint 1.10 [N35.3011°, W106.4718°]**

**STOP 4. Northern Flank of Sandia Mountains.**

## INTRODUCTION

The focus of this stop is the low-angle contact on the inside bend of a blind curve with relatively fast vehicular traffic. **Stay off the road and cross the road only when necessary and absolutely safe to do so.**

## STRATIGRAPHY

On right (north) side of road is the Upper Cretaceous Dakota Sandstone through Carlile Shale succession. The Carlile Shale of the Mancos Shale underlies a planar contact with overlying conglomeratic piedmont deposits of the Sierra Ladrones Formation (upper Santa Fe Group). Thin sandstone beds in the Mancos Shale may be correlative with the underlying Cretaceous Semilla Sandstone, a lenticular offshore bar deposit of the middle of the Carlile Member.

South of the roadcut are some of the most extensive Mesozoic outcrops in the Placitas area (Connell et al., 1995). These outcrops include Upper Triassic red beds of the Chinle Group and a faulted Middle to Upper Jurassic section of the Entrada, Todilto, Summerville, and Morrison Formations (Fig. 1.45; Lucas and Heckert, 1995; Anderson and Lucas, 2000; Lucas, 2018). The outcrops of Triassic and Jurassic strata at our first stop earlier today include (as mentioned previously) some of the same Triassic and Jurassic stratigraphic units, but are more completely exposed here.

Deposits of the Sierra Ladrones Formation record the transition from widespread aggradation to Pleistocene incision and valley entrenchment. Along the northern flank of the Sandia Mountains, Sierra Ladrones Formation strata are locally in fault contact with older Santa Fe Group deposits. The formation marks the final constructional phase of basin filling prior to development of the modern Rio Grande valley morphology (Connell, 2004; Connell et al., 2007). Lithofacies consist of interfingering piedmont and axial-fluvial deposits. Gravelly alluvium derived from the Sandia Mountains grade basinward into sand- and gravel-prone channel-belt deposits and associated overbank sediments of the ancestral Rio Grande.

Regional chronostratigraphic synthesis indicates that deposition of the Sierra Ladrones Formation spanned ~7 Ma to 0.8 Ma, with piedmont and axial components overlapping temporally but differing in geomorphic expression and preservation (Connell and Wells, 1999; Connell, 2004). These deposits postdate the principal phase of Miocene rift-flank uplift and widespread Santa Fe Group accumulation and represent a younger (Plio–Pleistocene) episode of basin aggradation.

## STRUCTURAL GEOLOGY

### Introduction

The northern flank of the Sandia Mountains forms a north-plunging structural ramp created by a 6.5-km (4-mi)-wide eastward step in the rift-bounding Rincon and San Francisco faults. Kelley (1977, 1982) interpreted the northern flank as a relay ramp associated with a dextral stepover between the Rincon and San Francisco fault systems. The Placitas fault zone is a complicated zone of steeply dipping, northeast-striking faults that is part of a breached relay ramp that accommodates an eastward step in the basin margin between the Rincon and San Francisco faults (Connell et al., 1995; Connell and Wells, 1999).

The geometry of the Placitas fault zone in the eastward stepover of the Albuquerque Basin has long been debated. Interpretations of low-angle contacts along the northern flank of the Sandia Mountains vary substantially, underscoring the need for careful distinction between depositional surfaces and structural discontinuities. This outcrop provides a useful setting to evaluate field relationships that bear directly on the structural evolution of the Sandia uplift and its basin margin.

The north-plunging ramp has been interpreted to represent the surface expression of major listric faults that define the eastern basin margin (e.g., Russell and Snelson, 1990, 1994). Woodward (1977) first proposed listric geometries for faults in the Albuquerque Basin. Using the downplunge method of cross-sectional construction, several workers suggested that the trace of the Placitas fault zone (northern structural boundary of the Sandia Mountains) is curved in map view (May et al., 1994; Russell and Snelson, 1994; Woodward and Menne, 1995). They interpreted this apparent curvature as indicative of a listric fault plane at depth; however, the mapped traces of the Placitas fault zone are rather straight (Connell et al., 1995), indicating a steep fault dip. Here the downplunge method has been misapplied, principally because the projection is nearly perpendicular to the Placitas fault zone (e.g., Connell et al., 1995; Connell and Wells, 1999). Instead, the Placitas fault zone likely acts as a transfer zone between the frontal faults of the Sandia Mountains and adjacent Hagan embayment (e.g., Connell and Wells, 1999; Karlstrom et al., 1999). The overall structure can be conceptually modeled as a breached relay ramp that formed between the basin-bounding Rincon and San Francisco faults. Ricketts et al. (2015) proposed that the Placitas fault zone may have an inheritance from an older, steeply dipping, northeast-trending strike-slip fault of Laramide age that was reactivated during Neogene time.

### Contact Between the Santa Fe Group and Mancos Shale: Fault or Unconformity?

Figure 1.46 shows images of a low-angle contact between the Santa Fe Group and the Mancos Shale. The low-angle contact has been alternately mapped as an erosional unconformity (e.g., May et al., 1994) or part of the Rincon fault (Russell and Snelson, 1994) and Ranchos fault zone (e.g., Connell et al., 1995). This planar feature dips of approximately 20° west. The

footwall and hanging-wall cut-off angles (with bedding) are ~30°, suggesting that a fault would have moved at low angles within the Placitas relay ramp after upper Santa Fe Group deposition, and after dips had already declined through footwall uplift and rotation.

Is this a low-angle, large-displacement normal fault, or is it primarily a depositional contact that has been modified by relatively minor fault displacement? Compared with other exposures along the rift, large-displacement faults would be expected to have wide damage zones exhibiting shear fabrics and meter-scale distributed deformation (e.g., Rawling et al., 2001). In such damage zones, clay cores and mixing zones are present. Refer to Station 4, Stop 1 of the Day 2 road log for examples of fault deformation in the Miocene Cerro Conejo and Zia Formations.

A depositional boundary would correspond to an angular or buttress unconformity. The presence of pebbly scours on the contact supports evidence for a depositional contact (Fig. 1.46); however, beds near the contact are slightly rotated, supporting a structural origin. Another scenario is that this contact is depositional in nature and has been modified by subsequent faulting. Given the rheological contrast between the overlying Sierra Ladrones Formation and the relatively soft underlying Mancos Shale, one might expect evidence for movement along the contact. In such a case, a narrow, weak damage zone can develop that can contain slickensides. Examining the width and complexity of a fault-damage zone would be insightful. Outcrop observations allow participants an opportunity to examine the rocks and decide for themselves what they think of this intriguing contact.

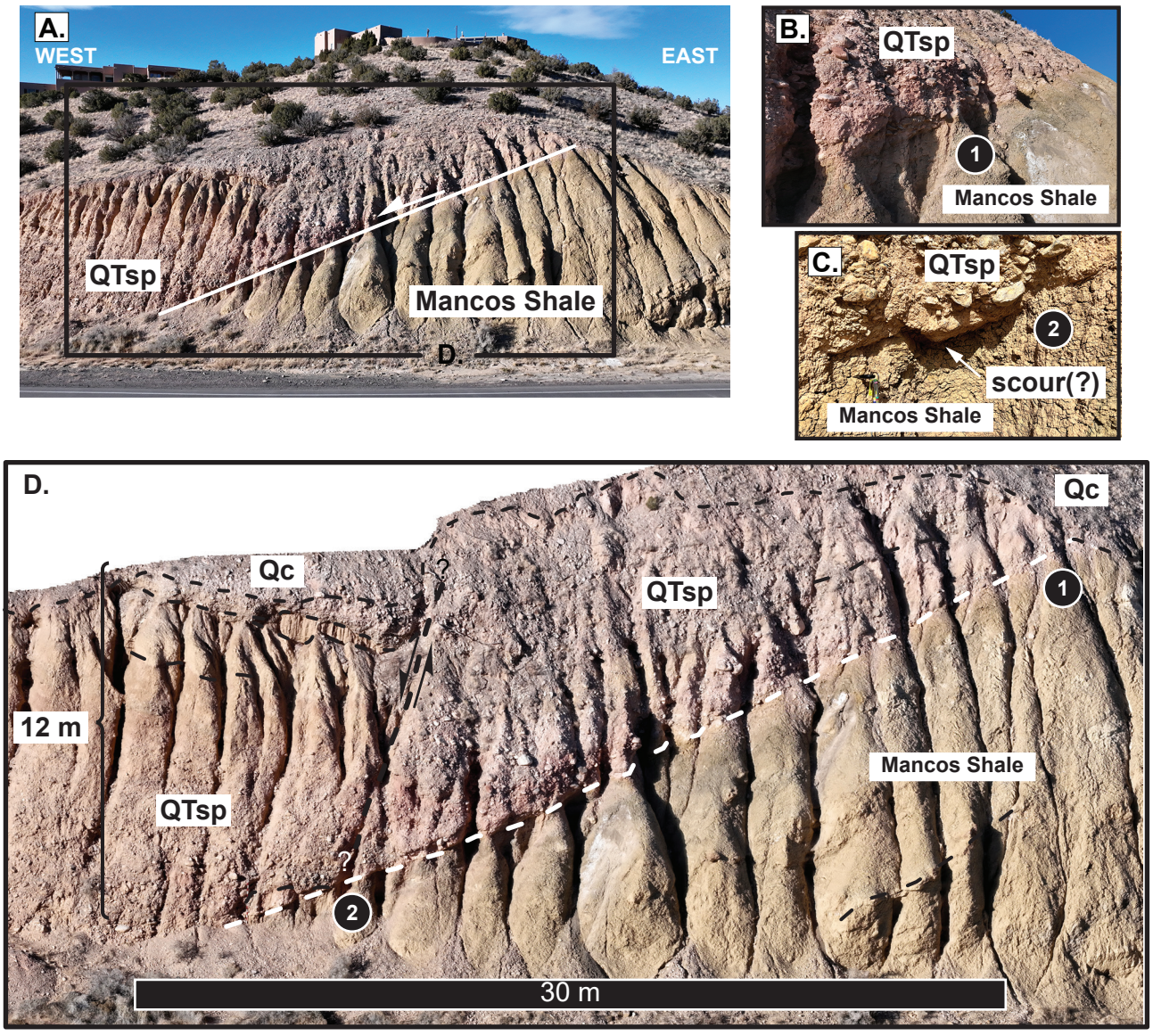



FIGURE 1.46. Contact between piedmont deposits of the Sierra Ladrones Formation (QTsp) overlying yellowish-brown Upper Cretaceous Mancos Shale. This outcrop has been alternately interpreted as an angular unconformity or a low-angle fault (e.g., May et al., 1994; Ricketts et al. 2015). A: Photograph of outcrop and interpretation of contact as a low-angle normal fault (modified from Ricketts et al., 2015). B: Closeup photographs of the contact. C: Likely pebbly scour of QTsp on Mancos Shale. D: Digital outcrop model showing the juxtaposition of QTsp over Mancos Shale. Numbers mark the approximate locations of photographs B and C.

### End of Day 1 Road Log

Drive west on NM 165 toward Bernalillo, New Mexico. Turn left onto on-ramp for southbound I-25 toward Albuquerque. South of the Tramway Boulevard/Roy Avenue exit (Exit 326), retrace route to the New Mexico Museum of Natural History and Science, or drive directly to the NMGS BBQ at Rio Grande Nature Center State Park (2901 Candelaria Road NW, Albuquerque, NM 87107), taking the Comanche/Candelaria Road exit (Exit 227) and turning right (west) onto Candelaria Road. Follow Candelaria Road to the end and turn right into the Rio Grande Nature Center parking lot.

## ACKNOWLEDGMENTS

We thank the Sandia Ranger Station (Cibola National Forest) and the Bureau of Land Management for facilitating access on public lands. We thank Mr. Max Dawkins for allowing access to Stop 3. We also thank Alexander Marx and Dakota FitsEmons for assistance with some of the figures.



The greater roadrunner (*Geococcyx californianus*) is a fast-running member of the cuckoo family and New Mexico's state bird. Roadrunners are widespread across desert, grassland, and woodland habitats and are a familiar symbol of the American Southwest. Photograph courtesy of Celestyn Brożek.



View of the Sandia Mountains from West Bluff Park, along the western bank of the Rio Grande. Photograph courtesy of Sean Connell.



Sandia Mountains after a dusting of snow. The pyramidal feature is locally known as “The Needle.” Photograph courtesy of Celestyn Brożek.



Sandia Mountains take from the Rio Grande Nature Center. Photograph courtesy of Celestyn Brożek.